Copyright Warning & Restrictions

The copyright law of the United States (Title 17, United States Code) governs the making of photocopies or other reproductions of copyrighted material.

Under certain conditions specified in the law, libraries and archives are authorized to furnish a photocopy or other reproduction. One of these specified conditions is that the photocopy or reproduction is not to be "used for any purpose other than private study, scholarship, or research." If a, user makes a request for, or later uses, a photocopy or reproduction for purposes in excess of "fair use" that user may be liable for copyright infringement,

This institution reserves the right to refuse to accept a copying order if, in its judgment, fulfillment of the order would involve violation of copyright law.

Please Note: The author retains the copyright while the New Jersey Institute of Technology reserves the right to distribute this thesis or dissertation

Printing note: If you do not wish to print this page, then select "Pages from: first page # to: last page #" on the print dialog screen

Order Number 9426997

Investigation of paraelectric PLT thin films using reactive magnetron sputtering

Kim, Hyun Hoo, Ph.D.

New Jersey Institute of Technology, 1994

U·M·I
300 N. Zeeb Rd.
Ann Arbor, MI 48106

ABSTRACT

INVESTIGATION OF PARAELECTRIC PLT THIN FILMS USING REACTIVE MAGNETRON SPUTTERING

by
Hyun Hoo Kim

The study of methods to prepare paraelectric perovskite PLT (Pb_{1-X} $La_XTi_{1-X/4}O_3$; x=0.28) thin films has been important because thin films of this high dielectric strength material are required to make high density capacitors for dynamic random access memory. In this research, paraelectric PLT thin films were prepared on multi-layer ($Pt/Ti/SiO_2/Si$) and MgO substrates in a unique way by the reactive magnetron sputtering method using a multi-component metal target. The individual control of each metal area on the sputtering target had considerable influence on the stoichiometry and electrical properties of the thin films. The effect of post-deposition annealing on as-deposited amorphous PLT films was studied as a function of temperature in the range of 450 °C to 750 °C. The inter-dependent relationship of the composition, crystalline structure and surface morphology in the films was studied as a function of annealing conditions. The chemical composition of the as-deposited and annealed films was measured by Rutherford back-scattering (RBS) and Auger electron spectroscopy (AES). The composition of PLT (28) thin film was: Pb, 0.73; La, 0.28; Ti, 0.88; O, 2.9.

The dielectric constant (ε_r) and dissipation factor ($tan\ \delta$) at low electric field measurement (500 V/cm) of the capacitors with the highest dielectric properties were 1216 and 0.018, respectively. Single crystal film at 650 °C were smooth and had the lowest leakage current density, 0.1 $\mu A/cm^2$, at the electric field of 0.25 MV/cm. However, the highest dielectric constant, 1216, and the highest charge storage density, 12.5 $\mu C/cm^2$, obtained with an annealing temperature of 750 °C. The research showed

that magnetron sputtering can be used to prepare paraelectric perovskite PLT (28) thin films with high dielectric constant, large charge storage density and relatively low leakage current for capacitor applications in active DRAM cells.

INVESTIGATION OF PARAELECTRIC PLT THIN FILMS USING REACTIVE MAGNETRON SPUTTERING

by
Hyun Hoo Kim

A Dissertation
Submitted to the Faculty of
New Jersey Institute of Technology
in Partial Fulfillment of the Requirements for the Degree of
Doctor of Philosophy

Department of Electrical and Computer Engineering

May 1994

APPROVAL PAGE

INVESTIGATION OF PARAELECTRIC PLT THIN FILMS USING REACTIVE MAGNETRON SPUTTERING

Hyun Hoo Kim

Dr. Kenneth Sohn, Dissertation Advisor — Date
Professor and Acting Chairman of Electrical and Computer Engineering, NJIT

Dr. Roy Cornely, Committee Member — Date
Professor of Electrical and Computer Engineering, NJIT

Dr. Haim Grebel, Committee Member — Date
Associate Professor of Electrical and Computer Engineering, NJIT

Dr. James Grow, Committee Member — Date
Associate Professor of Chemistry, NJIT

Dr. Walter Kosonocky, Committee Member — Date
Distinguished Professor of Electrical and Computer Engineering, NJIT

Dr. Richard Lareau, Committee Member — Date
Army Research Center, Fort Monmouth, NJ

BIOGRAPHICAL SKETCH

Author: Hyun Hoo Kim

Degree: Doctor of Philosophy in Electrical Engineering

Date: May 1994

Undergraduate and Graduate Education:

- Doctor of Philosophy in Electrical Engineering,
  New Jersey Institute of Technology, Newark, NJ, 1994
- Master of Science in Electrical Engineering,
  Louisiana State University, Baton Rouge, LA, 1987
- Master of Science in Electrical Engineering,
  Hanyang University, Seoul, Korea, 1984
- Bachelor of Science in Electrical Engineering,
  Dankook University, Seoul, Korea, 1982

Major: Electrical Engineering

Presentation and Publication:

Kim, H. H., K. S. Sohn, L. M. Casas, R. L. Pfeffer, and R. T. Lareau. "Preparation of PLT Thin Films using Reactive Magnetron Sputtering of Multi-Component Metal Target." 185th Society Meeting of Electrochemical Society. San Francisco. CA. May 22-27, 1994.

Kim, H. H., K. S. Sohn, L. M. Casas, R. L. Pfeffer, and R. T. Lareau. "Paraelectric and Mechanical Properties of PLT (28) Reactively Sputtered by Multi-Element Metal Target." The Ninth IEEE International Symposium on the Applications of Ferroelectrics. Pennsylvania State University. PA. August 7-10, 1994.

BIOGRAPHICAL SKETCH
(Continued)

Kim, H. H., and K. S. Sohn. "Investigation of Superconductor Thin Film on MgO Substrate with Buffer Layer." The Governer's Summer Research Fellowship in Superconductivity Conference. Princeton. NJ. July 31, 1989.

Kim, H. H., and B. H. Kim. "Investigation on Inception Voltage and Growing Processes of Treeing Phenomena in LDPE." Journal of Korean Electrical Institute. April. 32-36, 1984.

Kim, H. H., and B. H. Kim.. "A Study on Growth Control of Treeing Phenpmena in Low Density Polyethylene." Spring Meeting of Electrical material Society in Korean Electrical Institute. Seoul. May 28, 1983.

This thesis is dedicated to
my parents, my wife, Hyunyoo, and my two sons, Jongseok and Byongchul

ACKNOWLEDGMENT

I would first like to express my deepest gratitude to my advisor, Professor Kenneth S. Sohn, for his invaluable encouragement during the preparation of my thesis. I would not have been able to complete this work without his guidance and support. I am also grateful to the member of the dissertation committee, Professor Roy Cornely, Professor Haim Grebel, Professor James Grow, Professor Walter Kosonocky and Dr. Richard Lareau for their helpful suggestions and discussions.

I am further indebted to Mr. Luis Casas, Mr. Don Eckart and Dr. Robert Pfeffer, staffs of the Army Research Laboratory at Fort Monmouth, for their assistance in the material experiments and analysis of AES, XRD and RBS spectra. I extend my thanks to Professor Durga Misra and Mr. Wei Zhong for their help in the electrical measurements. I gratefully acknowledge the help I received from Mr. Vitaly Sigal, a technical staff of Material Engineering, in XRD analysis and SEM measurements.

Additional thanks go to my colleagues, Mr. Chang Kim, Dr. Byong Bahn and Dr. Jong Kim, who have provided their sharing of helpful opinions. I also wish to express my gratitude to Mr. Karl Ulatowski, Machine Shop Supervisor of Mechanical Engineering at NJIT, for his cooperation during the setup of internal construction in Triode Magnetron Sputtering System. I am especially grateful to Mr. Tony Lambiase for technical editing of the manuscript and thoughtful comments.

TABLE OF CONTENTS

TABLE OF CONTENTS
(Continued)

TABLE OF CONTENTS
(Continued)

LISTS OF TABLE

LISTS OF FIGURE

Figure **Page**

LISTS OF FIGURE
(Continued)

Figure **Page**

LISTS OF FIGURE
(Continued)

Figure **Page**

LISTS OF FIGURE
(Continued)

Figure **Page**

LISTS OF FIGURE
(Continued)

Figure **Page**

CHAPTER 1

INTRODUCTION

The ferroelectric elements in integrated semiconductor devices can be utilized in a variety of ways based on the piezoelectric, pyroelectric, dielectric and electrooptic properties. Compound ceramic oxides, which are well known as ferroelectric materials of PT family systems, are $PbTiO_3$ (PT), $Pb[Zr,Ti]O_3$ (PZT), $[Pb,La]TiO_3$ (PLT) and $[Pb,La][Zr,Ti]O_3$ (PLZT). Particularly, PLT films through a proper choice of lanthanum (La) content can be used for various device applications, including piezoelectric sensors, dielectric devices and electrooptic storage cells [1,2].

Ferroelectric thin films of PT systems with a high dielectric constant and low leakage current density have received dramatic attention for the development of memory devices [3]. Ferroelectric films, in the non-volatile random access memory (NVRAM) application, use a large value of the remanent polarization in the hysteresis property of the polarization versus electric field. In the dynamic random access memory (DRAM) application, the high dielectric constant of ferroelectric materials can be exploited by using a thin film capacitor as the charge storage element. On the La modified $PbTiO_3$ solid solution system (Pb-La-Ti-O system), PLT films with controllable composition and good crystallinity are highly desirable due to the relevant dependence of the memory devices. As the La content in the equilibrium phase diagram of the PLT system reaches 28 mol %, the ferroelectric tetragonal structure of PLT thin films is suddenly transformed into a paraelectric cubic phase. Paraelectric (non-ferroelectric) PLT films which offer good dielectric properties and extremely low leakage current density are, therefore, an excellent candidate for ULSI DRAM applications.

Several deposition methods have been used to synthesize ferroelectric ceramic thin films, including magnetron sputtering [4,5,6], ion beam sputtering [7,8], MOCVD [9],

metalorganic decomposition (MOD)[10,11], sol-gel solution method [12,13], and excimer laser ablation [14,15], etc.. Magnetron sputtering (dc or rf) of various deposition techniques is the most popular growth processing for ceramic oxide materials, because the desired composition of ferroelectric films is obtained easily from the compound target or a multi-element metal target. Paraelectric PLT (28) thin films in our experiments are prepared by reactive magnetron sputtering deposition using a multi-component metal target. The deposited films experience the various conditions of post-deposition annealing for the desired perovskite structure and good crystallinity.

The present work is organized into five parts. The first part describes the background and theory of ceramic oxide PLT material including the ferroelectric and paraelectric (non- ferroelectric) structures. The second part introduces the operation and advantages of a triode magnetron sputtering system, and explains the design and structure of a magnetron sputtering system and its calibration tests. The third part presents the preparation and experimental procedure of paraelectric PLT thin films. The PLT thin films are deposited on Pt/Ti/SiO_2/Si or Pt/MgO substrate by reactive magnetron sputtering using a multi-component metal target. The fabrication of ternary ceramic PLT thin films includes several conditions of post-annealing treatment for the desired perovskite phase with a high dielectric constant. The fourth part chiefly describes the material properties of PLT thin films. Paraelectric PLT (28) thin films are characterized for stoichiometric composition and cross-sectional profile by Rutherford back-scattering (RBS) and Auger electron spectroscopy (AES). They are analyzed for surface morphology by scanning electron microscopy (SEM), and evaluated for phase contents and crystallinity by X-Ray diffractometry (XRD). The fifth part introduces the electrical properties of these films which are analyzed by I-V plot, P-E measurement, V-t characteristics and dielectric measurements.

CHAPTER 2

BACKGROUND OF PLT MATERIALS

2.1 Ferroelectric State

Since Busch and Scherrer in Switzerland discovered the ferroelectric properties in 1935 [16], there has been increasing interest in ferroelectric ceramic oxides such as PT systems (namely, PT, PZT, PLT and PLZT). Ferroelectrics are a subgroup of the pyroelectric materials, which are a subgroup of the piezoelectric materials. Ferroelectrics, therefore, possess fundamentally both pyroelectric and piezoelectric properties, in addition to their unique ferroelectric properties. Ferroelectric materials usually show hysteresis effects in the relationship between dielectric displacement (or polarization) and electric field. A ferroelectric oxide is characterized by a net spontaneous polarization (or electric dipole moment) which can be switched or reoriented by the applied electric field. The spontaneous polarization (P_S) has its origin in the noncentrosymmetric arrangement of the B-site ions (i.e., Ti) in the unit cell [17].

In ferroelectric materials, there are regions of aligned electric dipoles, called domains, to produce the spontaneous polarization. The domains grow parallel to the field as an electric field is applied, and the polarization is increased as shown in Figure 2.1. The macroscopic polarization with an external field applied is composed of the aligned spontaneous polarization as well as electronic and ionic polarization generated by the external field. A maximum alignment of the spontaneous polarization occurs and the hysteresis curve saturates at maximum polarization (P_m) because additional electronic and ionic polarization produced by an increase in the field is quite small compared to the spontaneous polarization. The ionic and electronic polarization decrease to zero when the electric field is removed. The remanent polarization (P_r) is the spontaneous polarization that remains aligned with the previously applied field. In the hysteresis characteristic, the

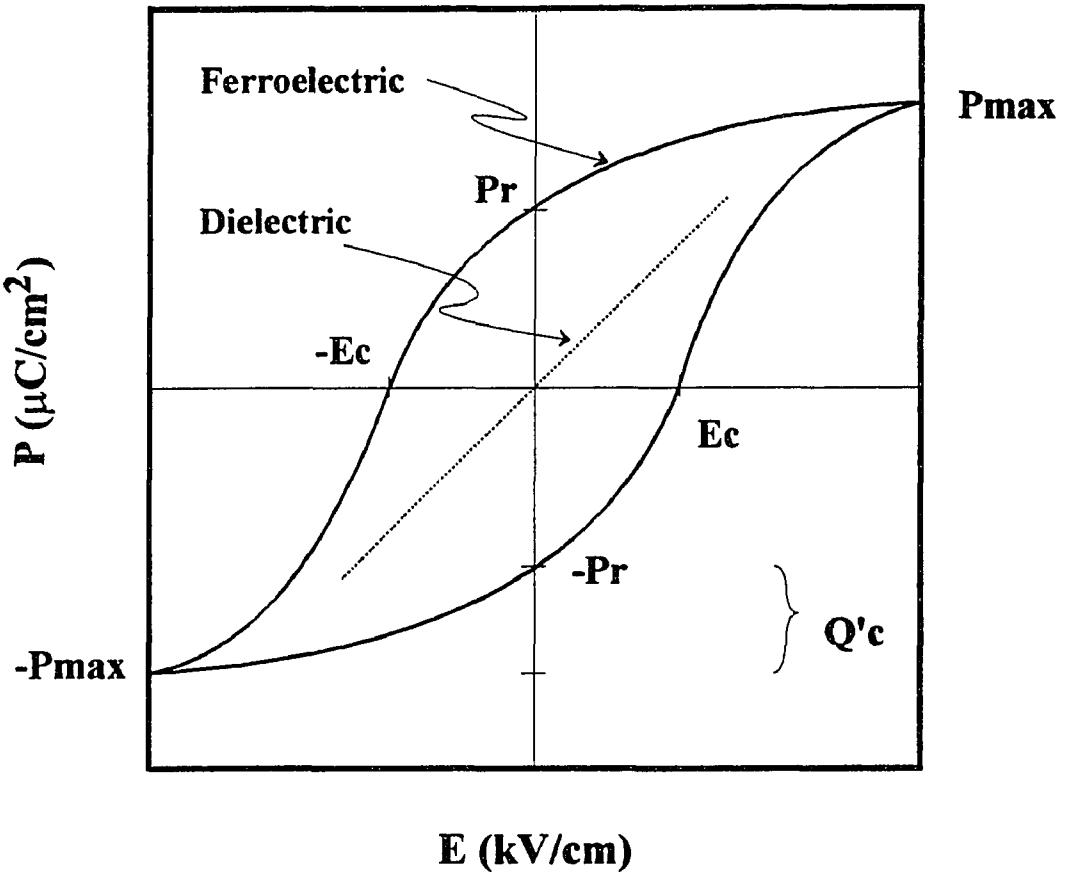

Figure 2.1 Typical polarization-electric field (P-E) characteristics for a ferroelectric and a dielectric.

magnitude of the reverse electric field, which decreases the net polarization to zero, is called the coercive field E_C. At this point the net polarization reverses polarity if the reverse applied field is increased further.

Ferroelectric PLT materials have a number of properties which make them useful in a variety of application [18,19,20], for example,

(1) high piezoelectric constant

(2) high dielectric constant

(3) relatively low dissipation factor

(4) high electrical resistivity

(5) fairly high pyroelectric coefficient

(6) high optical transparency

(7) high electrooptic coefficient

Although all these properties do not simultaneously combine to produce an optimum effect in any application, a number of desirable properties can be achieved by adjustable control of the La content in PLT thin films.

The perovskite structure in the ferroelectric phase of PLT oxide material assumes one of three structural formations: tetragonal, orthorhomic, or rhombohedral. The PLT solid solution system is a series of compositions modified by the solubility of substantial amounts of lanthanum oxide (La_2O_3) in the crystalline lattice of lead titanate ($PbTiO_3$). PLT material possesses the perovskite crystal structure described by the general chemical formula ABO_3 [19] as shown in Figure 2.2. The A element (Pb and La) is a large cation situated at the corners of the unit cell and the B element (Ti) is a smaller cation located at the body center. The oxygen atoms are positioned at the face centers. The chemical formula of the PLT system [21,22] can be generally expressed in two forms depending on the type of vacancies:

(A) $\mathbf{Pb_{1-x}La_xTi_{1-x/4}O_3}$

(B) $\mathbf{Pb_{1-\alpha x}La_xTiO_3}$

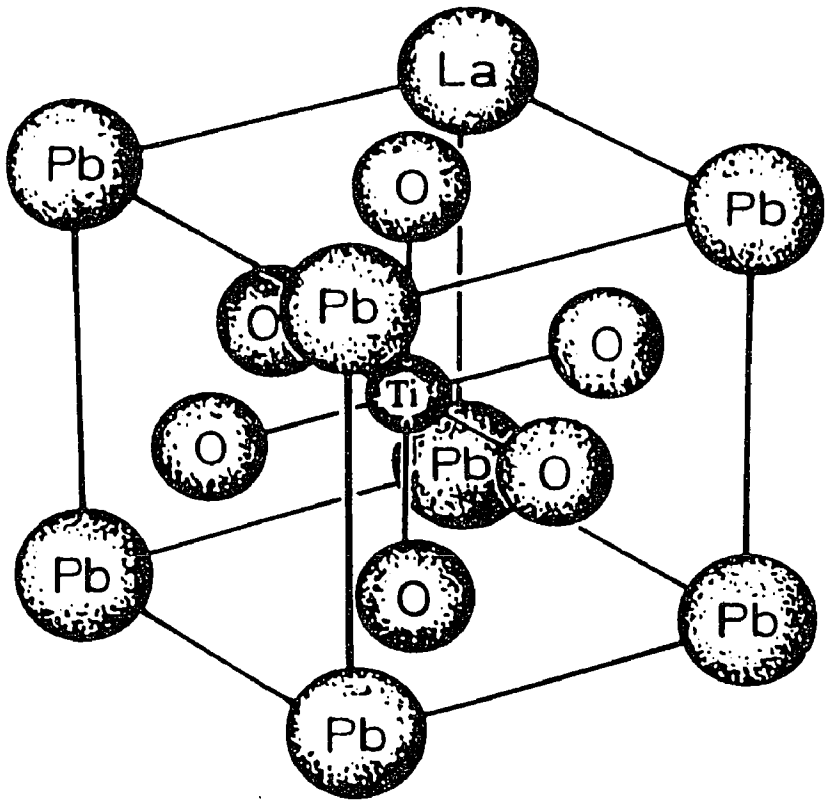

Figure 2.2 Unit cell of Pb-La-Ti-O system as a perovskite ABO_3 crystal structure

where α is called the vacancy distribution factor (or lead elimination factor) in the range $0.75 < \alpha < 1.5$, and essentially depends upon the partial pressure of the PbO, the amount of lanthanum (La), substrate temperature, and the partial pressure of oxygen [23]. In these formula, La ions replace Pb ions in the A-site of the perovskite ABO_3 ionic structure. Since La^{3+} (added as La_2O_3) substitutes for Pb^{2+}, electrical neutrality is maintained by the creation of lattice site vacancies. The actual location of these vacancies in either the A^{2+} sites or B^{4+} sites of the unit cell has not yet been completely reported despite numerous studies on the subject [19–23]. It is most probable that vacancies exist in both A- and B-site [21]. If both A- and B-site vacancies are present in the lattice, it is expected that the above formulation would provide excess Pb^{2+} ions which are expelled from the lattice (PbO vapor) during the annealing process. In fact, this excess PbO contributes to achieving full dense material by eliminating residual porosity before it becomes entrapped within the grains. Lead titanate ($PbTiO_3$) is a tetragonal ferroelectric perovskite material with the Curie temperature (T_C) of 490 °C, and its tetragonality, c/a, is 1.06 at room temperature. The addition of La to the bulk ferroelectric $PbTiO_3$ causes a unit cell contraction [24]. The c/a ratio and Tc decrease monotonically with increasing La concentration. Therefore, the effect of adding La of the PT system is to reduce the stability of the ferroelectric phases (reducing the Curie temperature) in favor of the paraelectric (non-ferroelectric) cubic phase.

The composition-structure relationship in the equilibrium phase diagram for the PLT system [23,25] at 1330 °C is given in Figure 2.3. Since the phase diagram in the Figure is applied only to films that form during deposition, it can not be directly formalized in PLT thin film using post-annealing treatment. Fox et al [26] discussed in detail that PLT films heat-treated by post-deposition annealing were evolved from the interdependent relationship between stoichiometric composition and crystallographic structure. A post-deposition annealing process is required for films deposited in the amorphous or partially amorphous state. The annealing parameters, that is, temperature, time and oxygen partial

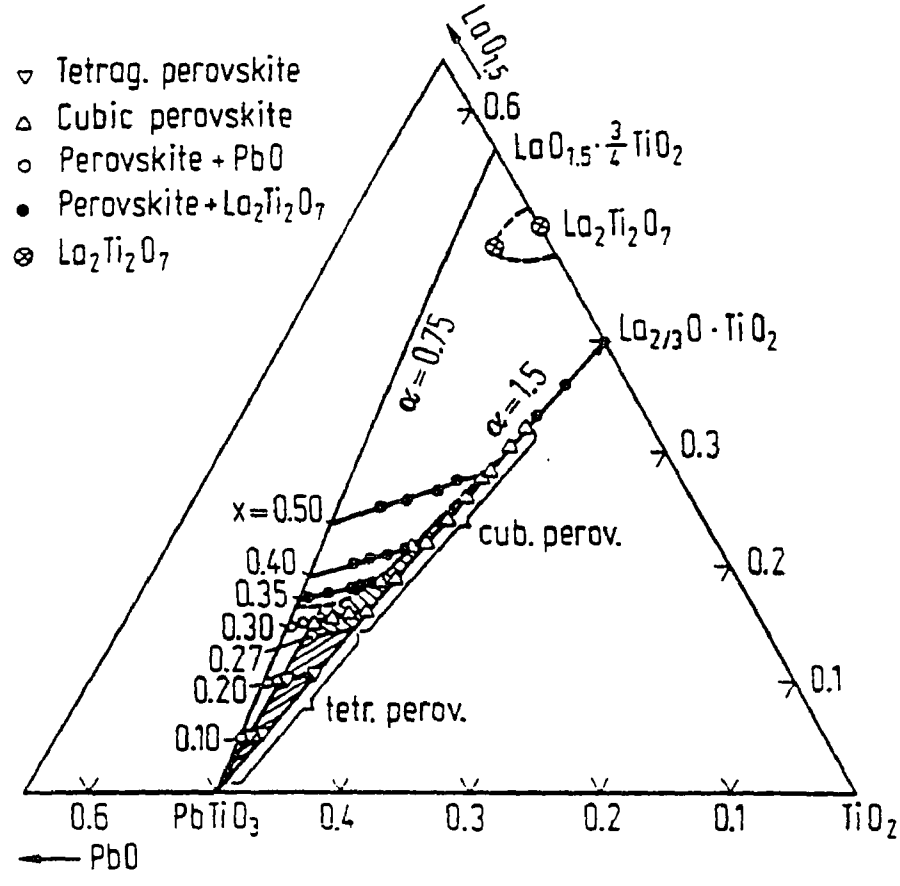

Figure 2.3 Equilibrium phase diagram for the PLT system at 1330 °C

pressure, have prominent influences upon crystallization and perovskite phase formation in PLT films [3]. Surface microstructures of the deposited thin film have commonly been introduced by the structure zone model (SZM) [27], as shown in Figure 2.4. Microstructures and morphologies of the thin film are classified by the deposition temperature and argon operating pressure. There are three microstructure zones in the SZM. Zone I ($T/T_m < 0.25 - 0.3$) is a porous structure consisting of tapered crystallites separated by voids. Zone II ($0.25 - 0.3 < T/T_m < 0.45$) has columns with relatively smooth surfaces. Zone III ($T/T_m > 0.45$) shows the recrystallized grain structure. The transition zone (subzone T) at the border between zone I and zone II exhibits a tightly packed fibrous structure. The post-annealed films are different from the microstructure of as-deposited films because of thermally induced surface and bulk diffusion. It is supposed that the final microstructure of PLT thin films using the post-deposition annealing is exhibited by a superposition of various zone structures in the SZM model due to the interdependent processes of crystallization and composition change caused by lead volatility.

2.2 Paraelectric State

There are two ways to perceive the paraelectric state in the Pb-La-Ti-O system. First, as the molar La content in the composition formula of the PLT system is equal to and higher than 0.28, the paraelectric phase with cubic perovskite structure appears in the PLT phase diagram as given in Figure 2.3. It is noted that its tetragonality (c/a) is unity and the Curie temperature is –25 °C [28]. Second, the ferroelectric behavior of PLT thin films disappears at a specific transition temperature with increasing temperature. The spontaneous polarization in ferroelectric film is a function of temperature. However, at high temperature, thermal energy destroys the domain structure of ferroelectricity. The specific temperature at which the spontaneous polarization disappears is called the ferroelectric Curie temperature. Above the Curie point (T_C), PLT material is suddenly

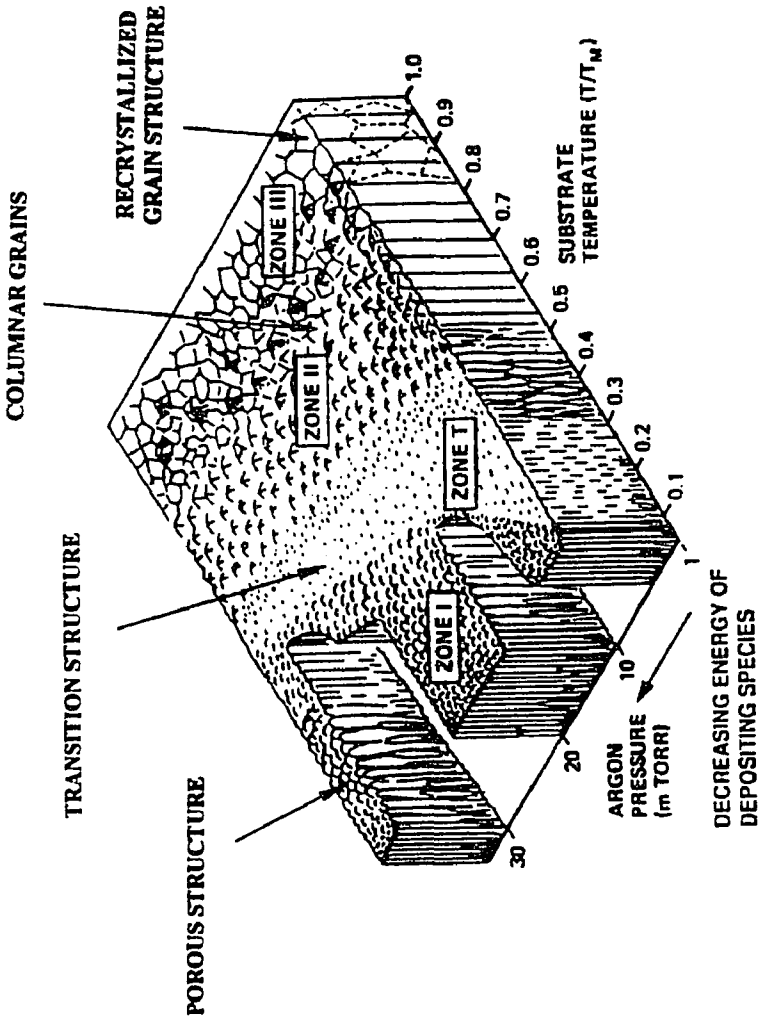

Figure 2.4 Thin film structure zone model (SZM) defined by T/T_m and the energy of depositing species

changed from ferroelectric (or noncentrosymmetric) tetragonal phase to paraelectric (or centrosymmetric) cubic state in the perovskite structure. As shown in Figure 2.5 (a), the ferroelectric state (i.e., spontaneous polarization) exists at a temperature below T_C, and also the spontaneous polarization equals zero above T_C.

The dielectric constant is not only a function of the electric field, but also a function of temperature. Figure 2.5 (b) shows the dielectric constant as a function of temperature. In the ferroelectric phase, the dielectric constant increases gradually as the temperature increases, and it becomes anomalously large at the Curie temperature. Above T_C, the dielectric constant can be frequently described by Curie-Weiss behavior:

$$\frac{1}{\varepsilon} = \frac{T - T_C}{C}$$

where, C is the Curie constant and

T_C is Curie temperature.

The dielectric constant, as a function of temperature, in the paraelectric phase of the PLT films can not be completely represented by the simple formula of Curie-Weiss behavior. Keizer et al [29] have developed models to interpret the anomalous dielectric characteristics. The dependence of the dielectric constant on temperature for the paraelectric phase of PLT (28) thin films can be modified by the power series of the temperature as the following:

$$\frac{1}{\varepsilon} - \frac{1}{\varepsilon_{max}} = C_1 - C_2(T - T_{max}) - C_3(T - T_{max})^2$$

where, C_1, C_2 and C_3 are constants, depending on the stoichiometric composition.

Dey and Lee [30] discussed that the ferroelectric thin films with hysteresis effect exhibited a number of disadvantages for semiconductor memory applications. The time-

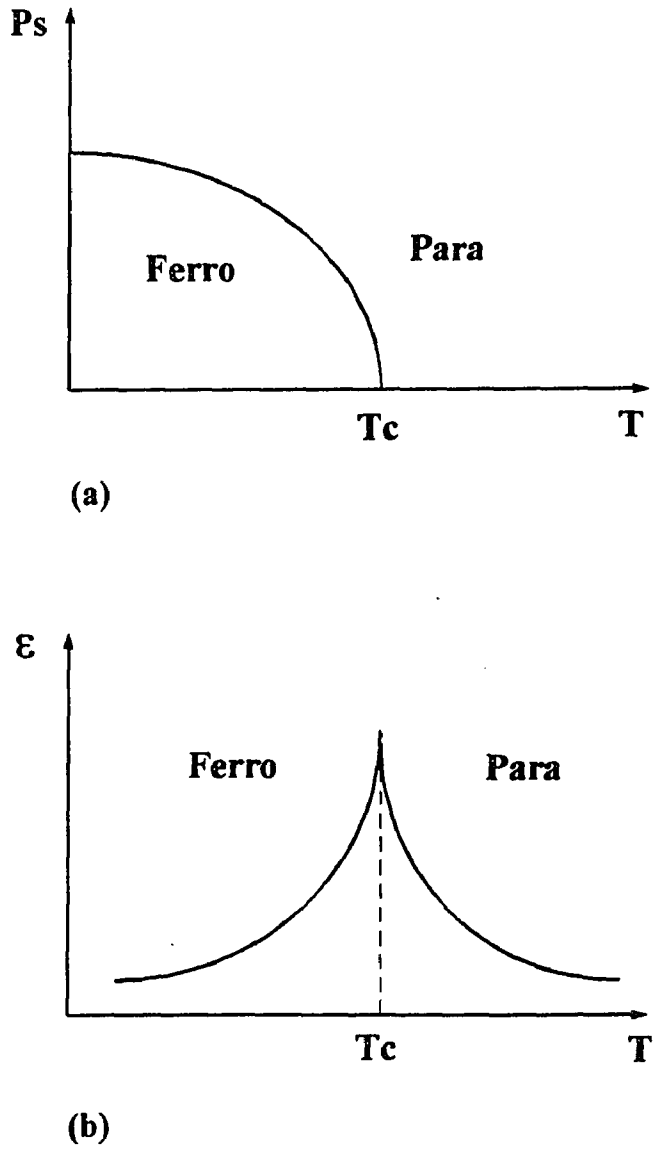

Figure 2.5 The dependence of (a) spontaneous polarization and (b) relative dielectric constant on temperature (near Curie temperature).

dependent polarization reversal processes in the saturation arm between P_r and P_m of a hysteresis loop are relatively slow. This processes, in terms of domain reorientation and phase switching, produce a potential fatigue (time-dependent degradation in charge storage density) and severely limit the charging and discharging speeds of the capacitors. Therefore, nonswitching cubic paraelectric films with high dielectric constant should offer outstanding advantages over switching ferroelectrics.

Figure 2.6 shows polarization versus electric field (or called P-E) characteristics for normal dielectric, paraelectric, and ferroelectric thin films. The typical P-E characteristic of a ferroelectric film exhibits the hysteresis loop with the positive and negative remanent polarization values. Conversely, paraelectric PLT film behaves like a normal dielectric material at a low electric field, and has no remanent polarization in the absence of an electric field. At a high electric field, the nonlinear behavior is demonstrated in paraelectric films. The dielectric and electrooptic effects of ternary ceramic PLT thin films are greatly affected by the La content, and they reach maximum effect near the phase boundary (x = 0.28) between the ferroelectric tetragonal and the paraelectric cubic structure [22].

2.3 Potentials of PLT Material for DRAM Capacitor

With the successful development of dynamic random access memory (DRAM) technology, the reduction in cell size has required reducing the area of the planar storage capacitor. It is, therefore, necessary to increase the charge storage density on the capacitor to maintain adequate operation. The required increase in charge storage density has been achieved through improvements in processing technology, reduction of the dielectric thickness, and innovations in the cell design [31]. However, the thin dielectric materials such as conventional dielectrics as well as Ta_2O_5 and Si_3N_4/SiO_2 do not appear to be sufficient for ultra large scale integration (ULSI) DRAMs. As a result, a new

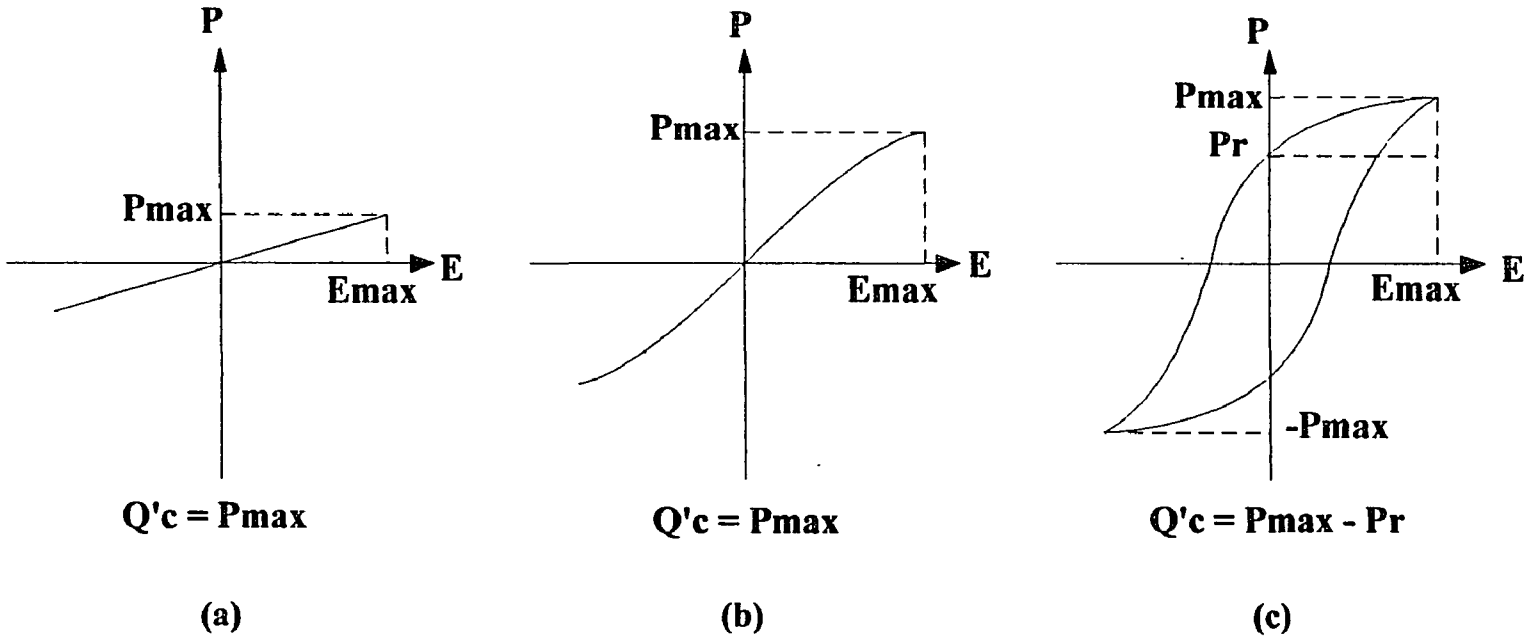

Figure 2.6 Polarization-electric field (P-E) plots of (a) linear capacitor for dielectric, (b) nonlinear capacitor for paraelectric, and (c) hysteresis loop for ferroelectric.

dielectric material that permits a capacitor with higher charge storage per unit area and is compatible with ULSI processing is required for use in ULSI DRAMs.

Ferroelectric materials as an alternative dielectric with a higher dielectric constant have been widely considered by a large of number of researchers [31,32]. There are numerous important requirements that have to be satisfied by the dielectric material for future generations of DRAMs and they are as follows:

(1) high charge storage capacity per unit area,

(2) low leakage current density,

(3) low defect density,

(4) high reliability,

(5) compatibility with silicon integrated circuit processing technology, and

(6) stability with the two capacitor electrodes.

Table 2.1 shows key parameters required for the electrical properties of recent ULSI DRAMs.

Table 2.1 Key parameters required for the electrical properties of 64 and 256 Mb DRAMs.

Parameter	64 Mb	256 Mb	Comment
Memory cell area (μm^2)	0.7-1.0	0.25-0.34	—
Storage capacitor area (μm^2)	2-6 0.2-0.5	0.7-2 0.07-0.17	Trench Planar
Storage charge density ($\mu C/cm^2$)	1-5 10-50	2-11 20-115	Trench Planar
Leakage current density ($\mu A/cm^2$)	2-25 20-250	3-35 30-360	Trench Planar
Dielectric thickness (nm)	10-200	10-200	—

A DRAM memory circuit uses charge storage on a capacitor to represent binary data values. The most common DRAM memory cells are based on the one-transistor (1-T) design to reduce the size of DRAM. This has the advantages of a small memory cell area made possible by the use of only one transistor and one storage capacitor in the circuit design. The 1-T cell is also comparatively easy to fabricate, operates at less power, and is more reliable than other designs using multiple transistors. Figure 2.7 (a) shows a typical memory cell with a single transistor and capacitor for charge storage. The 1-T cell of the basic DRAM technology was invented by Dennard [33]. Its concept is that the "0" and "1" binary information is stored on the capacitor by charging or discharging the capacitor through the transistor. The transistor connected to the word line isolates the storage capacitor from the bit line, and as soon as the transistor is turned on, the capacitor is connected to the bit line so that information is written and read. A cross-sectional structure of 1-T DRAM cell [34,35] with a paraelectric capacitor is shown in Figure 2.7 (b). Similar to the conventional 1-T memory cell, the single transistor as a pass transistor provides a path to the capacitor. During operation, a positive or zero voltage is on the bit line for the "1" or "0" state, respectively. However, the critical factor in the design of a 1-T DRAM cell is the charge storage density which fundamentally determines the effectiveness of the memory cell to maintain the distinction between "0" state and "1" state.

Recent researchers [36,37] suggest that the improvement in the relative dielectric constant using a thin insulating material such as tantalum pentaoxide (Ta_2O_5; $\varepsilon_r \sim 20$-25) and yttrium oxide (Y_2O_3; $\varepsilon_r \sim 12$-16) is 3 to 6 times over that of SiO_2, while the net gain in charge storage density is only a factor of two at best. This is due to higher leakage current and lower dielectric breakdown strength. The requirement for high charge storage capacity per unit area is focused on dielectric material with an extremely high dielectric constant. The ability of the dielectric constant with the use of new dielectrics can

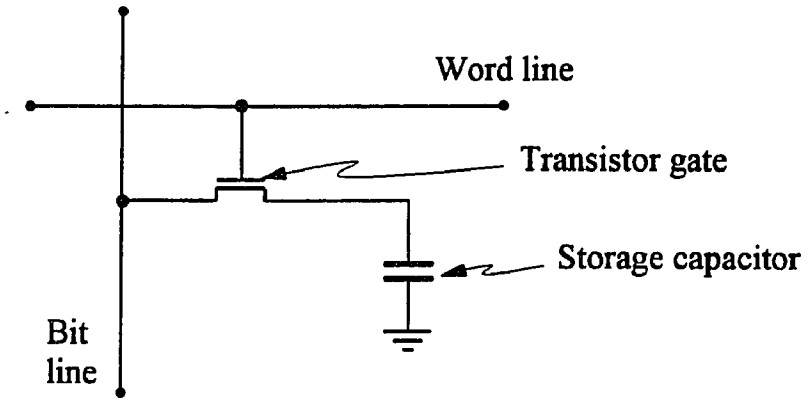

(a)

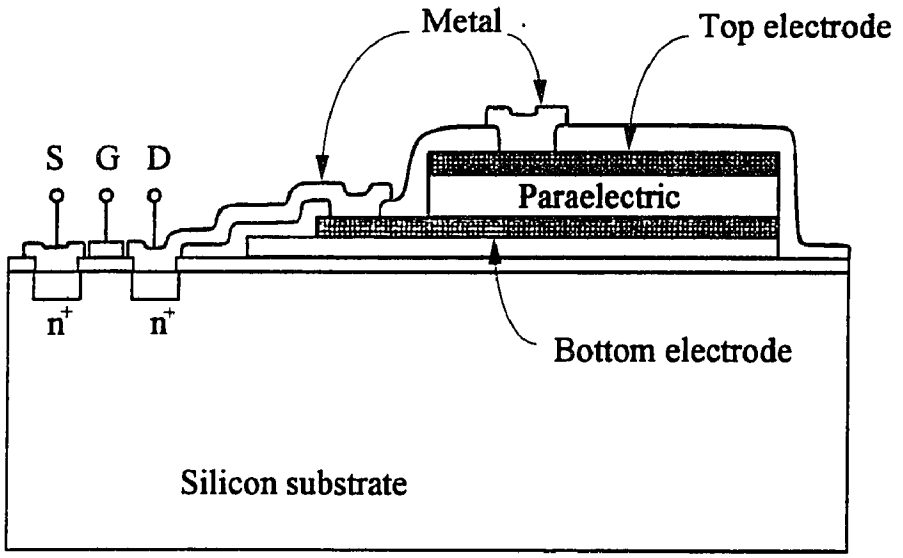

(b)

Figure 2.7 (a) Circuit elements of one-transistor (1-T) DRAM cell, and (b) Cross-sectional structure of 1-T cell involving paraelectric capacitor.

withstand a sufficiently large electric field, because the charge storage capacity is proportional to the dielectric constant and the applied electric field.

In recent reports for DRAM operation [38], a PZT film of 400 nm thick is equivalent to a 1.6 nm SiO_2 film subjected to a 2.5 V voltage (5.5 $\mu C/cm^2$). The 200 nm film has a polarization of 9 $\mu C/cm^2$ equivalent to a 1.0 nm SiO_2 film with a 2.5 V voltage. Paraelectric PLT (28) films of 500 nm thick have a polarization of 5.7 $\mu C/cm^2$ with a 2 V voltage. The largest charge storage capacities reported for ONO (oxide/nitride/oxide) and Ta_2O_5 dielectrics correspond to a 2.5 nm SiO_2 film. The film thickness of the dielectric has been reduced to less than 10 nm in order to retain a sufficient charge storage in current DRAM technologies. A further reduction in thickness may have a deleterious impact such as a direct tunneling through thin dielectric films and has reached the fundamental limit in processing technology.

Another important capacitor dielectric requirement for any potential DRAM is low leakage current density. High leakage current has limitation in the operation since the cells require more frequent refreshing, use more power, and limit the maximum field that may be applied across the device. Figure 2.8 shows the leakage current density as a function of the electric field for the various dielectric materials [39,40]. The PZT and PLT films exhibit superior leakage characteristics compared to other dielectric films at high fields.

Charge storage density, in ferroelectric thin film, corresponds to the difference between the maximum polarization and the remanent polarization in hysteresis loop. The ferroelectric PZT films for DRAM operation present some disadvantages such as time dependent polarization reversal processes in the saturation of the hysteresis loop. These processes not only cause a potential fatigue (time-dependent degradation of Q_C) problem but can also increase loss tangent and seriously limit the switching speed of the capacitors. The hysteresis property is not actually desirable in DRAM application, and the capacitor operates only as a linear capacitor. Therefore, paraelectric cubic PLT films with extremely

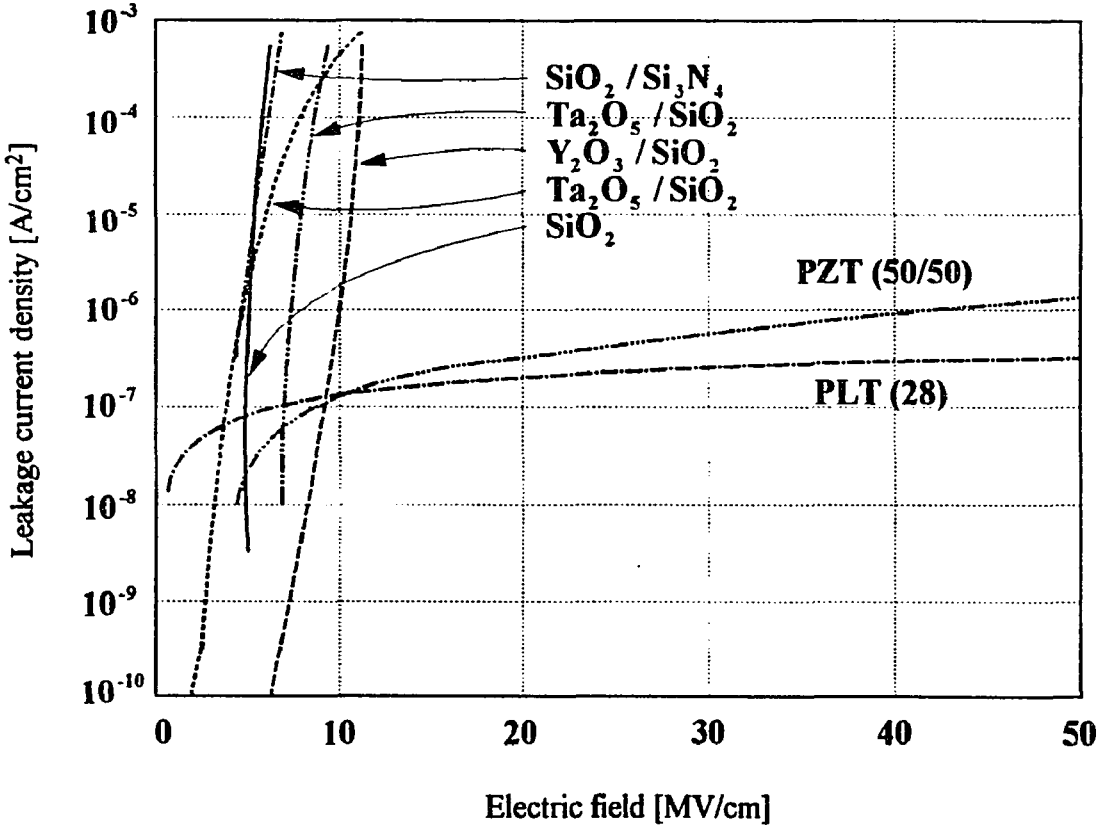

Figure 2.8 Comparison of leakage current density of PLT thin film with other dielectric materials. PLT film shows superior characteristic to other DRAM dielectric

high dielectric constant and normal dielectric characteristics should offer significant advantages over ferroelectric films.

Charge storage densities, leakage current densities, and dielectric thickness in recent ULSI DRAM technologies with planar capacitor are basically required to be in the range of 20–115 $\mu C/cm^2$, 30–36 $\mu A/cm^2$, and 0.01–0.2 μm, respectively [41]. Paraelectric PLT thin films are a potentially attractive candidate for the storage dielectric capacitor in future DRAMs. Nonswitching cubic paraelectric PLT thin films with a linear dielectric characteristic offer significant advantages over conventional dielectrics and are also preferable to nonlinear switching ferroelectric thin films for the operation of ULSI DRAMs.

2.4 Objectives of Research

Ferroelectric thin films have been developed in semiconductor memories that are optimized for a variety of applications. These are static random access memories (SRAMs) that are required for high speed applications; dynamic RAMs (DRAMs) that are designed for computer storage; and nonvolatile RAMs (NVRAMs) that are used for read-only-memory. The important characteristics of ferroelectric materials are specified by special properties for all types of memory devices of the memory application as follows. Nonvolatile ferroelectric memories utilize a ferroelectric thin film capacitor as a nonvolatile storage element and make use of the hysteresis property of polarization versus voltage characteristics. The high dielectric constant of ferroelectric materials can be exploited by a thin film capacitor as the storage element in DRAM devices. Here, the hysteresis property of ferroelectric is not desirable, and the capacitor operates similar to a linear capacitor of normal dielectric for charge storage. Consequently, the paraelectric PLT (28) thin films with excellent dielectric properties are expected to offer significant advantages for ULSI DRAM technology.

Many researchers have used various deposition techniques for preparation of ferroelectric oxide thin films. Adachi et al [42] succeeded in the epitaxial PLZT thin films on sapphire and MgO substrates by rf magnetron sputtering method from an oxide powder target. Schwartz et al [43] prepared ferroelectric PLT thin films by the sol-gel solution method. Watanabe et al [44] fabricated amorphous PLT (15) thin films by metal organic chemical vapor deposition (MOCVD) at low temperature. Quin et al [45] and Fox et al [46] also made ferroelectric PLT thin films by a multi-ion-beam reactive co-sputtering technique. The common interests in preparing PLT thin films of high quality by different deposition methods include stoichiometry control, suitable microstructure, uniformity, reproducibility, and process compatibility with semiconductor technology.

To date, preparation of PLT thin films with correct composition is so difficult that their electrical properties for memory device technologies have not been investigated sufficiently. Thus, this study begins with a development of high dielectric properties in ferroelectric oxide materials for ULSI DRAM application. The first purpose of the present research work is to prepare paraelectric PLT thin films by a multi-component metal target of triode magnetron sputtering technique which is designed in our laboratory. Subsequently, a post-deposition annealing treatment for the as-deposited films is carried out to crystallize into the desired perovskite phase. The material and electrical characteristics of the films are also investigated by a variety of analytic methods. RBS and AES are used in order to achieve the desired stoichiometric composition of PLT (28) thin films. XRD is also used to determine the crystalline structure and lattice constant of PLT thin films. The surface microstructure is analyzed by SEM topography. The dielectric and electrical characteristics such as P-E, I-V and V-t measurements are investigated to illustrate the potential use of PLT (28) thin films in DRAM application.

CHAPTER 3

TRIODE MAGNETRON SPUTTERING SYSTEM

3.1 Introduction

Presently, the most important factor in the preparation of ferroelectric oxide films is the deposition method. In the ferroelectric thin film (FTF) growth processes, Krupanidhi [47] reported that the deposition techniques could be primarily specified in terms of the growth processes with and without the presence of low energy bombardment during deposition. The growth processes with low energy bombardment included, magnetron sputtering, ion beam sputtering, excimer laser ablation, electron cyclotron resonance plasma-assisted growth, and plasma-enhanced chemical vapor deposition (PECVD). The deposition techniques without bombardment included sol-gel synthesis, metalorganic decomposition (MOD), thermal and e-beam evaporation, CVD, MOCVD, and MBE. Table 3.1 summarizes the various growth techniques for recent FTF processing of PT systems [47].

Sol-gel processing in chemical solution methods and magnetron sputtering of the above mentioned methods have been reported as successful preparation techniques because of better control of the film composition. The sol-gel technique has received significant attention due to easier fabrication of a large area, excellent lateral uniformity and low cost. However, sol-gel deposition has a number of disadvantages such as the inability of exact thickness control for thin films and difficulty of small feature deposition. Due to the recent requirements for ultra large scale integration (ULSI) of ferroelectric oxide/semiconductor thin film-based devices, rf or dc magnetron sputtering of physical deposition techniques have received dramatic attention [18,47]. The multi-component target sputtering, or multiple targets sputtering, appears to be a suitable method to deposit stoichiometric thin films with controllable thickness and high growth rate.

This chapter briefly introduces the theoretical background and construction of

Table 3.1 Various deposition techniques for ferroelectric thin film based on the presence of bombardment

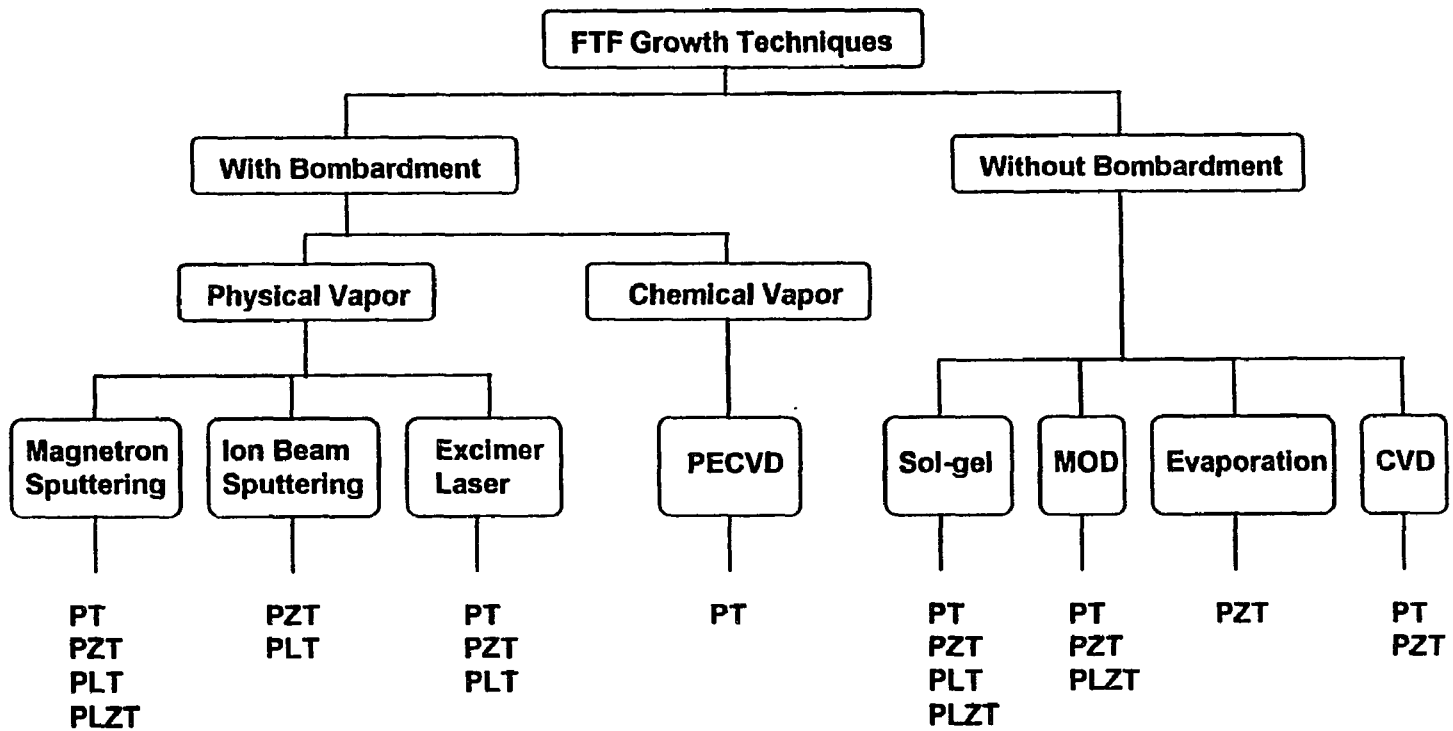

triode magnetron sputtering which was designed in our laboratory, and the basic tests for its calibration. Finally, the ternary ceramic oxide of PLT thin film with a high dielectric constant and a low leakage current is deposited reactively by our triode magnetron sputtering.

3.2 Triode Magnetron Sputtering

3.2.1 Magnetron Sputtering

Sputtering is an atom-by-atom process. Atoms are ejected from the surface of a target under ion bombardment and subsequently deposit to the substrate. Sputtering as a phenomenon was first observed to coat mirrors in the 1850s [48]. In the 1940s, sputtering was used to a significant extent as a commercial deposition process. A typical magnetron sputtering process shown in Figure 3.1 has a shaped and closed path magnetic field to trap and concentrate the electrons produced in the discharge at the target surface. The electrons are confined to above the target materials. The high density cloud of electrons promotes ionization of the sputtering gas in the region close to the target surface, and the target is negatively biased to attract ions to the target. The high energy impact of these ions on the target dislodges atoms from the material which are collected on the substrate surface. Due to the high ionization efficiency of this process, low power levels may be used, and at the same time high deposition rates are achieved. Because electron leakage is restricted by the magnetic field, bombardment of the substrate is minimized and heating of the growth film and substrate is substantially reduced.

The magnetron sputtering process has many advantages [48,49]. The primary advantages are:

(1) high deposition rate,

(2) ease of sputtering any metal, alloy, or compound,

(3) high-purity of the deposited films,

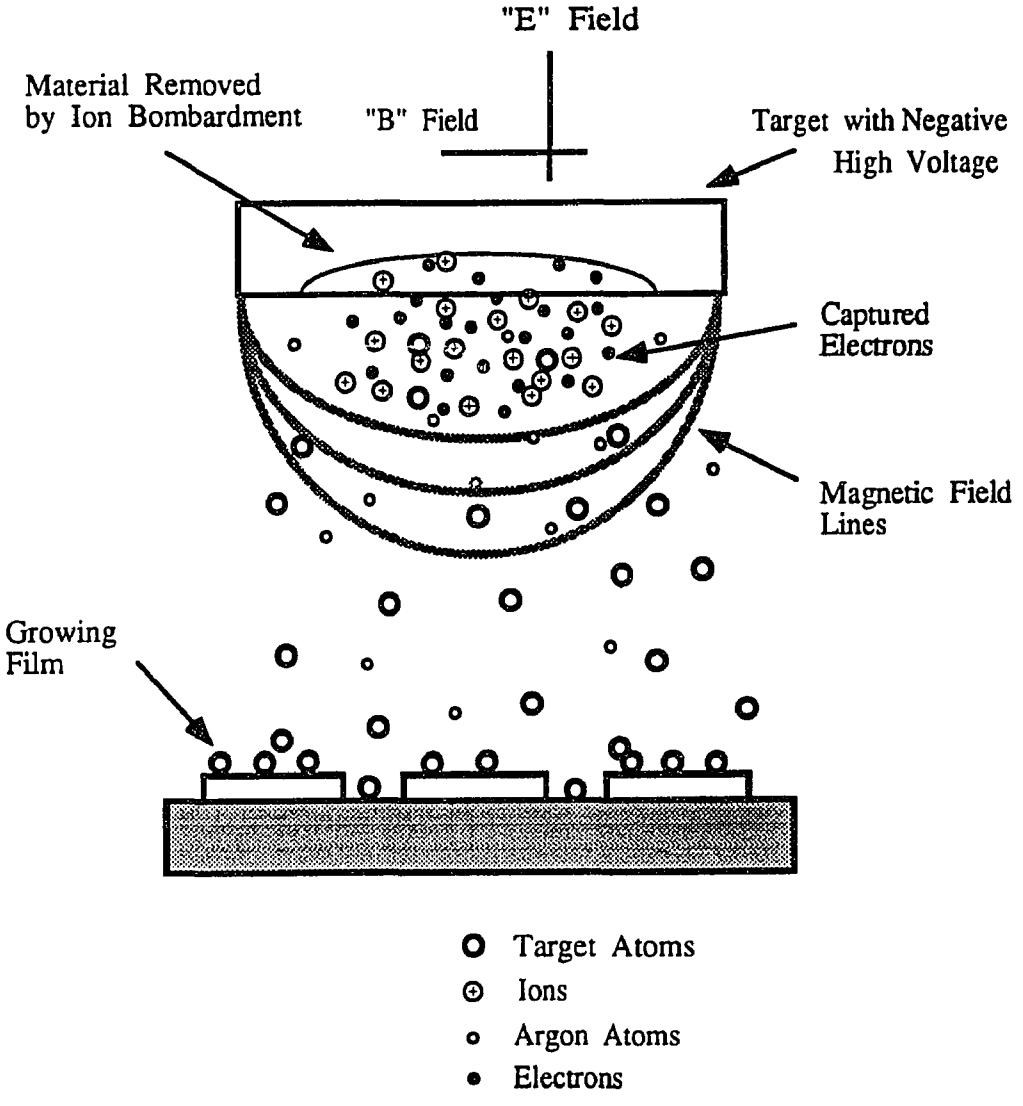

Figure 3.1 Basic operation of magnetron sputtering system

(4) extremely high adhesion of films,

(5) excellent coverage of steps and small features,

(6) ability to coat heat sensitive substrates,

(7) ease of automation, and

(8) excellent uniformity on large area substrates.

Magnetron sputtering, because of the above advantages, is a very powerful technique which can be used in a wide range of applications.

The advantages of a triode technique in a triode magnetron sputtering are that a very high ion density is produced, the processing pressure is relatively low and the plasma current density for the deposition films can be controlled independently with the plasma voltage. Therefore, the deposition rate of triode magnetron sputtering is higher than that of diode magnetron sputtering. There are also some disadvantages in terms of the heated filament. First, the thermionic filament is impractical in the reactive sputtering process. Second, the filament of the refractory metal contributes to contaminate the deposited films. The filament is subject to burnout and its power dissipation adds heat to the chamber area.

3.2.2 Construction of Triode Magnetron Sputtering System

Figure 3.2 shows a frontal picture of a triode magnetron sputtering system, including the vacuum chamber, power supply, and system control console. The block diagram of the sputtering system is shown in Figure 3.3. In this section, the triode magnetron sputtering system is discussed in terms of its structure and the details of its construction. A generalized magnetron sputtering system consists of a high vacuum system, a sputtering source assembly, and a substrate holder in its basic formation. The design and characterization of a triode magnetron sputtering system will be presented.

The vacuum system used for this triode magnetron sputtering system was previously an asymmetrical reaction ion etch system, model 640, built by Plasma-Therm,

Table 3.2 Partial pressure in the sputtering chamber before introducing the argon gas

PARTIAL PRESSURE

287SEC VF 2.5X10^{-6}TORR

EMUL 1.20 KV OFF

UNIT 1
T/MA 5.0E-0

MATL/MASS	FACTOR	TORR
HYDROGEN	2.319	3.4E-8
HELIUM	7.143	1.0E-8
WATER	1.333	8.7E-7
N2 / CO	1.029	4.3E-8
OXYGEN	1.053	9.7E-9
ARGON	.947	4.6E-9
0	1.000	.0E-0 N
0	1.000	.0E-0 N
0	1.000	.0E-0 N
0	1.000	.0E-0 N
0	1.000	.0E-0 N
0	1.000	.0E-0 N

INFICON QUADREX 200

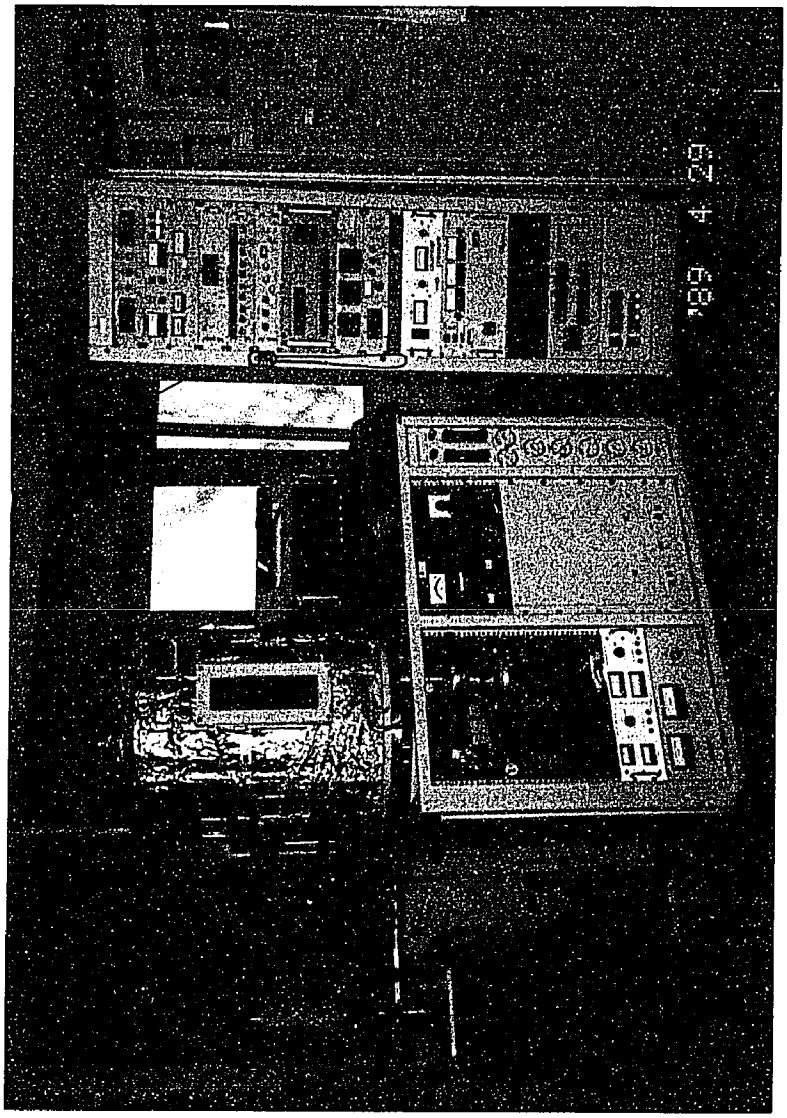

Figure 3.2 Front picture of triode magnetron sputtering

Inc [50]. The dimension of bell jar chamber is 32-inches high by 24-inches outer diameter. The vacuum system consists of a turbomolecular pump, rough and process mechanical pump. A residual gas analyzer (Leybold–Heraeus, Inficon, Quadrex 200) is attached to a flange between the base of the bell jar and the turbomolecular pump. It is used to monitor vacuum chamber performance, such as, various residual gases, and to detect vacuum leaks and contaminants. The lowest base pressure observed in the vacuum chamber has been 2.5×10^{-6} Torr. The partial pressures of residual gases in the vacuum chamber is shown in Table 3.2.

The target source assembly is a TRI–MAG, model 383, sputtering source by L.M.Simard, Inc., and TRI–MAG stands for triode and magnetron sputtering system. This sputtering source has an exceedingly high deposition rate for thin film research. In the triode system, ions are generated in low voltage (50–70 V) and high current (2–15 A) arc discharge between a thermionic filament (tantalum) and a main anode. The magnetic field design is the key factor governing the operation of the magnetron in the planar magnetron system. It is responsible for the effective trapping of the electrons and the uniform erosion of the target material. Unique characteristics of thin film deposition is given by an E×B field for plasma confinement close to the target surface. The magnetic structure under E×B field is configured to give exceptionally uniform target erosion and to permit the sputtering of insulators as well as magnetic materials. The source of the permanent magnets for the magnetron system is a ferrite, so called "ceramic 8", and its magnetic flux strength is around 250 Gauss [51]. Figure 3.4 shows the entire sputtering source assembly, including the water lines and the electrical connections, based on the above essential limitations. The power block diagram of the triode magnetron sputtering source is given in Figure 3.5. The substrate holder is located above the sputtering source assembly so that the deposited thin films have a high purity due to the sputtering-up position. The substrate holder is made of a 4 inch diameter copper disk.

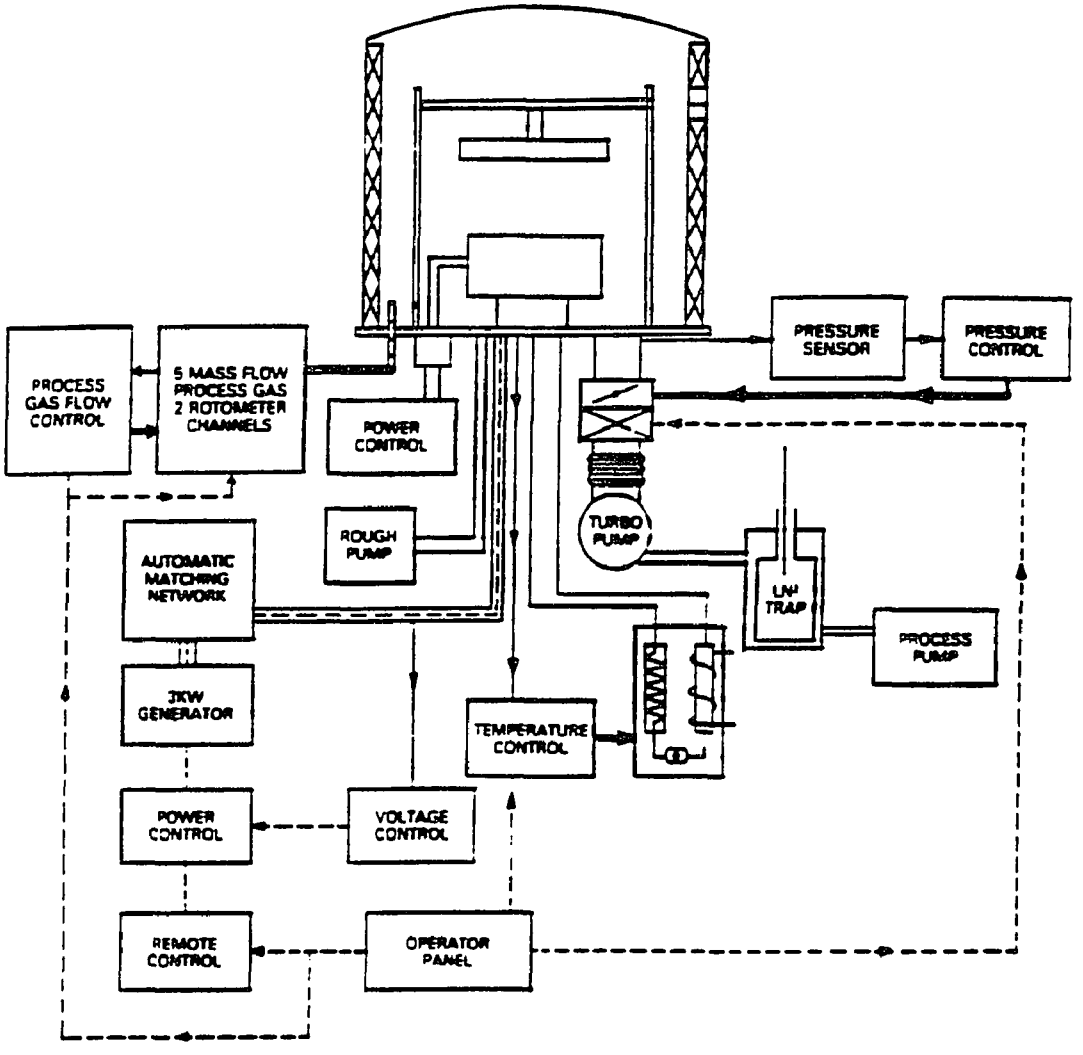

Figure 3.3 Block diagram of triode magnetron sputtering

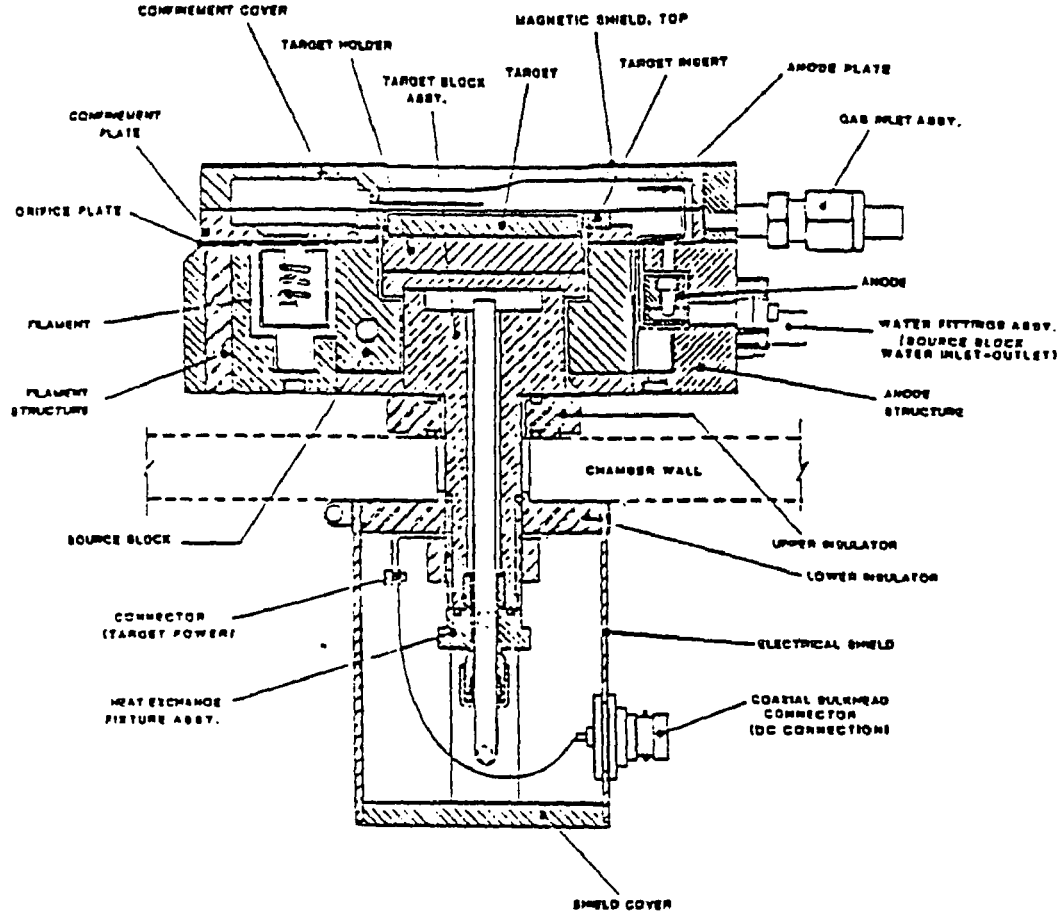

Figure 3.4 Entire sputtering source assembly

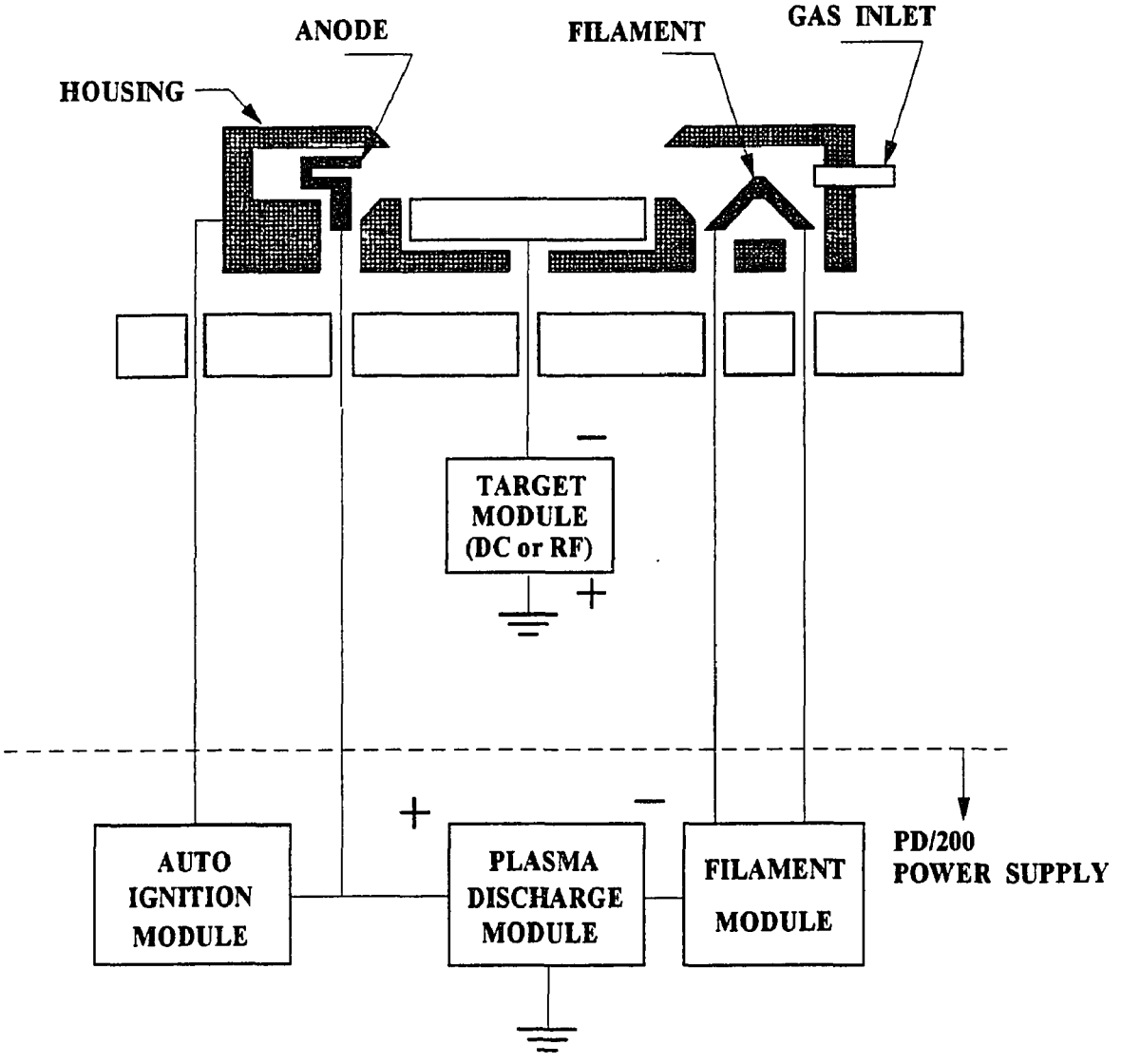

Figure 3.5 Power block diagram of triode magnetron sputtering source.

3.3 Calibrating Tests of Triode Magnetron Sputtering

In order to calibrate the rf triode magnetron sputtering system for thin film deposition processes, the effects of different glow discharge conditions were investigated in terms of the deposition rate measurements. The basic parameters for calibrating experiment in our rf triode magnetron sputtering were rf power input, gas pressure, plasma current, and target to substrate distance. Because a knowledge of the deposition rate is necessary to control film thickness and to evaluate optimal conditions which are an important consideration in preparing better thin films, the deposition rates of copper as a testing material under the various sputtering conditions were investigated.

3.3.1 RF Power Effect

The deposition rates dependent on the rf power are shown in Figure 3.6, and the deposition rates increase linearly with increasing rf power input. The sputtering conditions were: 70 mm distance between target and substrate, 20 mTorr argon gas pressure, 5 A plasma current, and 60 minutes deposition time. In this Figure, the curve "a" shows the deposition rate of a sample in the center location "1" on the substrate holder. The curve "b" demonstrates the average value of deposition rates at four positions "2", "3", "4", and "5" whose distance from the substrate center is 25 mm, respectively. Each deposition rate on location "2", "3", "4", and "5" was with maximum 5 % range of the average value on the curve "b". The temperatures of the substrate holder caused by ion bombardments of sputtered atoms and thermionic filament in a triode system also increase with increasing rf power. It is expected that the linear increasing curve of substrate temperatures occurs mainly by ion bombardment with increasing rf power, because the plasma current causing the thermionic filament is a fixed parameter during the growing processes.

3.3.2 Target to Substrate Distance Effect

Figure 3.7 shows the effect of distance between the target and substrate in the deposition

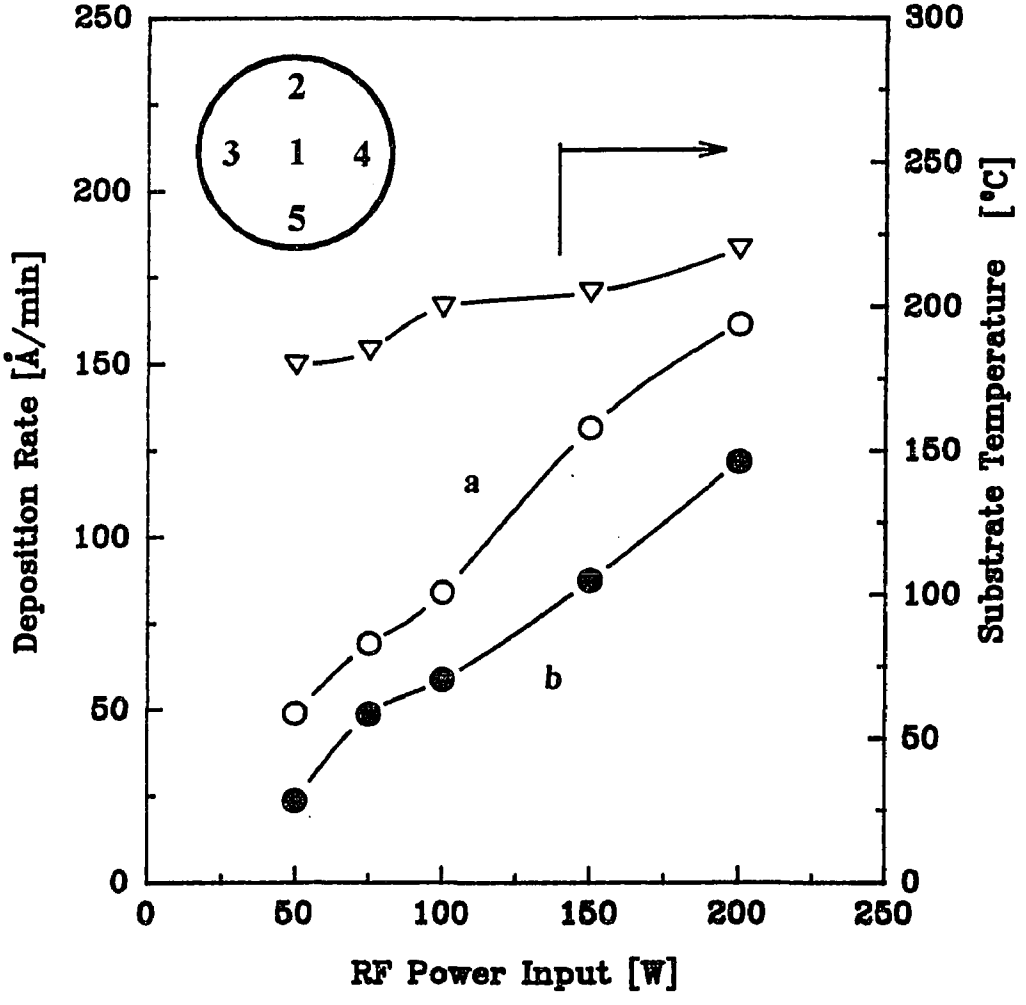

Figure 3.6 Deposition rate dependent on rf power input (a) deposition rate of the center "1" on the substrate holder, and (b) average of deposition rate of at four positions "2", "3", "4" and "5" with distance of 25 mm from the center

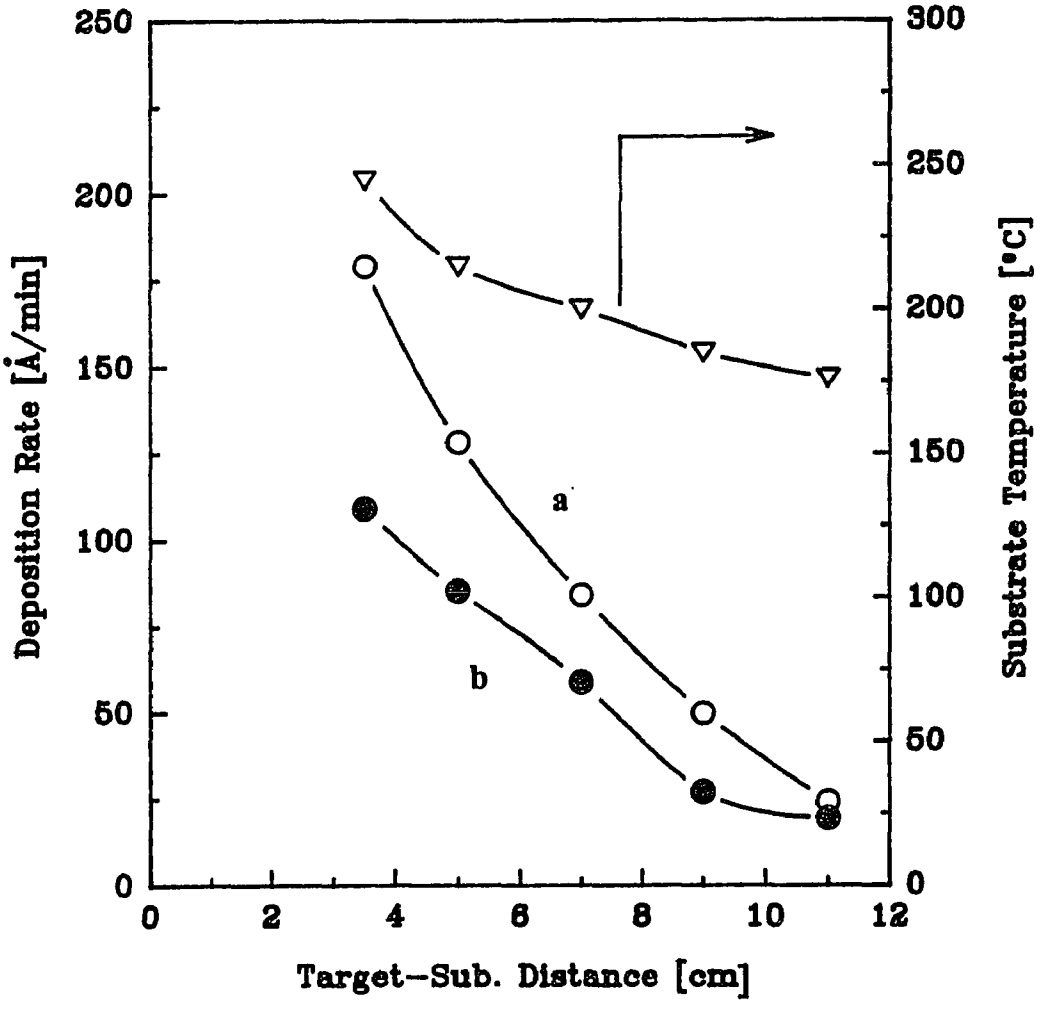

Figure 3.7 Deposition rate dependent on distance between target and substrate

rate curve. The deposition rates as shown in this Figure decrease with the increasing target to substrate distance. This means that the deposition rates are inversely proportional to the transit distance of copper atoms, and the probability of deposition on the substrate gradually becomes low with increasing transit distance. The measurements of substrate temperature is similar to the curve of the deposition rates under the same sputtering conditions.

3.3.3 Plasma Current Effect

The advantages of a triode system is that a high ion density is produced and the plasma current density for the deposition films can be controlled independently with the plasma voltage. Figure 3.8 shows the deposition rates as a function of the plasma current. The sputtering conditions were: 70 mm distance between target and substrate, 20 mTorr argon gas pressure, 100 W rf power input, and 60 V plasma voltage. The deposition rates increase linearly with increasing plasma current. As the plasma current is gradually increased, electrons caused by a thermionically heated filament are increased. These electrons accelerate toward the main anode where they then ionize a large portion of argon gas molecules. The process occurring in the triode system relies on the abundance of electrons generated by the thermionic filament to ensure sufficient ionizing collisions. Thus, the ion population at the target surface is increased with increasing electrons, and the deposition rates increase. The surface temperatures on the substrate holder depend effectively on the plasma current in the triode system and this is shown in this Figure. The curve of the substrate temperature increases with increasing plasma current, and it is expected that the increasing temperature on the substrate is caused by the sputtering deposition and by the thermionically heated filament.

3.3.4 Argon Sputtering Pressure Effect

Figure 3.9 shows the deposition rates with the different sputtering pressure of argon gas at

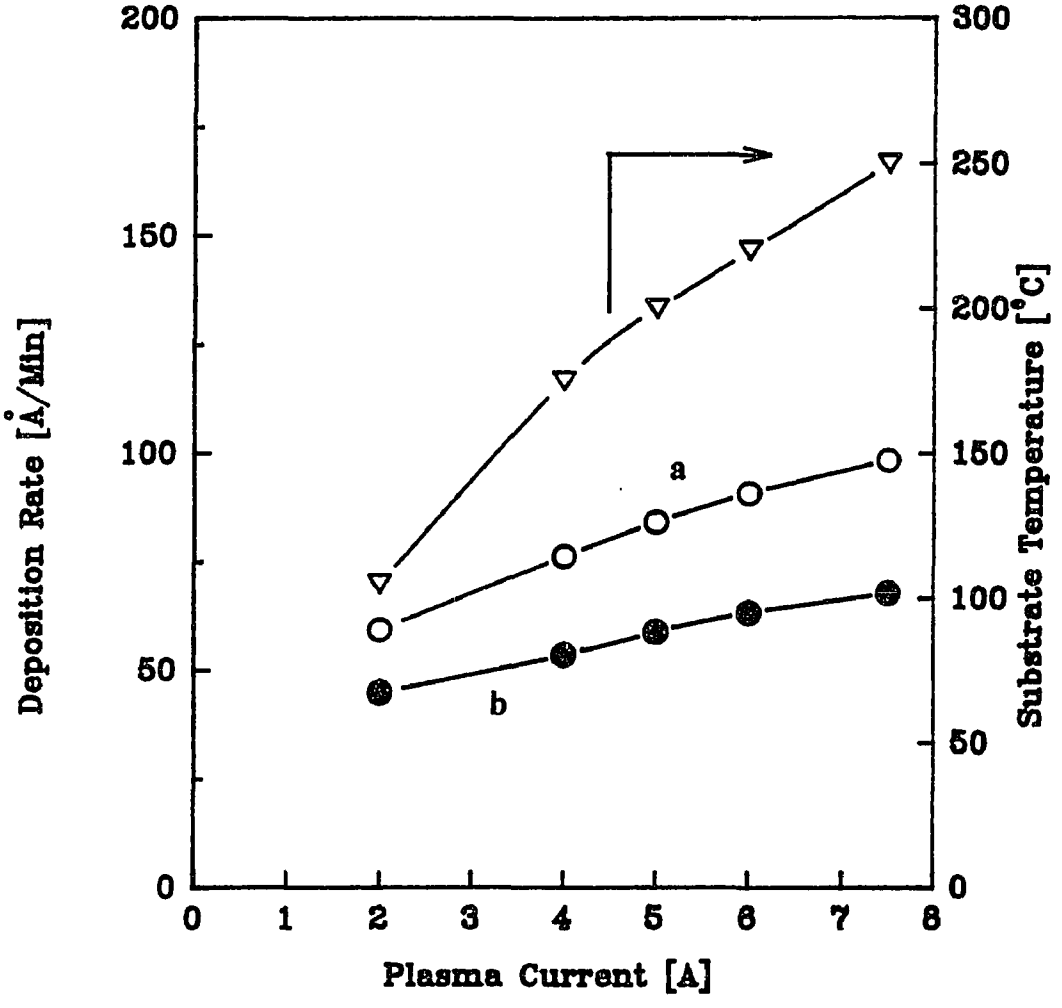

Figure 3.8 Deposition rate dependent on plasma current

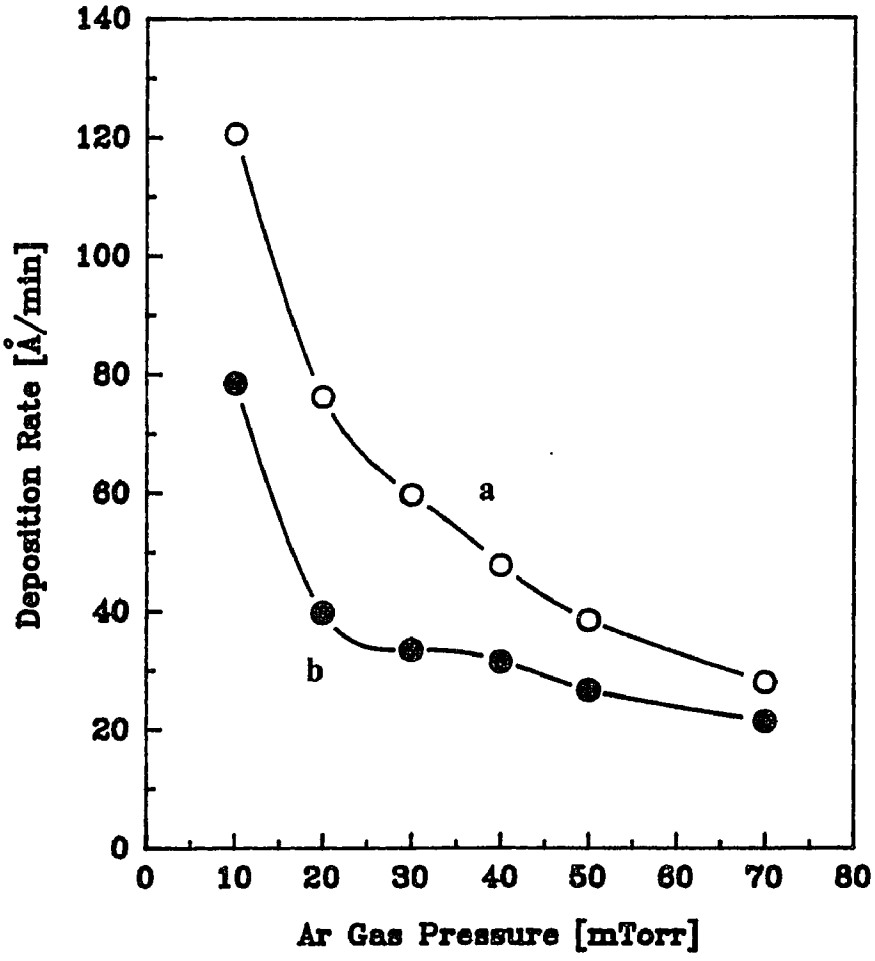

Figure 3.9 Deposition rate dependent on argon sputtering pressure

70 mm distance between target and substrate, and 125 W rf power input. As the sputtering pressure of argon gas is increased, the deposition rates decrease due to the scattering between the argon gas and the sputtering particles. The mean free path conspicuously decreases at higher sputtering pressures. Thus, the probability of collision between argon atoms and sputtering atoms increases with a higher argon sputtering pressure, and the probability of a sputtering atom reaching the substrate without colliding with an argon atom is reduced.

Figure 3.10 shows the residual gas with the variance of the argon sputtering pressure after 60 minutes from the starting of the sputtering deposition process. The sputtering conditions are same with the Figure 3.9. Mass 18 is the water (H_2O) peak. 20 and 40 AMU in mass axis are Ar++ and Ar+ ions, respectively. As shown in this Figure, the peaks of Ar++ and Ar+ ions increase absolutely at a higher Ar sputtering pressure. Conversely, the water peaks keep almost constant with a rising sputtering pressure.

3.4 Simulation of Magnetron Sputtering System

A triode magnetron sputtering system which was designed in our laboratory was simulated by the SIMION program [52], and the simulation of electron trajectories in the sputtering system is given in Figure 3.11. The two dimensional structure of the sputtering source assembly in the triode magnetron sputtering system was reduced by half scale to the actual system. The magnetic flux strength of the system was 250 Gauss. The potential of the main anode was a positive 50 voltages, and the substrate holder and housing of the target assembly were grounded. It was assumed that Ar gas was not introduced into the chamber in order to analyze the electron trajectories toward the main anode without collision. The electron trajectories in the sputtering system are confined directly above the target surface, as shown in this Figure. It shows that the electrons are trapped to the target surface by the force of the E×B field as shown in Figure 3.1. An electron, emitted from the filament, travels toward the main anode with the helical path. High electron

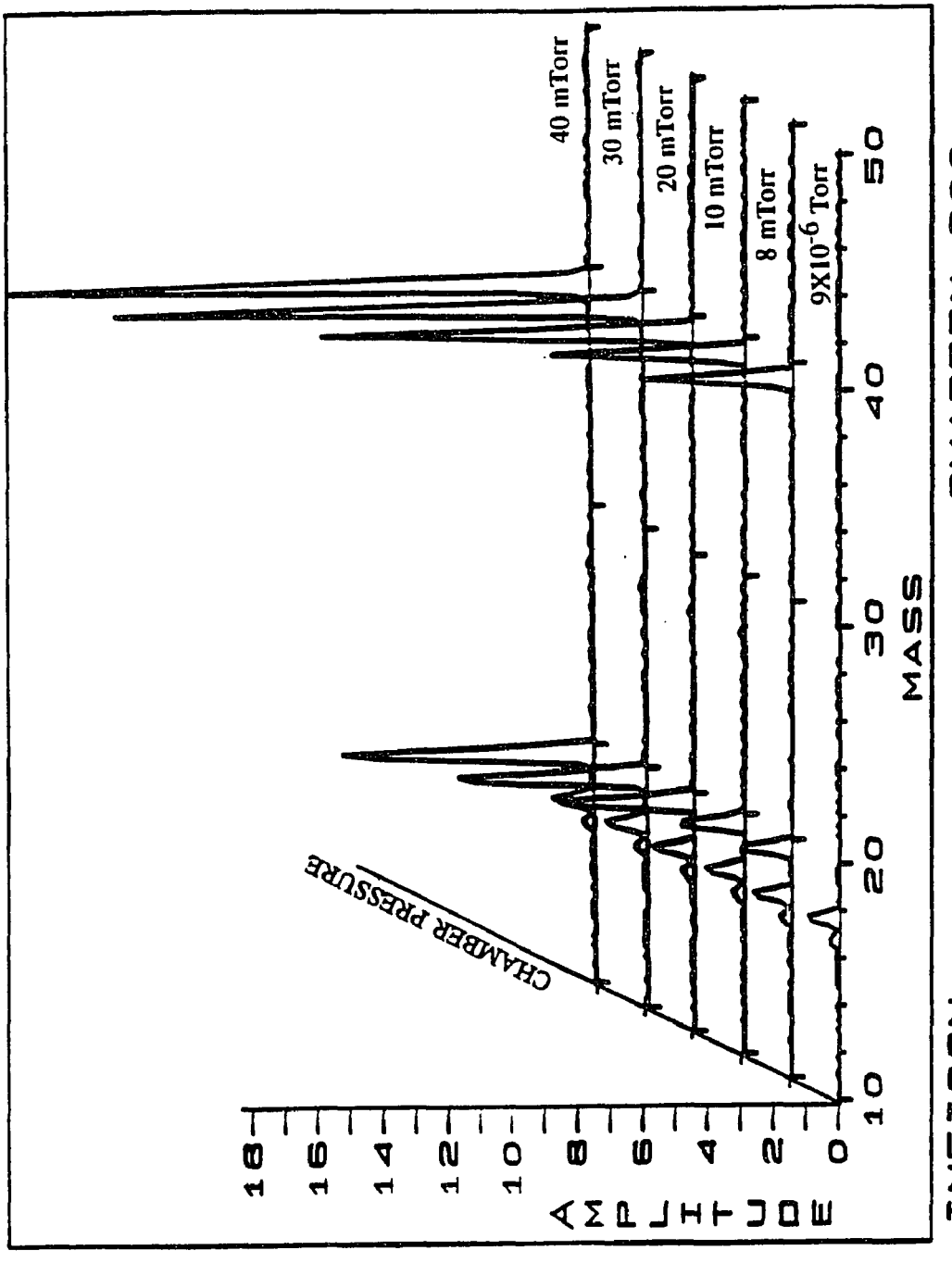

Figure 3.10 Residual gas pressure with increasing argon gas pressure

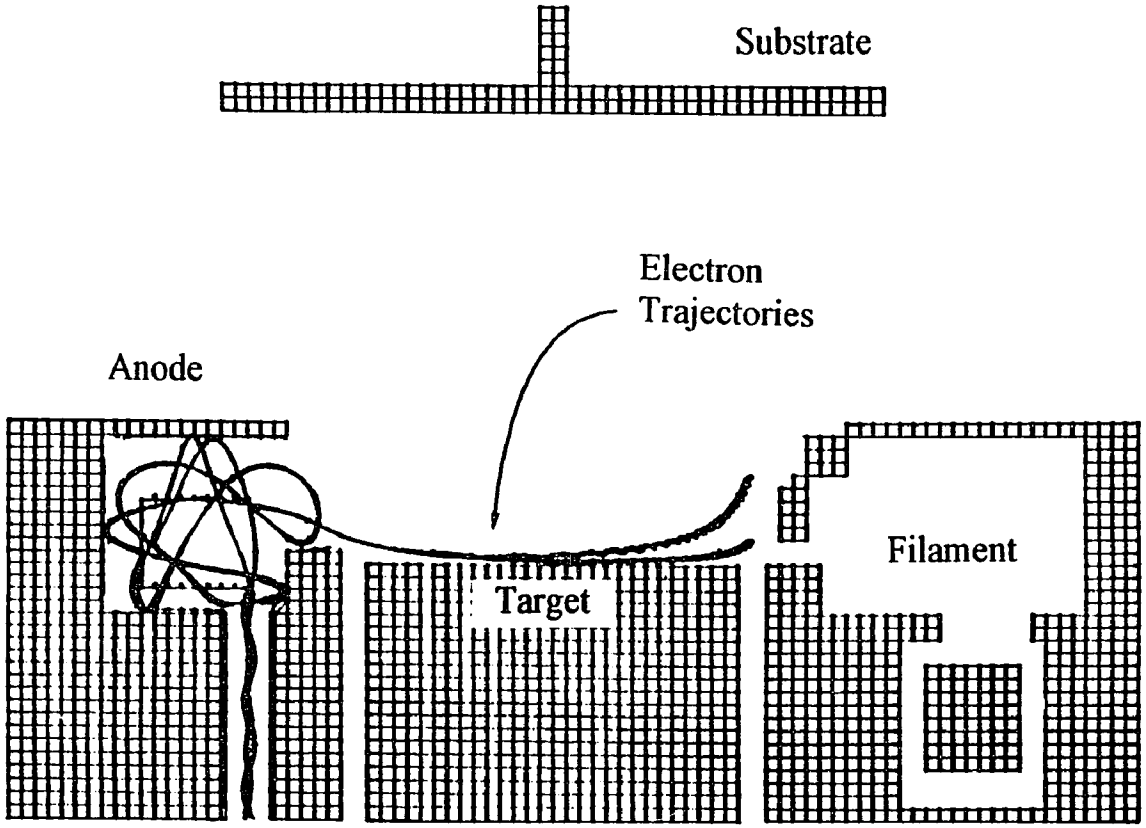

Figure 3.11 Representative simulation of electron trajectories in magnetron sputtering.

density magnetically confined near the target produces more ionization in terms of its bombardment.

The height of the electron trajectory from the target surface is closely related to the magnetic field and electric field. We can assume that the action of a magnetic field (along the Z axis) perpendicular to the electric field (along the Y axis) is to produce electron motion along an X axis. The equations of motion will then be [53]:

$$\ddot{y} = \frac{e}{m}[E(y) - B\dot{x}]$$

$$\ddot{x} = \frac{e}{m}B\dot{y}$$

$$\dot{x} = \frac{e}{m}By$$

where, E is the electric field,

B is the magnetic field strength,

e is the magnitude of electronic charge, and

m is the electron mass.

After substituting in the y dependencies of E and $\dot{x}$, the differential equation will be:

$$\ddot{y} = \frac{eE}{m} - \left(\frac{Be}{m}\right)^2 y$$

Thus, the resulting differential equation can be solved:

$$y = \frac{eE_o}{m\omega^2}(1 - \cos\omega t)$$

where, $\omega^2 = \frac{eE_o}{md} + \frac{e^2B^2}{m^2}$

and d is the thickness of dark space. In the absence of the electrical field, ω is equal to eB/m. This is known as the cyclotron frequency [53]. It is noted that the traveling height of an electron is also related to the thickness of dark space from this solution of the above equation. The maximum height, y_{max}, of the electron from the target surface, assuming no collisions, can be found by considering the gains and losses of potential and kinetic energy [54]:

$$\frac{1}{2}m\dot{x}_{\max}^2 = e(V - V_T)$$

where, V_T is the negative target voltage and V is the potential at y_{max}. Since $\dot{x} = Bey/m$, then y_{max} can be obtained:

$$y_{\max} = \frac{1}{B}\left[\frac{2m}{e}(V - V_T)\right]^{1/2}$$

This expression holds both within and without the dark space, and is a better approximation at lower pressures.

Figure 3.12 shows the trajectories of argon ions with the changes of their location after bombardment by electrons. The sputtering conditions are same with the procedure of Figure 3.11, and the target potential is a negative 200 voltages. Argon trajectories are concentrated largely upon the center of the target surface and slightly closer to the filament. The erosion profile of the target surface caused by Ar ion bombardment is shown in Figure 3.13, and thoroughly corresponds with the results of simulation that shows the collision of Ar trajectories. This erosion shape is mainly dependent on magnetic field strength, magnetic field shape and target material, and is controlled primarily by the magnetron design. It is known that the position and shape of this erosion directly affects the thickness distribution of deposited film on the substrate. Therefore, the geometry of

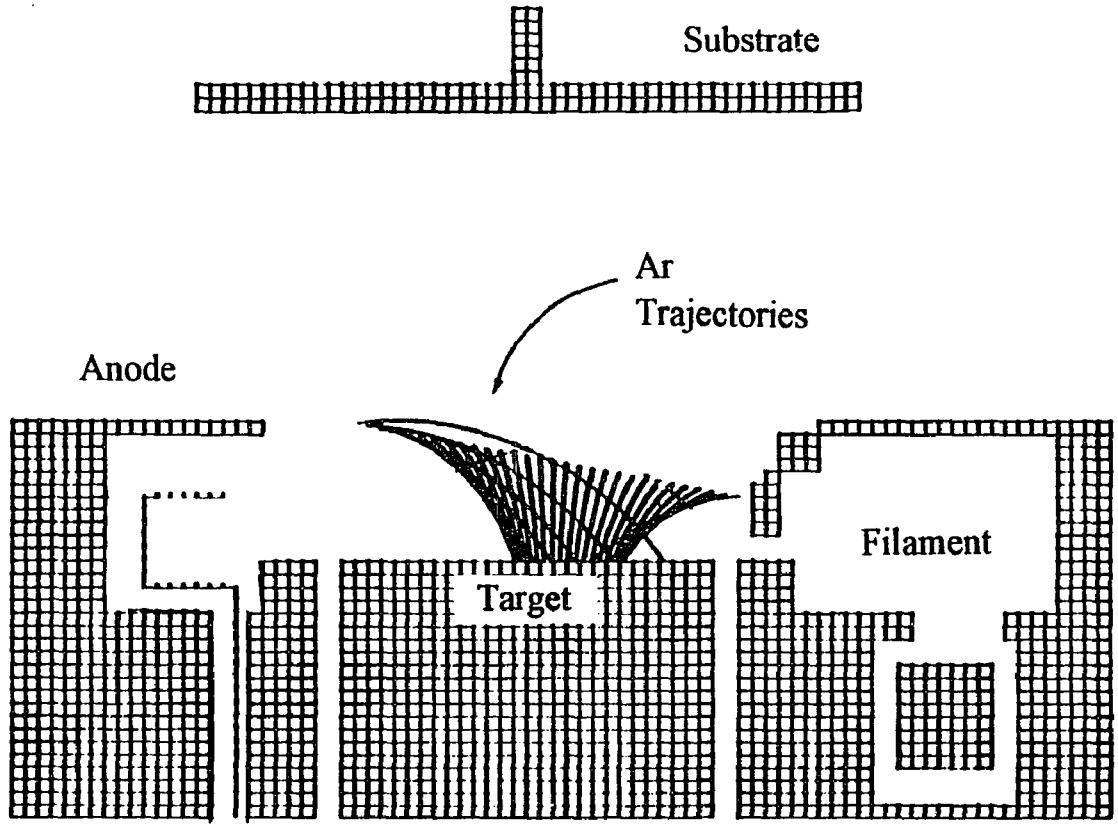

Figure 3.12 Simulation of argon ions trajectories after bombardment with electron

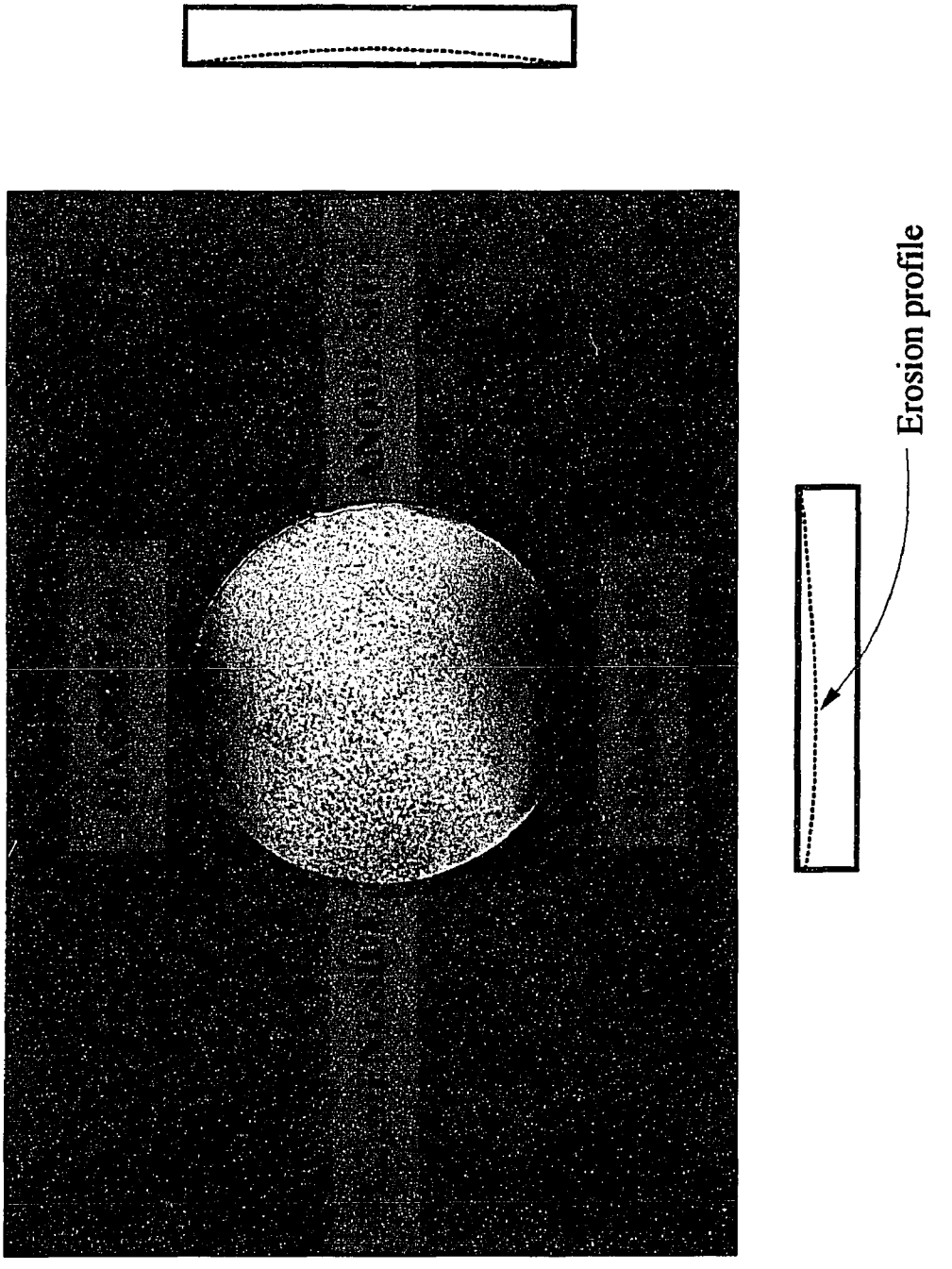

Figure 3.13 Picture of erosion profile in target surface

the magnetron source is an important parameter for a magnetron sputtering system.

3.5 Discussion

The results of calibration tests with four different sputtering conditions demonstrates that the deposition rate of rf triode magnetron sputtering is relatively higher than that of the conventional sputtering system. This means that the higher deposition rate is probably caused by a high ion density in the triode and magnetron system. The surface temperatures, in the substrate holder, are particularly increased with increasing plasma current in a triode system. It is evident that the results of electron and Ar ion trajectories simulated by the SIMION program correspond well with the actual processes of triode magnetron sputtering and the erosion profile of the target surface. The erosion area bombarded by Ar ion is sputtered widely on the whole target except on both magnet-sides. Therefore, rf triode planar magnetron sputtering, which was designed in our laboratory, is a powerful deposition system.

CHAPTER 4

EXPERIMENTAL PROCEDURE

4.1 Substrate Preparation

Substrates of PLT thin films were typical MgO or Pt/Ti/SiO_2/Si multi layer which consisted of (100) n-type Si with 500 nm thermally grown SiO_2, 50 nm Ti, and 200 nm Pt metal. Prior to the fabrication of multi layer substrates, n-type Si (100) of 1 Ωcm resistivity was degreased in trichloroethylene for 5 min, and rinsed in acetone. The substrates were dipped in dilute HF solution (HF : H_2O = 1 : 10) for 30 sec, and rinsed in deionized water for 5 min. Table 4.1 shows the growth conditions of thermally steam oxidation for SiO_2 layer. Table 4.2 illustrates the sputtering conditions for Ti as an isolation barrier and Pt metal as a buffer layer and a lower electrode.

The electrical characteristics of a metal-dielectric-metal (MDM) capacitor for DRAM cells are dependent upon the properties of the ferroelectric material and electrode. There are numerous important requirements, regarding the MDM capacitor, that must be satisfied by the correct choice of lower electrode materials, and these include [55]:

(1) low resistivity

(2) suitable electrical properties of the metal/dielectric interface

(3) good adhesion with underlayer

(4) thermal and morphological stability

(5) excellent action as a buffer barrier

High temperature post-annealing treatment, in order to transform the amorphous pyrochlore state of deposited PLT (28) thin films to cubic perovskite phase with excellent dielectric properties, can sometimes cause an undesirable interdiffusion and chemical reaction between lower electrode and PLT oxide. To reduce the interfacial problems, Pt is commonly used as the electrode materials. However, the Pt layer on the Si substrate has a

Table 4.1 Growth conditions of thermally oxidation for SiO_2 layer on Si.

Oxidation Step	Conditions
Pre-Cleaning	H_2O:HF = 100:1 1 min.
Rinse	DI Water, 1 min.
Spin Dry	Under N_2 Gas
Steam Oxidation	
Bubbler	530 SCCM
O_2 Flow	7.5 *l*/min.
Temperature	1050 °C
Time	115 min.
Thickness	475 nm Good Uniformity
Refractive Index	1.45

Table 4.2 Typical sputtering conditions for isolation barrier of Ti and buffer layer of Pt.

Sputtering conditions	Ti	Pt
Power density (W/cm^2)	0.92	0.78
Gas pressure (mTorr)	20	20
Distance (mm)	5	5
Sputtering gas	Ar	Ar
Sputtering Time (min)	20	40
Thickness (nm)	50	200
Temperature (°C)	55	70
Triode supply		
Plasma voltage (V)	55	55
Plasma current (A)	3	3

serious adhesion problem, a peeling-off phenomena due to its high thermal expansion coefficient. It is usual to use Ti, TiO_2, or Ta thin layer to solve the problems of thermal and interfacial stability. Currently, Sreenivas et al [56] have studied the stable metallization of Pt/Ti bilayer under the various environments for ferroelectric thin film capacitors. Kondo et al [57] and Olowolafe et al [58] reported that the material behavior of Ti and Pt was investigated to improve the adhesion with the substrate.

4.2 Target Design

The target sources of magnetron sputtering technique for multi-component ferroelectric thin films are generally specified in 3 ways as shown in Figure 4.1. Magnetron sputtering has special and considerable advantages in the range of usable plasma pressure, and in limiting electron bombardment of the film. Figure 4.1 (a) shows the rf sputtering method of a ceramic oxide pallette or mixed powder oxide target. Since the components of powder oxide may have widely different sputtering yields, the target composition must be adjusted by the amount of each component, as well as the additional PbO which is normally added to the target to compensate for loss of Pb from the sputtered thin films. However, the powder target process shows a number of disadvantages including [59,60]:

(1) difficulty in pressing a large-diameter disk,

(2) target cracking due to heating during sputtering,

(3) reproducibility problem in terms of oxygen deficiency and stoichiometric variations on the target surface, and

(4) low sputtering rate.

As described above, there is a limit in the strict control of film composition for such a sputtering system with powder target. Figure 4.1 (b) shows dc or rf reactive sputtering of a multi component metal target, while Figure 4.1 (c) shows the reactive sputtering using multiple metal targets. It is known that the sputtering rate of a metal target is higher than the rate of oxides and insulators [59]. Although the evidence is not yet conclusive, the

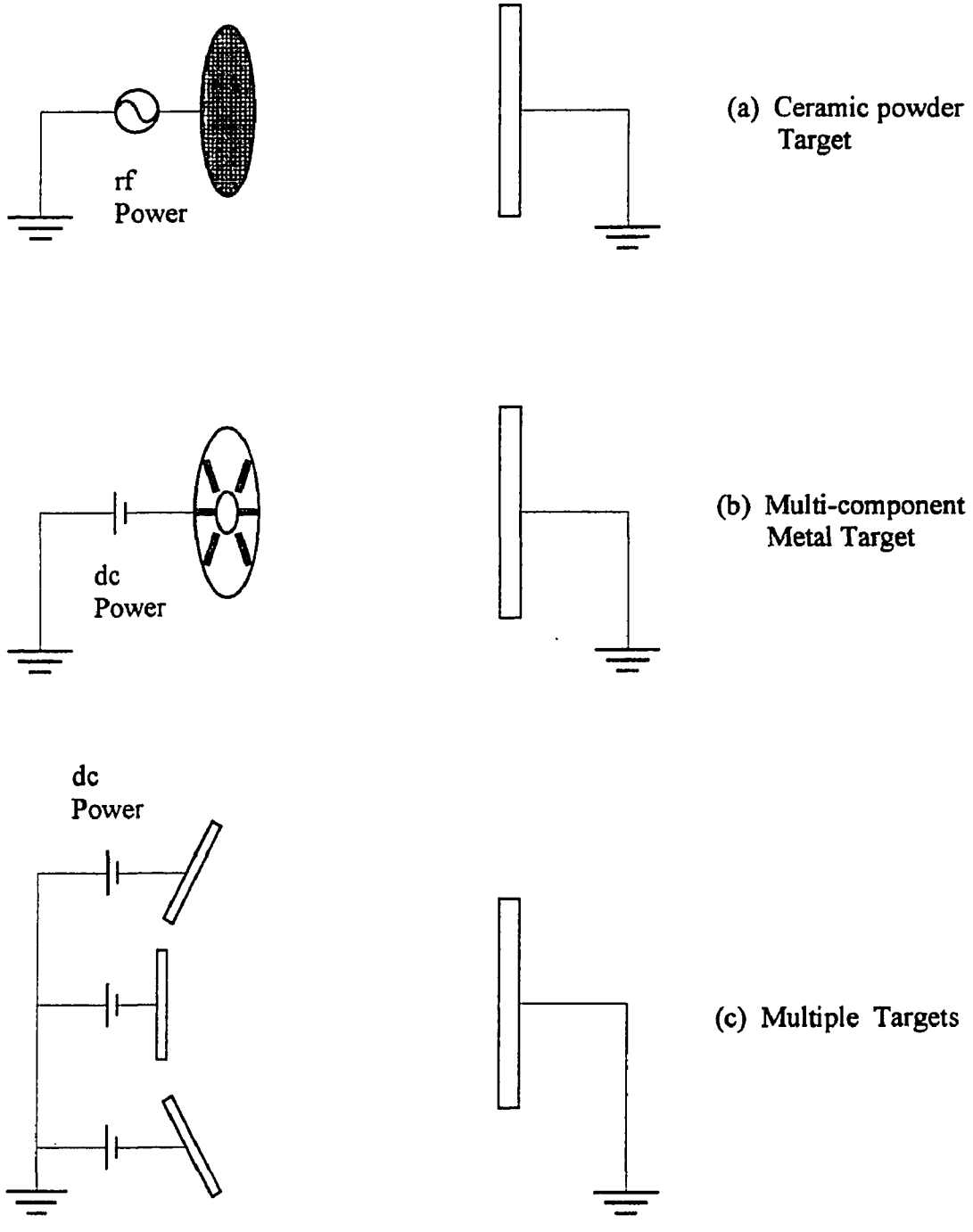

Figure 4.1 Sputtering depositions of compound ceremic oxide films with different target formations.

sputtering rate for metal targets or a multi-component target is a factor of 2 or 3 higher than for a ceramic powder target, and lower substrate temperature processing is possible. The multi-component metal target offers a number of advantages. They include [61,62]:

(1) the potential for higher sputtering rates due to smaller binding energy.

(2) the possibility for larger area target,

(3) high stability and purity of target,

(4) convenience of modification of the target composition, and

(5) the ability to incorporate dopant metal such as a La of lead titanate.

A reactive magnetron sputtering system that can control the target areas of individual metal elements is highly desirable for the preparation of the complex compound films. In order to control, interdependently, each metal element in PLT thin films, a reactive magnetron sputtering system with a multi-component metal target is used for the PLT deposition in this study.

The task, to deposit high-quality material, is to produce films with low impurity and correct stoichiometric composition. Target metals of multi-component film should be extremely pure. The original metals of the multi component target consist of Pb (99.999%), La (99.9%), and Ti (99.97%). Several sectors of La, and a thin circular plate of Pb, are located on a 2.25 inch diameter and 0.25 inch thick disk-shaped Ti target. A typical schematic diagram of the multi component metal target is given in Figure 4.2. The number of atoms deposited onto a unit area on the substrate is determined not only by the target configuration, the incident ion energy, sputtering yield, and magnetron design, but also by complex scattering phenomena within the plasma. Thus, the simple expression of the number of atoms, n, modified by Ochiai et al [63] is written as:

$$n = \alpha g Y t$$

where, α is a constant depending on the sputtering conditions (gas pressure, target power,

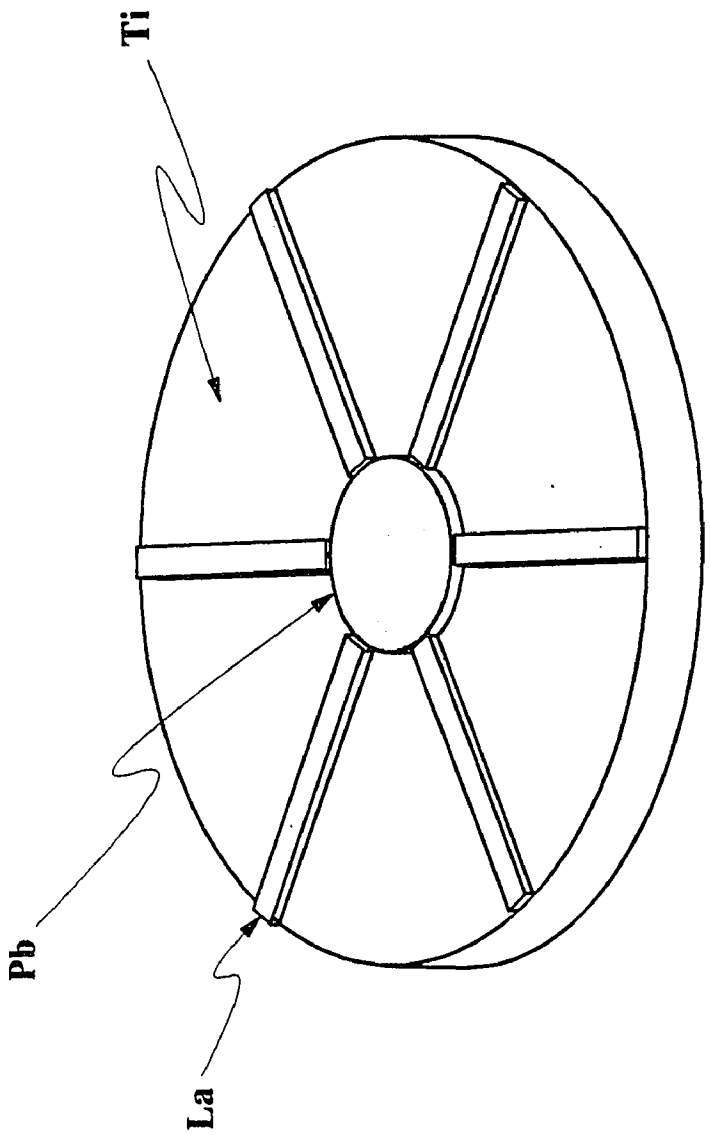

Figure 4.2 Multi-component metal target design for PLT film.

and plasma current, etc.)

g is a geometric factor,

Y is the sputtering yield (atoms/ion), and

t is the sputtering time.

The content of an element in the deposited films is proportional to the fraction of the element in the multi-metals target. As proposed by Fukami et al [64] and Hase et al [65], the ratio of the Pb/La area on Ti disk target is actually determined by the modified Sigmund's method [66,67] which considers (1) sputtering yield for Pb, La, and Ti metal, (2) Ti diameter due to (Pb+La)/Ti = 1/1, (3) composition ratio of Pb/La on the deposited thin films. The film composition predicted for the ith element (C_i) is given by:

$$C_i = \frac{Y_i}{\sum Y_i A_i} \times 100 \qquad \text{(atom \%)}$$

where, i corresponds to Pb, La, and Ti for PLT material,

Y_i is the sputtering yield, and

A_i is the occupied area on the target.

The area ratio of each metal element on the target surface is estimated from the above formula. The relative composition for the paraelectric PLT (28; i.e., $Pb_{0.72}La_{0.28}Ti_{0.93}O_3$) film is calculated to be:

Pb : La : Ti = 14.08 : 11.70 : 74.22

in the target area of each metal. The exact chemical composition of post-annealed PLT thin films is characterized by Rutherford backscattering (RBS) and Auger electron spectroscopy (AES).

4.3 Sputtering Conditions

A reactive magnetron sputtering is carried out by introducing an oxygen (purity 99.99 %) and argon (99.999 %) gas mixture. Sputtering parameters such as power, sputtering pressure, gas composition, substrate-target distance and substrate temperature thoroughly affect the physical and chemical characteristics of the deposited PLT films. The details of the multi-component target and sputtering conditions used in this experiment are summarized in Table 4.3. The substrate temperature was measured by a chromel-alumel thermocouple attached to the substrate holder. Table 4.4 shows partial pressures in the chamber during PLT deposition using magnetron sputtering with a multi-component metal target.

The primary factors, in the preparation and crystallization of PLT thin films, are the adjustable control of oxidation kinetics and of the Pb content of the films, because Pb tends to re-evaporate from the substrate at high temperature. Generally, the sputtering rate in reactive sputtering deposition decreases rapidly with increasing oxygen partial pressure. When the oxygen partial pressure is high, the surface of the target metals is oxidized and an altered thin layer is formed. Oxygen gas pressure, dependent on the sputtering rate, is completely different among Pb, La, and Ti metals. The oxidation decreases with an increase in sputtering power and increases with an increase in partial pressure of oxygen. The applied power must be greater than the threshold for each component in order to maintain constant sputtering conditions and uniform composition in the final films for a multi-component metal target [68].

In plasma processing techniques such as a reactive magnetron sputtering technique, various target-substrate geometries can affect the deposition process of multi-component oxide films. Consequently, there are several control problems which should be considered in the stoichiometry of multi-component thin films using a reactive magnetron sputtering method [69,70].

Table 4.3 Optimized sputtering conditions for PLT deposition.

Sputtering conditions	PLT thin films
Power density (W/cm^2)	0.86
Gas pressure (mTorr)	20
Target-substrate distance (cm)	4
Sputtering gas	Ar : O_2 = 50 : 50
Deposition rate (nm/min)	2.8
Thickness (nm)	200
Substrate temperature (°C)	160
Triode supply	
Plasma voltage (V)	60
Plasma current (A)	3

Table 4.4 Partial pressure in the sputtering chamber after introducing the gases.

Material / Mass	Factor	Torr
Hydrogen	2.319	2.4 E - 8
Helium	7.143	NA
Water	1.333	4.6 E - 7
Nitrogen / CO	1.029	8.0 E - 8
Oxygen	1.053	2.5 E - 6
Argon	0.947	2.7 E - 6
Emulation 1.20 KV		Total pressure 2.5 E - 5

(1) The formation of an altered layer at the target surface due to the different sputtering yields in the multi-component target, the different diffusion coefficients, the concentration gradient, and the temperature gradient

(2) The different composition between the target surface and the deposited film due to the complex sputtering phenomena, particularly reactive processing

(3) Resputtering in terms of negative ion effects

(4) Electron bombardment effect by secondary electrons emitted from the oxide target

Many technical methods have been proposed in order to improve these disadvantages in a magnetron sputtering process. Adachi et al [71] increased the operating pressure to reduce the energy of the neutralized negative ions in terms of causing multiple collisions for the plasma procedure. Sandstrom et al [72] and Terada et al [73] reported unconventional sputtering geometries (so called, off-axis sputtering) to minimize the bombardment of growing films by secondary electrons and ions emitted from the target. The bias sputtering mode, in addition, is able to influence the properties of the deposited films by changing the sputtering flux and energy of incident particles [74]. The charged particles are controlled by changing the electric field of bias sputtering. In multi-component oxide sputtering, the constituent elements arriving at the surface of the substrate usually have different sticking coefficients, especially if the elements have large differences in vapor pressure. The sticking coefficients can also be changed by low energy ion bombardment of the growing film by applying a small bias to the substrate [53], and this bias sputtering is important in small adjustments of the stoichiometry.

The reactive sputtering deposition for good oxide films is governed by the processes [75,76]:

(1) formation of a reproducible oxide layer on the target surface,

(2) the stability of the oxide species formed during transport in the plasma, and

(3) nucleation and growth on the substrate surface.

In this study, the specific techniques, such as off-axis sputtering and bias sputtering, are not taken into consideration, owing to the low deposition rate and intricate plasma process in the reactive sputtering method with triode and magnetron system. The operating pressure used, 20 mTorr, is known to be a relatively high pressure in the magnetron sputtering processes, to suppress the energy of negative ions as discussed by Adachi et al [71]. In order to control the composition of deposited PLT films in spite of the different composition between target surface and growth films, the modified Sigmund's method is used under the optimizing sputtering conditions.

4.4 Post-Annealing Conditions

The most difficult factor to control in the stoichiometric composition of PLT films is the Pb concentration. A non-stoichiometry of Pb content results from evaporation by heat treatment such as substrate temperature during the deposition or post-deposition annealing method. The heated substrate process influences the overall plasma phenomena of reactive sputtering, and consequently an excess Pb content is required in the target composition. Therefore, the post-deposition annealing for as-deposited PLT thin films is not only more preferential treatment, but it also can achieve a chemically stable compound by the similar method with the formation of ceramic bulk films. PLT thin films deposited reactively by magnetron sputtering are in the amorphous or partially amorphous state, and the as-deposited films subsequently require a post-annealing heat treatment. Since ferroelectric compound oxide films are normally processed at a very high temperature, their characteristics such as structural, electrical and mechanical properties, change especially with the annealing conditions during the cooling-down step. A heat treatment followed by a slow cooling-down at high temperature can considerably relieve the internal stresses of as-deposited thin films. The post-annealing process for perovskite structure of paraelectric PLT film can strongly affect the film composition due to lead volatility. Pb evaporation during annealing treatment can be particularly influenced by the annealing

conditions such as annealing temperature, annealing time, oxygen partial pressure and starting composition. The post-deposition heat treatment introduces an interdependency between composition and crystalline structure evolution. Simultaneous crystallization and Pb vaporization produce a relation between composition and the crystallographic structure that is dependent on the kinetic mechanism of two processes. The structural phases within the PLT thin film after post-deposition annealing depend on the starting composition, the amount of crystallization, and the quality of lead oxide volatility [26].

In our experiments, the substrate heat has not been used during the reactive magnetron sputtering deposition of PLT in order to minimize the unbalanced effect in the deposition rate of each metal element [61,62], suppress the Pb evaporation and reduce the inter-reaction between the PLT film and substrate. The PLT thin films were annealed in a fused quartz tube furnace with flowing oxygen at a flow rate of 0.2 *l*/min. In the annealing profile for all PLT films, the heating rate was 15 °C/min and the cooling rate was 5~6 ° C/min. The ranges of the annealing temperature and annealing time for this experiment were 450~750 °C and 5~60 min, respectively.

4.5 Metal-Dielectric-Metal Capacitor

Metal-dielectric-metal (MDM) structures for electrical and dielectric measurements are fabricated on multi-layer ($Pt/Ti/SiO_2/Si$) and MgO substrates as shown in Figure 4.3 (a) and (b). Through a suitable choice of the electrode material and the deposition method for the ferroelectric ceramic oxides, it is possible to control the electrical properties of the MDM structure and in particular to influence the electrical resistance. The effect of the electrode material, on the electrical properties of ferroelectrics, has not been completely studied yet.

However, contact between the electrode metal and the ferroelectric oxides is generally specified by neutral, ohmic and barrier type [77,78]. In the case of neutral contact, the electronic work functions of the metal (W_m) and the ferroelectric oxides (W_f)

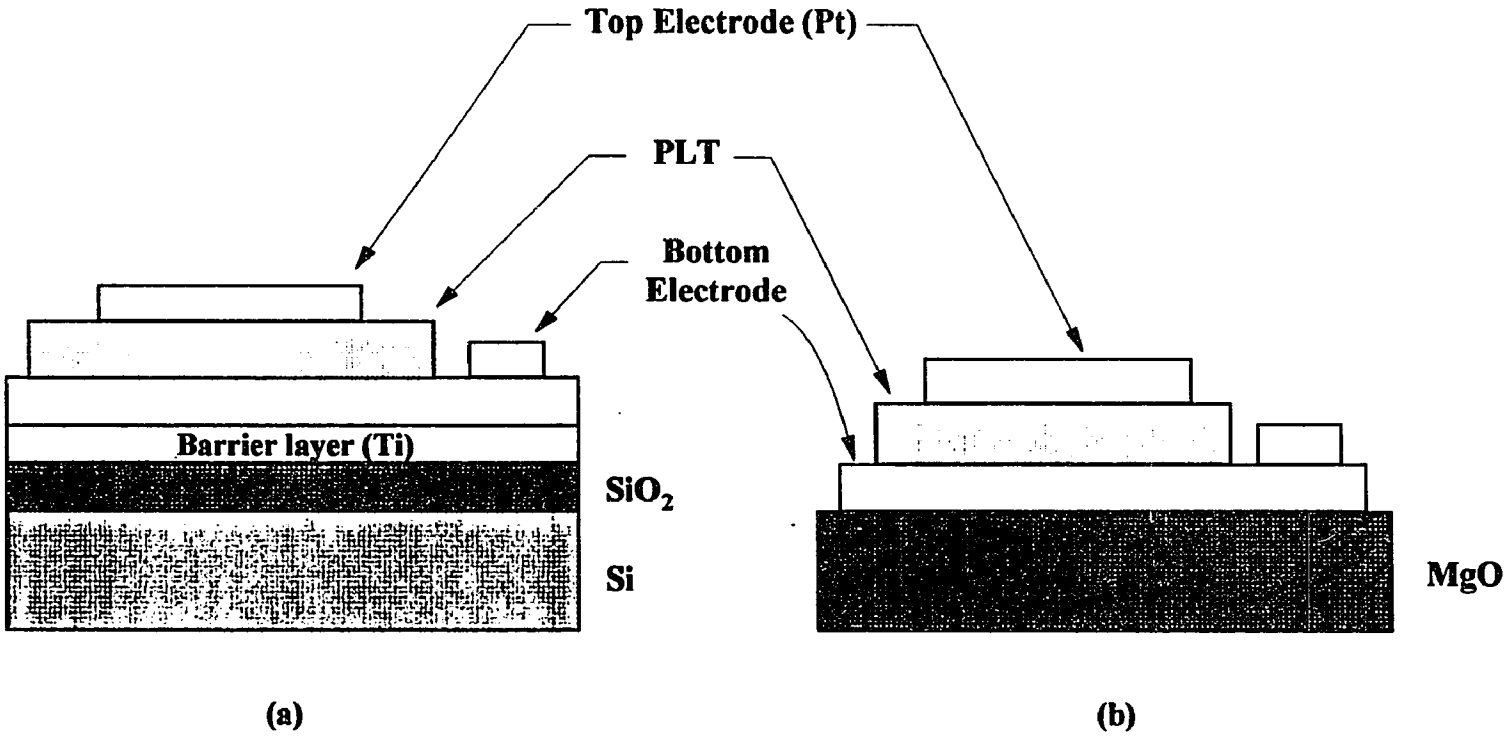

Figure 4.3 Capacitors with structure of (a) Pt/PLT/Pt-multilayer (Ti/SiO_2/Si) substrate and (b) Pt/PLT/Pt-MgO substrate.

are equal, while the conditions of ohmic and barrier contacts are $W_m > W_f$ and $W_m < W_f$, respectively. The barrier contacts form a high specific electrical resistance, owing to a depletion layer occurring at the metal-ferroelectrics interface. This is the reason for nonlinearity in the current-voltage characteristic curves. Therefore, the electrodes on MDM capacitor should be of ohmic contact, so that they present a small electrical resistance and good adhesion at the interface, and do not cause changes in the electrical properties of the ferroelectric oxides. Magnetron sputtering to obtain ohmic electrodes for paraelectric PLT thin films is a known deposition method. Among the various electrode materials, Pt as a top and bottom electrode is also used because of the potential advantages in its electrical characteristics.

CHAPTER 5

MATERIAL ANALYSIS AND DISCUSSION

Paraelectric lead lanthanum titanate (PLT; 28 mol %) thin films are prepared by a multi-component metal target using the previously described magnetron sputtering system. The as-deposited amorphous films are crystallized into the cubic (or paraelectric) perovskite structure by a heat treatment at an annealing temperature ranging from 450 to 750 °C. The post-annealing treatment, used for crystallizing the films in this study, affects the film composition due to Pb evaporation. The electrical properties of the perovskite PLT thin films are strongly dependent upon the stoichiometric composition and crystalline structure. The dielectric properties of the films reach maximum values near the ferroelectric-paraelectric phase boundary (La content of 28 mol %) in the equilibrium phase diagram of PLT system as previously mentioned in Chapter 2. Therefore, it is necessary to analyze the material characteristics of PLT thin films such as chemical composition, crystalline structure and surface microstructure.

The primary concern in PLT (28) thin film deposition is the stringent control of stoichiometric composition. AES (Perkin-Elmer, PHI 660, scanning Auger microscopy) and RBS (General Ionex, model 4117, Tandetron ion accelerator) measurements are used for analyzing the relative composition ratio of Pb, La, Ti and O of the PLT thin films. The depth profiles of the films are also measured using AES, and the exact thickness of PLT (28) thin films is identified by RBS analysis. The crystalline phases and lattice parameters of thin films is characterized by an X-ray diffractometer (Rigaku, D/MAX system and philips, vertical diffractometer) using CuKα radiation. The microstructure of the films is also investigated by SEM (ISI, SIII-A(K)).

5.1 Chemical Composition Analysis

5.1.1 Stoichiometric Composition by AES

The chemical compositions of PLT thin films are identified by a semiquantitative Auger electron microscopy (AES) analysis using a Perkin-Elmer PHI 660 scanning Auger microscopy (SAM). A primary electron beam of 5 KeV is utilized to stimulate Auger transitions within the films. The AES system is evacuated to a base pressure of 1×10^{-10} Torr by an ion pump and turbomocular pumps, and the pressure is then raised to 5×10^{-8} Torr by Ar gas. A 4 KeV Ar^+ ion beam for 2 min is also used to simultaneously remove surface contaminations on the films. This is done to insure that the films have been sputter-cleaned prior to the AES analysis. All signals are clearly labeled, along with intensity values for relevant peaks used for quantitation. The detailed conditions of the AES analysis are summarized in Table 5.1.

It is necessary to evaluate the effect of instrumental parameters on the measured Auger signal in order to determine the relationship between the Auger electron signal and

Table 5.1 AES analysis conditions

Primary electron beam voltage	:	5 KeV
Primary electron beam current	:	1 ± 0.02 μA
Ion beam voltage	:	4 KeV
Base pressure	:	$1x10^{-10}$ Torr
Scanning speed	:	100 eV/sec
Surface cleaning	:	4 KeV Ar^+ ion bombardment at $5x10^{-8}$ Torr

the atomic concentration. The important instrumental variables are the primary electron beam current, the primary beam energy and the dN(E)/dE spectrum. Figures A.1, A.2 and A.3 are Auger energy spectra of each pure Pb, La or Ti metal. These values are very similar to the data values of pure elements tabulated in a handbook of Auger electron spectroscopy [79]. In Figure A.1, the Auger spectrum of pure Pb shows only a Pb peak at 93 eV. Ti Auger signals, as shown in Figure A.3, are detected at 386 eV and 417 eV. However, the Auger spectrum of pure La, as shown in Figure A.2, indicates La signals at 82 and 631 eV, and an intense O signal at 516 eV because La oxidizes rapidly in air. The surface of pure La metal is quite rough and appears to be porous.

A simple approximation of quantitative analysis can be accomplished by a comparison of Auger signal intensity in the test sample to that of the pure elemental standard. The elemental atomic concentration of element, C_X, in the test sample is expressed as:

$$C_x = \frac{I_x(\text{test})}{I_x(\text{standard})}$$

where I_X (test) and I_X (standard) are the peak-to-peak Auger signal intensity from the film and standard, respectively. The atomic concentrations of PLT thin film, however, can not be calculated directly from the Auger energy spectra of pure elements. There are several inherent sources of error in the above formula. The most important factors are: (1) matrix effects on the Auger electron escape depth and backscattering factors, (2) chemical effects on peak shapes, and (3) surface topography [79,80]. The Auger electron escape depth in the test film may be different from that of the pure elemental standard. Since the magnitude of the Auger signal is proportional to the number of atoms in the analysis volume, a larger escape depth will cause a corresponding increase in the Auger signal. Chemical effects can change the peak shape and thus lead to an error when using peak-to-

peak heights in the differentiated spectrum for a measurement of the Auger signal. A smooth surface generally produces a larger Auger signal than a rough surface [80]. Besides, surface roughness on the films will degrade the Auger signal intensity. This effect is minimized by determining concentrations from the above equation since surface roughness is expected to decrease all Auger peaks.

A standard of known composition, which is close to that of the actual films, should be used to obtain the highly accurate quantitative analysis. Figure A.4 shows the energy spectrum and relative composition of a perovskite PLT thin film analyzed by Rutherford backscattering spectrometry measurement. RBS results of PLT ceramic oxides, which are chosen as a composition standard, are used to calibrate the Auger transition intensities, in order to increase the semiquantitative accuracy of the Auger technique. Figure A.5 presents the Auger spectrum for the same PLT film with the result of RBS analysis. Elemental relative sensitivity factors of the perovskite PLT thin films for semiquantitative analysis are calculated from AES analysis based on the RBS results. The atomic concentration for each element in a PLT film can be obtained by multiplying the peak-to-peak height by an elemental relative sensitivity factor. Table 5.2 shows relative Auger peak-to-peak height and relative sensitivity factors for a PLT film. These values are

Table 5.2 Relative Auger peak heights and relative sensitivity factors for a standard PLT film.

Elements and peak voltage (eV)	Peak-to-peak height	Atomic concentration	Relative sensitivity factor (RSF)
Pb, 93	175.6	0.144	1.182
La, 626	19.2	0.044	0.511
Ti, 418	56.4	0.132	0.555
O, 511	248.9	0.680	0.400

considerably different from the previous AES results of pure elements utilized in an Auger electron spectroscopy handbook [79].

Figure A.6 shows the AES analysis of an as-deposited PLT film prepared under the same conditions as the film that is used as a standard for the calibration of AES data. All Auger signals of Pb, La, Ti and O are detected within the PLT films. No impurity element is observed in the Auger spectrum, except a small contamination of the carbon signal which comes from the KL_2L_2 transition at 271 eV. It seems that the carbon contamination on the film surface is largely caused by handling. The chemical composition of the as-deposited PLT film is analyzed by Auger peak-to-peak height and the relative sensitivity factor from the Table 5.2, resulting in a composition of $Pb_{1.44}La_{0.28}Ti_{0.82}O_{4.6}$. It seems that a relatively large amount of Pb element is detected in the composition of the as-deposited PLT film without a heat treatment.

Figure A.7 (a) and (b) show the typical results of Auger analysis on the perovskite PLT (28) thin films annealed at 650 °C for 5 min. The observed signals of all elements are Pb $N_{6,7}O_{4,5}O_{4,5}$ at 93 eV, La $M_5N_{4,5}N_{4,5}$ at 627 eV, Ti $L_3M_{2,3}M_{4,5}$ at 418 eV, and O $KL_{2,3}L_{2,3}$ at 512 eV. The Auger signals of Ti consist of Ti $L_3M_{2,3}M_{2,3}$ at 386 eV and Ti $L_3M_{2,3}M_{4,5}$ at 418 eV. The peak of Ti $L_3M_{2,3}M_{4,5}$ at 418 eV, which is not sensitive to the bonding state, is used to obtain the chemical composition of the PLT film. The stoichiometric compositions in Figure A.7 (a) and (b) are:

(a) Pb : La : Ti : O = 0.72 : 0.28 : 0.88 : 2.9

(b) Pb : La : Ti : O = 0.72 : 0.28 : 0.75 : 3.1

In compositional analysis of the paraelectric PLT films, the ratio of Pb and La is the most important quantity, because the evaporation of Pb depends upon the conditions of the post-annealing treatment. It is also suggested that its ratio has tremendous effects on the electrical properties of the PLT films, and the relationship between the chemical composition and the electrical properties will be discussed in next chapter.

5.1.2 AES Depth Profile

Auger electron microscopy is also used to check the carbon contamination and the composition uniformity across the thickness of paraelectric perovskite PLT thin films. The Auger depth profile of the as-deposited PLT film on $Pt/Ti/SiO_2/Si$, as a function of etching time, is shown in Figure A.8. The amorphous PLT film is nonuniform near the film surface, and the Auger data shows a Pb enrichment on the surface of the as-deposited film. Although the higher Pb concentration in the near-surface region of the film can not be explained precisely, the sputtering rate of Pb has been reported to be higher than that of La or Ti metal [62,64]. It would lead to an increasing slope in the Pb profile near the film surface. A Pb enrichment on the surface region has also been observed from rf-magnetron sputtering using a multi-target by Adachi et al [68]. It seems that this effect is a general phenomenon of the as-deposited film and is not related to a specific deposition method. Carbon contamination is not observed in the depth profile of the amorphous PLT film except for the carbon absorption on the film surface as shown in Figure A.8.

The AES depth profiles for the post-annealed films are shown in Figure A.9 (a) and (b). The AES profiles for PLT thin films annealed at 650 °C for 5 min are remarkably different from that of the as-deposited film near the surface region. The Pb content of the heat-treated films decrease at the surface, suggesting that this fact is due to the evaporation of Pb from the surface during the post-annealing process. The typical depth profile shows relatively uniform distribution of the components (Pb, La, Ti and O) into the depth of the film.

5.1.3 Rutherford Back-scattering Analysis

Rutherford back-scattering is used to investigate the stoichiometry of PLT thin films, as well as to calibrate the Auger spectrum signal to an elemental concentration of AES characterization. Figure A.10 (a), (b), (c) and (d) illustrate the RBS spectra of the PLT thin films with the different area ratio of a multi-component metal target. An annealing-

heat treatment for all PLT films is applied under the same condition at an annealing temperature of 650 °C for 5 min. The changes of the normalized compositions as shown in the spectrum analysis of the RBS for each metallic components of PLT thin films shows a similar tendency with the relative composition ratio in target area of metal elements. It is mentioned that the content of an element in the deposited PLT films is proportional to the fraction of the element in the target metal. It is noted that the relatively big signal of oxygen is detected due to the inherent sensitivity of the RBS system.

5.1.4 Discussion

The atomic concentrations in ternary ceramic PLT films, as the results of compositional analysis, could not be directly estimated by the comparison with the Auger spectra of pure Pb, La, and Ti as shown in Figure A.1, A.2 and A.3. The Auger signal of each element in the PLT films is observed to be slightly shifted in comparison with the value of pure metal. It is expected that the shift of the Auger peak signal is caused by matrix effects. Therefore, the relative sensitivity factor for each element is calculated, and the results are summarized in Table 5.2.

Compositional control of the PLT thin films is accompanied with the changes in relative area ratio of the multi-component metal target. Figure 5.1 shows the relationship between the relative composition of the perovskite PLT thin films and the corresponding area ratio of the multi-component metal target specified by six different types. The black star means the ideal composition ratio of paraelectric PLT ($Pb_{0.72}La_{0.28}Ti_{0.93}O_3$) thin film in a ternary oxide Pb-La-Ti-O system. The white star expresses the compositional area ratio of target element estimated by the modified Sigmund's method. Table 5.3 enumerates in detail the schematic results of Figure 5.1 analyzed by AES and RBS measurements. The content of La is the important factor, in this study, because the paraelectric state of the PLT thin films is determined by the La content in the phase diagram of Pb-La-Ti-O system as shown in Figure 2.3. The dielectric and electrical

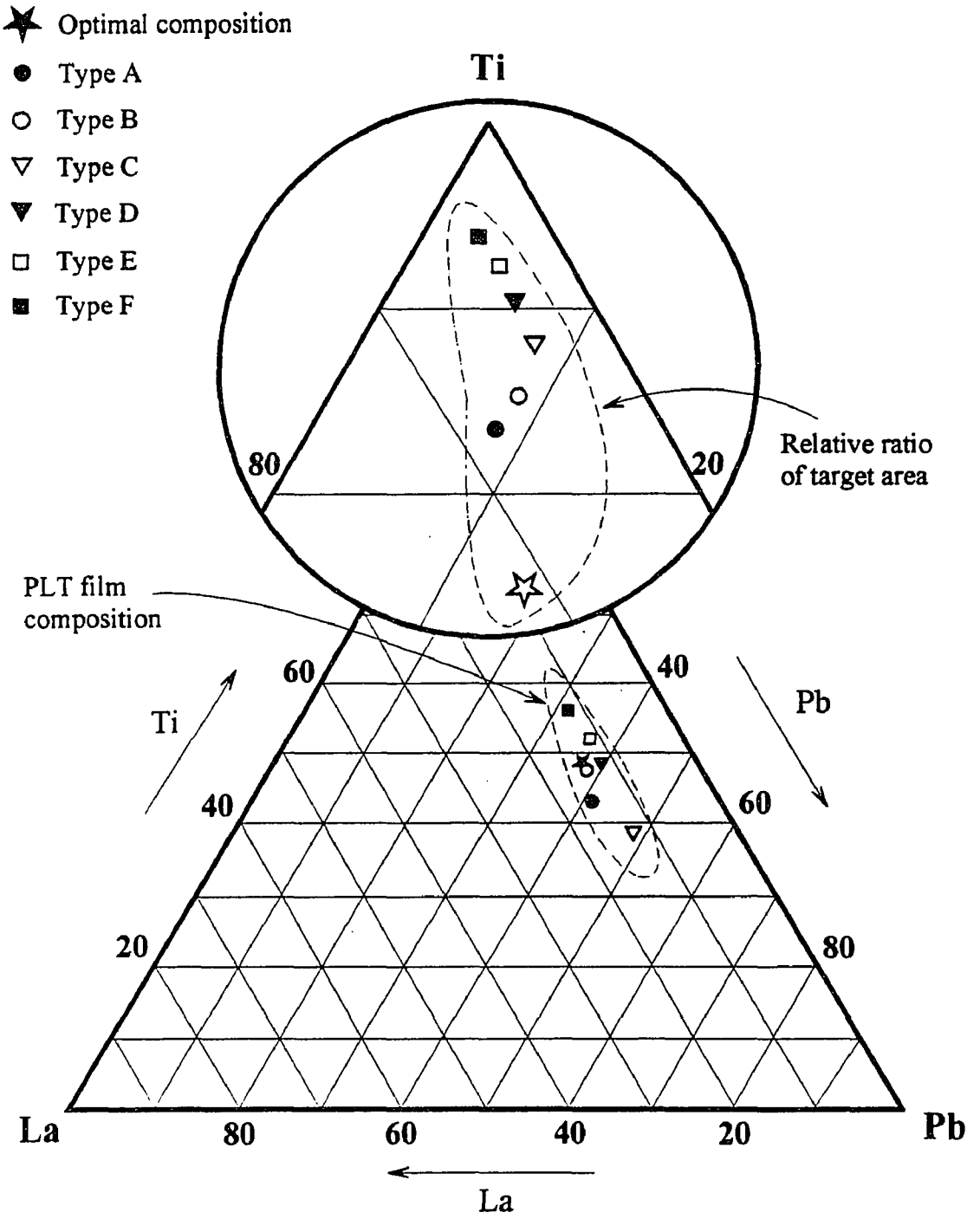

Figure 5.1 Relationship between the relative composition of sputtered PLT films and the corresponding area ratio of multi-component metal target.

Table 5.3 Relative composition of PLT thin films by AES analysis, and the corresponding area ratio of multi-component metal target.

Types	Relative ratio of target area			Relative ratio of deposited film			Chemical composition		
	Pb	La	Ti	Pb	La	Ti	Pb	La	Ti
A	8.38	5.85	85.76	38.62	14.81	46.56	0.72	0.28	0.88
B	7.60	7.80	84.60	41.14	16.00	42.86	0.72	0.28	0.75
C	7.60	4.41	87.97	48.42	12.67	38.91	0.72	0.19	0.58
D	5.19	4.41	90.41	39.74	11.97	48.29	0.72	0.22	0.87
E	3.70	4.41	91.89	36.52	12.17	53.30	0.72	0.24	1.00
F	2.77	4.41	92.83	32.08	11.67	56.25	0.72	0.26	1.25
Ideal ratio	14.08	11.70	74.22	37.31	14.51	48.19	0.72	0.28	0.93

characteristics, consequently, depend on the paraelectric perovskite phase. In order to compare the AES analysis of the PLT thin films with the chemical composition by the general formula of the PLT system ($Pb_{1-x}La_xTi_{1-x/4}O_3$; La content of 28 mol %), the accurate coefficients of the stoichiometric composition (Pb, La, Ti and O) for the perovskite structure (ABO_3) should be 0.72, 0.28, 0.93 and 3, respectively. The close composition of PLT films, as shown in Figure A.7 (a), is Pb of 0.73, La of 0.28, Ti of 0.88 and O of 2.9. In conclusion, the observed composition of the AES analysis shows that the PLT (28) film deposited reactively by the multi-component metal target using a magnetron sputtering system has a close stoichiometric composition. Furthermore, the criterion of RBS analysis provides accurate quantitation in chemical composition of the paraelectric PLT films to act as standards for AES characterization.

5.2 Crystalline Structure Analysis

5.2.1 Annealing Temperature Effect

The crystalline structure of the films is examined by X-ray diffractometer (XRD; 30 KV, 20 mA) using Cu Kα radiation. The effect of a post-annealing treatment on XRD patterns of paraelectric PLT thin films is presented in Figure A.11. The preparation of these films is of the same thickness (200 nm) and annealed for the same time (5 min). The accurate composition of these films belongs to the type D as shown in Table 5.3. As-deposited PLT films produce XRD spectrum consistent with an amorphous structure. The formation of a broad hump in the films treated annealing temperature below 450 °C shows around $2\theta = 30°$ as shown in Figure A.11 (a). It has been reported that the structure of PLT films under a heat treatment of low temperature may correspond to the metastable pyrochlore phase [42,81]. The general formula of the pyrochlore is $A_2B_2O_7$. The (100) and (110) peaks do not appear clearly in as-deposited films. After PLT films are annealed at a temperature above 550 °C, XRD patterns exhibit the formation of the stable

perovskite phase as shown in Figure A.11 (b), (c) and (d). Tetragonal splitting peaks of perovskite structure are not observed on the XRD spectra of PLT films. Typical diffraction peaks of the cubic perovskite phase such as (100), (110), (200) and (211) orientation arise completely in all PLT films. The other peaks are identified as related to the substrate, either Pt or Si. It seems that the intensity of each peak in XRD patterns increases up to the highest temperature of 750 °C. The numerical data of XRD patterns, as shown in Figure A.11, are also summarized in Table 5.4. The effect of heat treatment with increasing annealing temperature results in the increasing intensity for each peak, while FWHM of each diffraction peak seems to be gradually reduced. Also, it is certainly observed that the angular shifting of all diffraction peaks trends toward a higher angle with an increase of post-annealing temperature. It is expected that the films may be influenced by changes of internal stress with increasing temperature [82] or by reduction of the amount of Pb element incorporated within the cubic perovskite structure [22].

Figure A.12 shows the XRD spectra of the paraelectric PLT films as a function of annealing temperature for crystallization. The preparation conditions of these films are the same; i.e., same thickness (200 nm) and same annealing time (5 min). The chemical composition of these films belongs to the type A as illustrated in Table 5.3, and in particular the film annealed at 650 °C exhibits the diffraction pattern with the stoichiometric composition of $Pb_{0.73}La_{0.28}Ti_{0.88}O_{2.9}$. As-deposited PLT film presents the broad amorphous pattern, and the (111) main peak and (200) peak of platinum (Pt) are uniquely observed. Schwartz et al [43] and Dana et al [83] found that the (200) peak of Pt was also detected in the XRD spectrum of the as-deposited PLT thin films with a thickness of about 400 nm. On the contrary, Shimizu et al [81] reported that the Pt (200) peak was not observed in the as-deposited PLT films with a thickness greater than 500 nm, and conversely the (200) peak of the perovskite PLT structure appeared only around $2\theta = 45.5$ with a heat treatment of high temperature (up to 900 °C). It is expected, as a

Table 5.4 The detailed XRD data for the results of Figure 5.10.

Orientation / Annealing temp.	(100)			(110)			(200)			(211)		
	2θ	Intensity	FWHM	2θ	Intensity	FWHM	2θ	Intensity	FWHM	2θ	Intensity	FWHM
450 °C	—	—	—	—	—	—	46.3	339.9	0.337	57.1	6.1	0.420
550 °C	22.3	13.2	0.279	31.9	24.3	0.435	46.1	227.1	0.288	56.1	8.0	0.434
650 °C	22.5	10.2	0.530	32.0	26.6	0.398	46.3	249.2	0.330	57.2	8.2	0.730
750 °C	22.6	57.2	0.232	32.1	21.1	0.347	46.4	421.5	0.279	57.5	13.2	0.430

result of this study, that Pt (200) peak and PLT (200) peak of the XRD patterns may be overlapped like the results of Schwartz et al and Dana et al.

The paraelectric perovskite phase according to the XRD patterns is detected for all films in the temperature range of 550 to 750 °C. The trend of these XRD patterns corresponds relatively to those of Figure A.11. The film annealed at 650 °C shows a small (210) orientation peak of the cubic perovskite structure. Also, the intensity of each diffraction peak is directly proportional to the effect of rising annealing temperature. The sharpness of the peaks indicates good crystallinity in the perovskite PLT films. The heat treatment of PLT (28) thin films at 650 °C for 5 min results in the formation of the paraelectric perovskite structure with a lattice constant of $a = c =$ 0.394 nm and oxygen-to-oxygen distance of 0.279 nm.

Figure A.13 demonstrates XRD step scans over the angular range from $2\theta = 54$ to $2\theta = 59$ in order to observe the (211) peak shift of the films annealed at 550, 650, and 750 °C. This peak shifts from d = 0.1633 nm to d = 0.1609 nm with a rise of annealing temperature. It seems that the slight shift is due to the changes of compressive stress in the internal film and Pb evaporation within the perovskite phase with increasing temperature.

Figure A.14 presents the diffraction pattern as a function of temperature for the PLT films of a chemical composition type B as shown in Table 5.3. At 550 and 650 °C, both PbO around $2\theta = 30$ and polycrystalline perovskite phases coexist, because of the excess Pb content as shown in Figure 5.1. The perovskite peaks are observed at 750 °C only, and the PbO peaks completely disappear at high temperature. Sayer [61] reported that the crystallization of amorphous ferroelectric films was initiated around 400 °C and completed between 600 and 700 °C, depending on the film preparation method and annealing conditions. It is suggested that, for a good characteristic of PLT thin films, the relationship between the composition and the crystal structure caused by Pb evaporation is interdependent .

Figure A.15 illustrates the XRD spectra of PLT thin films on a single-crystal MgO (100) substrate. As-deposited film shows only one peak of MgO substrate and amorphous phase along the diffraction spectrum. Two peaks of the perovskite PLT film appear, and their intensities are increased with changes of annealing temperature. It is thought that the PLT films deposited on MgO substrate suffer compressive stress along the crystalline plane of the films by an annealing heat treatment. Hence, this stress may transform the polycrystalline films into c-axis and a-axis oriented films [84].

5.2.2 Annealing Time Effect

Figure A.16 shows the XRD patterns of the perovskite films as a function of annealing time at the annealing temperature of 650 °C. As-deposited film is obviously amorphous, and the (111) peak of platinum and other substrate peak is observed. In the PLT (28) thin films annealed at 650 °C, an elevated annealing time shows only the typical formation of the perovskite phase, and the intensity of the diffraction peaks increases further. It is apparent that the slight shift of typical PLT peaks occurs in the films annealed for a prolonged annealing period.

5.3 Surface Microstructure Analysis

It is known that as-deposited thin film presents microstructures of densely packed fiber with a smooth surface as shown in SZM zone I or zone T of Figure 2.4 [27]. The as-deposited PLT film is smooth and shows a featureless surface as exhibited in Figure A.17. This shiny morphology of the as-deposited films is expected to be modified by a post-annealing treatment. Figure A.18 presents a typical SEM topography for the PLT thin film annealed at 650 °C for 5 min. It is likely that the film surface is also relatively smooth, and belongs to the SZM zone II. The segregation phenomena on the delimiting surface of the PLT (28) thin film annealed at 750 °C for 5 min are shown in Figure A.19. Murakami et al [85] and Opila [86] have reported that the segregation along grain

boundary appears frequently in Pb-based ceramic films in the presence of oxygen due to Pb evaporation. It is suggested that this phenomena occurs to reduce thermal strain within the film during post-annealing treatment. However, the films deposited by substrate heat treatment shows relatively less segregation because the phase formation grows slowly without the evidence of a remarkable grain boundary.

Figure A.20 (a) and (b) show cracking on the multi-layer substrate and a lack of adhesion on MgO substrate in terms of the post-annealing treatment of high temperature at 750 °C for 60 min. High temperature annealing, in particular, results in thermal segregation by Pb evaporation and grain densification, and finally leads to the formation of hillocks or craters. The serious crack, caused by the prolonged heat treatment, is accelerated by thermal stress in terms of a mismatch in thermal expansion coefficients between PLT film and substrate.

CHAPTER 6

ELECTRICAL ANALYSIS AND DISCUSSION

All electrical measurements for DRAM application are performed utilizing a MDM configuration capacitor using the paraelectric PLT (28) thin films of 200 nm thick as a dielectric layer. Dielectric measurements are carried out on a Boonton 7200 capacitance meter with a peak voltage of 10 mV (i.e. 500 V/cm) and a frequency of 1 KHz. The most frequently used test to characterize ferroelectric or paraelectric PLT thin films is a typical Sawyer-Tower circuit [87]. This is an excellent measurement technique for establishing the relationship of polarization to electric field. Polarization-electric field (P-E) characteristics for charge storage density is investigated by an HP54501A digitizing Oscilloscope and Wavetek (Model 270) Function Generator. Additional electrical characteristics such as, current-voltage (I-V) plot for leakage current density and voltage-time (V-t) measurements for charging transient, are of interest for a capacitor dielectric of the 1-T DRAM cell. These topics are the subject of reliable characteristics and the transient behavior of paraelectric PLT (28) thin films. The current-voltage characteristics for leakage current density are measured by an HP4145B Semiconductor Parameter Analyzer.

6.1 Dielectric Characteristics

6.1.1 Effect of post-annealing temperature

The dielectric constant and dissipation factor (loss tangent) as a function of post-annealing temperature are presented in Figure 6.1. The dielectric constant increases significantly and the dissipation factor decreases slightly, as the annealing temperature is increased. The dielectric properties are dependent on the changes in the stoichiometric composition as

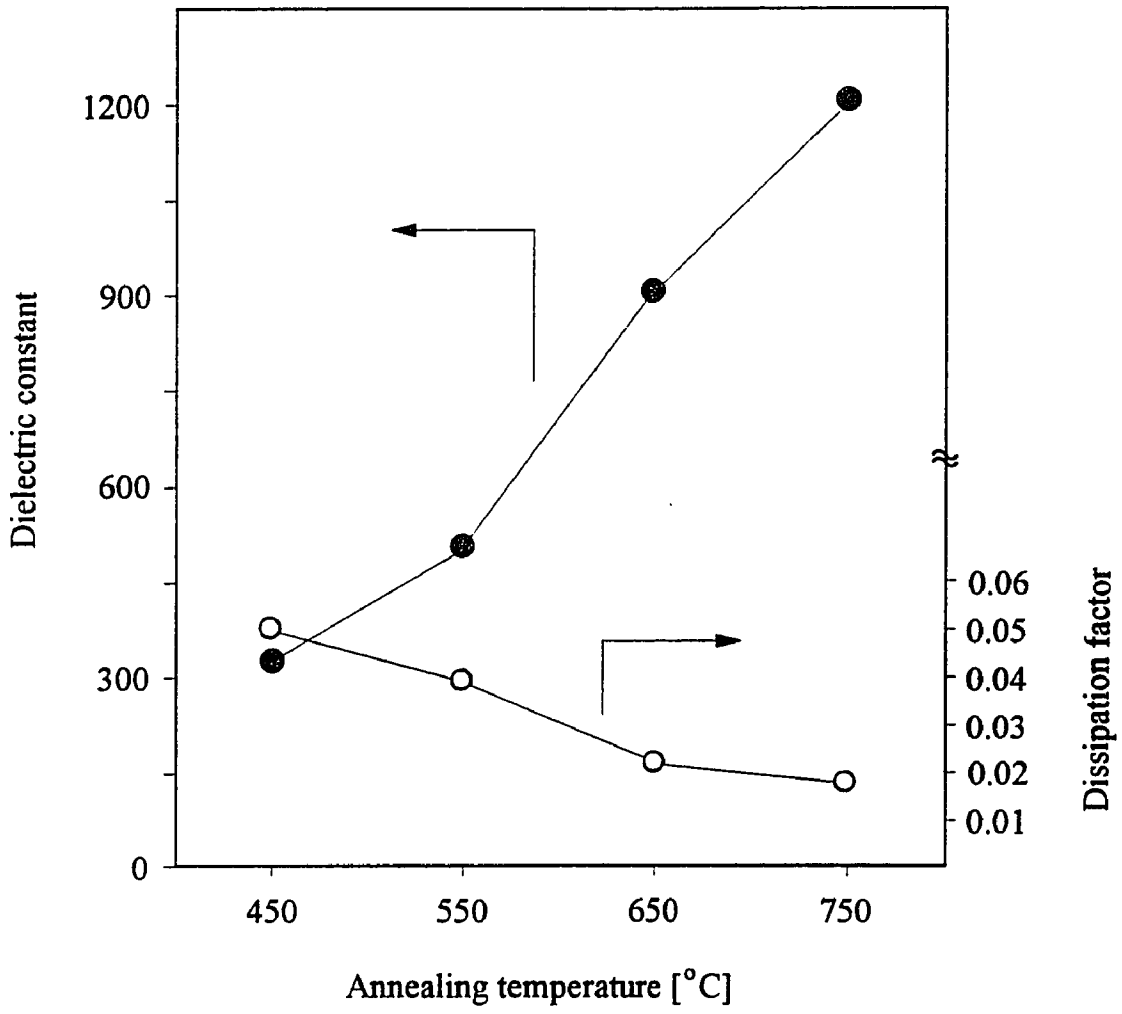

Figure 6.1 Dielectric constant and dissipation factor of PLT (28) thin films as a function of post-annealing temperature.

well as in relative quantities of amorphous and crystalline structures with variation of annealing heat treatment. Thus, with a rise in annealing temperature, the amorphous phase and the excess PbO structure with poor dielectric properties disappear and are transformed to the crystalline structure, i.e., the paraelectric perovskite PLT phase. Conversely, the dissipation factor reduces from 0.051 to 0.018 with the increasing annealing temperature, and with the dependence on the existence of the amorphous and excess PbO phases.

The dielectric constant of the PLT thin films, in this study, is sometimes difficult to measure, because of the low resistance of the films and the presence of microcracks and porosity caused by high temperature treatment. Fox et al [88] have commented that the dielectric properties can be expressed by morphological conditions of the thin films with coexistence of the three phases such as perovskite PLT phase, excess PbO and air. The excellent dielectric properties of PLT thin films are achieved by the continuity of the perovskite PLT phase. The PbO phase and porosity resulting from Pb evaporation give rise to the discontinuity of the perovskite PLT phase in the thin films. The PbO phase has a higher conductivity than the perovskite PLT phase. The dielectric constant decreases and the dissipation factor increases due to the presence of excess PbO phases in the films annealed at lower annealing temperature.

6.1.2 Effect of temperature

Figure 6.2 shows the relative dielectric constant of the PLT film annealed at 650 °C and for 5 min at the temperature range of 30~120 °C. The dielectric constant of paraelectric PLT (28) thin film decreases slightly as a function of temperature. The peak of dielectric constant, the so called Curie temperature, is not observed in this temperature range. It is expected that the dielectric peak of the film with the change of temperature is similar to the Curie temperature reported by Keizer et al [29].

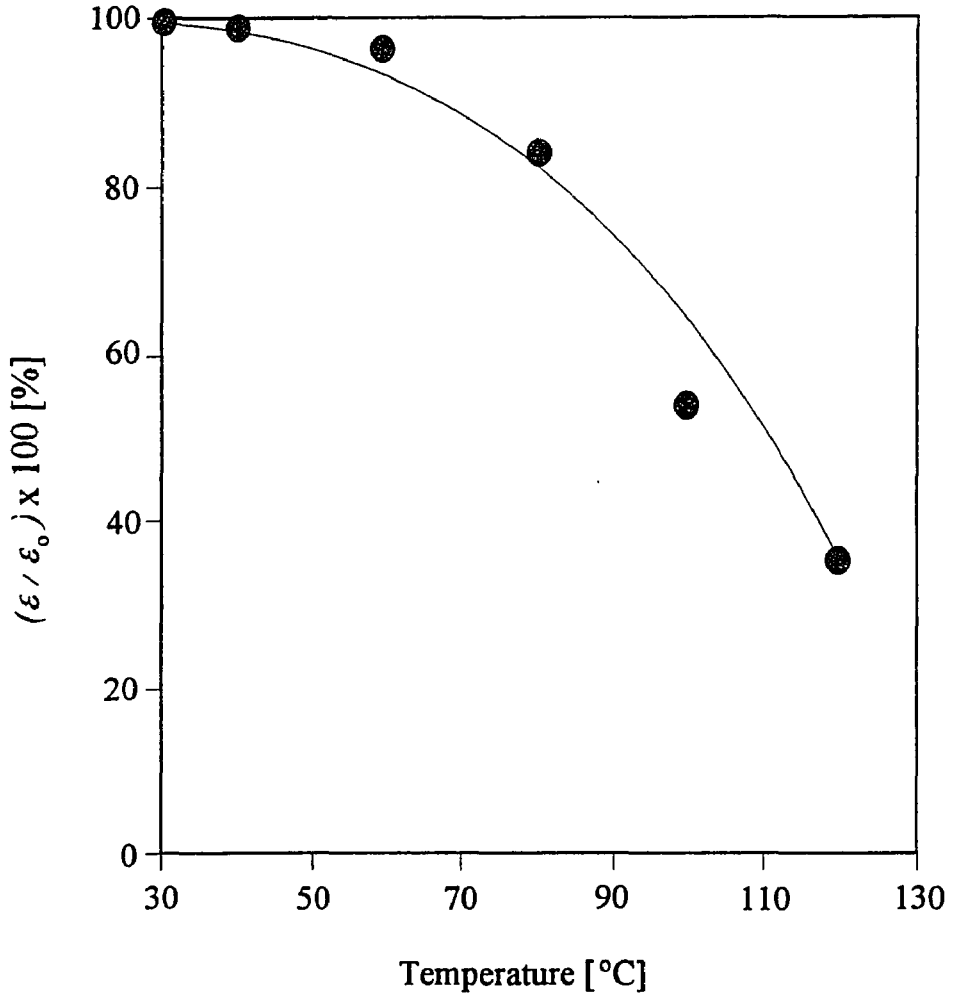

Figure 6.2 Dielectric constant of 200 nm PLT (28) thin film with different tempersture.

6.1.3 Effect of La content in PLT films

The dependence of the dielectic constant on various La concentrations of PLT thin films is demonstrated in Figure 6.3. All PLT films are annealed by the same condition of post-deposition heat treatment at 650 °C for 5 min. The dielectric constant increases with a rise in La concentration. This phenomenon results from the lowering of the Curie temperature, as shown in the results of Adachi et al [42]. This is due to the La content increases slightly in the chemical composition of the PLT films. The dielectric properties are closely related to the changes in chemical composition of PLT thin films. The dielectric constant and dissipation factor of PLT (28) thin film are around 904 and 0.023, respectively.

6.1.4 Discussion

The perovskite PLT phase, from the results of various effects mentioned above, primarily exhibits (100) orientation for nearly stoichiometric composition. However, it may be noted that small changes of the composition and crystallinity produce substantial changes in the dielectric characteristics of the PLT thin film. The main reason for a poor dielectric properties at low annealing temperature may be explained by low crystalline phases of the PLT films. Since the intensities of the perovskite phases increase with an increase in post-annealing temperature as illustrated by the results of XRD patterns, it is expected that the dielectric characteristics of paraelectric PLT thin films correspond well with the crystalline structure and the excellent dielectric properties of PLT thin films are achieved by the continuity of the perovskite structure. The best results of dielectric constant and dissipation factor at low field measurement (500 V/cm), as shown in Figure 6.1, are approximately 1216 and 0.018 in $Pt/Ti/SiO_2/Si$ substrate, respectively. Actually, the measured dielectric constant is tremendously different from the value of bulk PLT films reported by Hennings et al [22]. It is supposed that porosity and the segregation

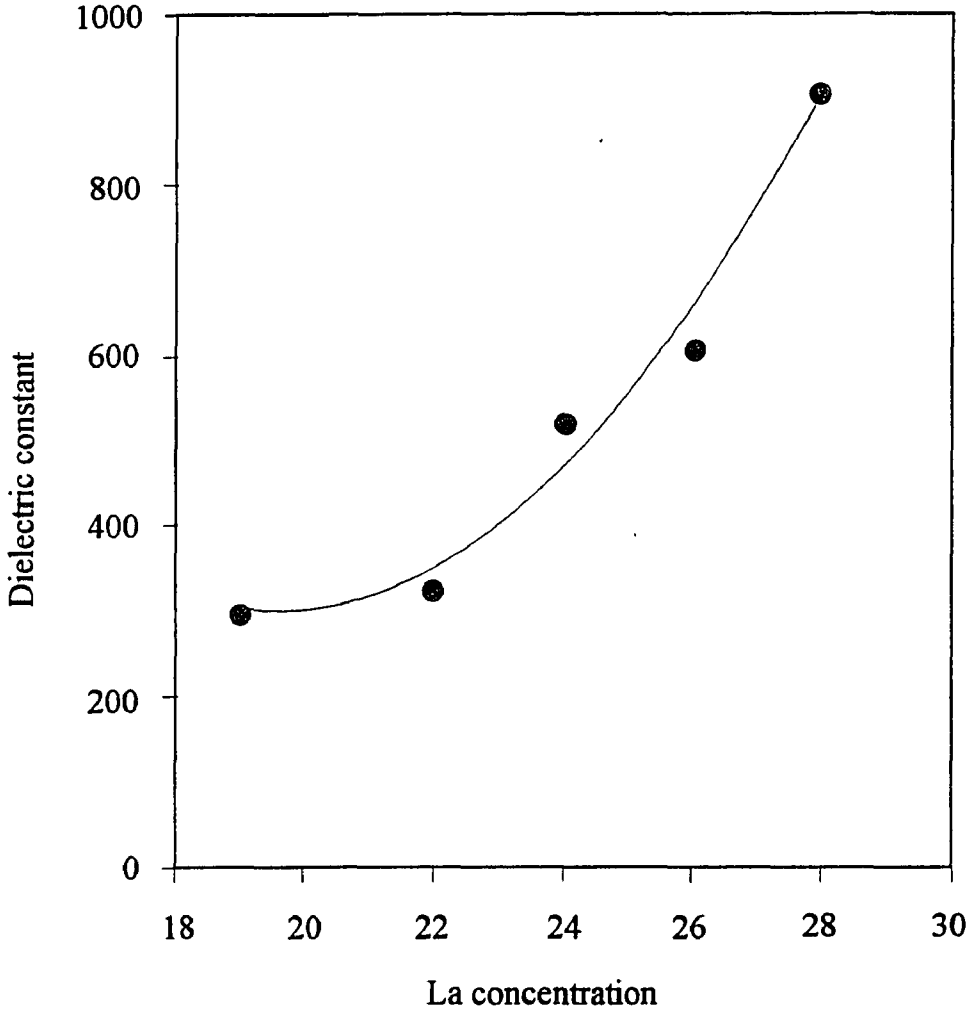

Figure 6.3 Changes of the dielectric constant with increasing La concentration of PLT films as described in Table X.

phenomena produced by Pb evaporation considerably affect the dielectric properties of PLT thin films.

6.2 Polarization-Electric Field Characteristics

The polarization-electric field (P-E) characteristics of the paraelectric PLT (28) thin films are measured using a typical Sawyer-Tower circuit with a 500 Hz sine wave as shown in Figure 6.4. The P-E measurements of the films under different peak voltages are presented in Figure B.1. The paraelectric PLT (28) thin film is annealed at 650 °C for 5 min. The P-E curve at low peak voltage of 1 V (50 KV/cm) is similar with the linear behavior of a normal dielectric material as shown in Figure B.1 (a). The P-E characteristics are gradually developed to the paraelectric state of nonlinear behavior, as the peak voltage increases enough. The charge storage density (or polarization) is around 10.3 $\mu C/cm^2$ at the peak voltage of 4 V (200 KV/cm). The polarization is proportional to the electric field, and the relative dielectric constant is constant by means of the formula, $P=\varepsilon_o(\varepsilon_r-1)E$, only at a low field. The polarization is gradually saturated with the increasing peak voltages, due to the paraelectric characteristics, and the above equation for dielectric properties can not be automatically applied to the paraelectric phase. The approximation of dielectric constant with different peak voltage is obtained by the effective dielectric constant, K_{eff}, defined as the following [20]:

$$K_{eff} = \frac{Q_C'}{\varepsilon_o E_{\max}}$$

where, Q_C' is the charge storage density, and E_{max} is the maximum electric field. The above mentioned equation shows that the effective dielectric constant is approximately 580 at a peak voltage of 4 V.

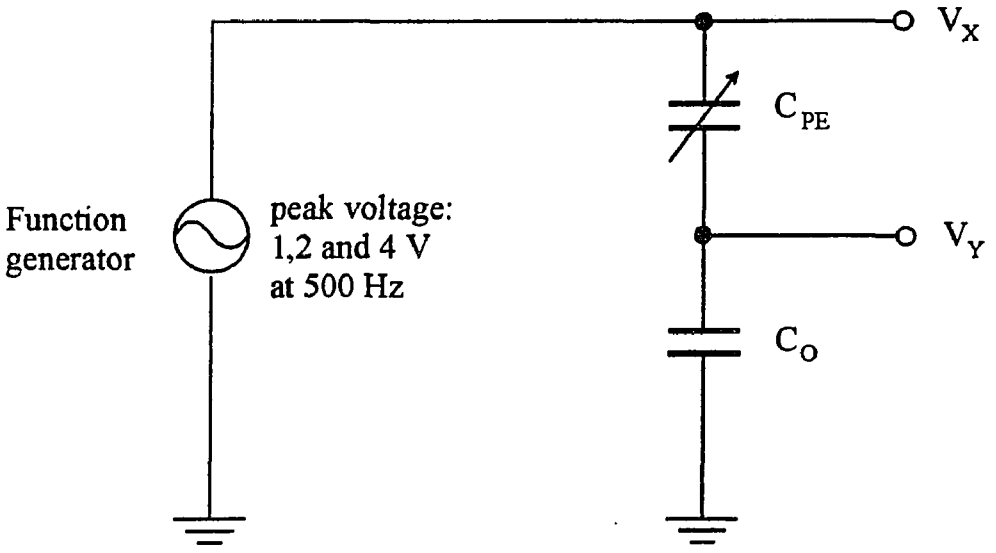

Thickness : 200 nm
Area : $3.14 \times 10^4\ \mu m^2$
C_{PE}: 1.26 and 1.69 nF
C_O: 68.7 nF

Function generator : Wavetek Model 270
Digitizing Oscilloscope : HP54501A

Figure 6.4 Typical Sawyer-Tower circuit for polarization-electric field measurement.

Figure B.2 shows the P-E characteristics with different peak voltage for the PLT (28) film heat-treated at 750 °C for 5 min. The P-E curve at a peak voltage of 2 V presents the prominent paraelectric nonlinear behavior. The charge storage density at the peak voltage of 4 V (200 KV/cm) is around 12.5 $\mu C/cm^2$ as shown in Figure B.2 (c), and the effective dielectric constant is about 706. Figure B.3 describes the P-E characteristics as a function of annealing temperature at the same peak voltage of 4 V. The formation of the paraelectric state in PLT (28) films with increasing post-annealing temperature is obvious at a glance from this Figure. It is expected that some degree of crystallinity, with different annealing temperature, has an influence upon the paraelectric nonlinear characteristics of the films.

Recently, Adachi et al [1] reported that the polarization of PLT (28) thin films exhibited a slim hysteresis loop. But the La contents of 28 mol % in their films were the chemical composition in the powder target of rf-magnetron sputtering. Therefore, the La contents of PLT thin films were practically lower than those of target material, and their P-E hysteresis with slim loop obviously showed the ferroelectric behavior of PLT thin films.

6.3 Leakage Current Characteristics

The leakage current density is one of important limiting factors for the DRAM capacitor dielectric. High leakage current places important limitation in the operation of a unit cell. It is necessary, to prevent the capacitor from discharging between refreshing cycles, that the leakage current per unit area should be low. There are several transport mechanisms of leakage current in a MDM capacitor [38,89], and also there are two distinct regions specified by the electric field. Ohmic behavior is the dominant process at low electric fields. The leakage current density of ohmic characteristics is expressed:

$$J = A\frac{E}{kT}\exp\left[\frac{-E_a}{kT}\right]$$

where, E is the applied electric field,

A is a constant related to thermally excited electron hopping, and

E_a is the activation energy.

Under high fields, the leakage current exhibits exponential behavior which is governed by oxygen vacancy diffusion, space charge limit current injection, grain boundary potential barrier, tunneling, Schottky emission, or Poole-Frenkel emission [90]. The leakage current characteristics of PLT thin films vary exponentially with the square root of the electric field. This is mainly due to Schottky emission or Poole-Frenkel emission of the various mechanisms at high electric fields. Schottky emission occurs at the contact interface between the paraelectric film and electrode, and Poole-Frenkel emission occurs largely in the bulk film. The Schottky emission is analogous to thermionic emission and governed by the following equation [89]:

$$J = A^* T^2 \exp\left[\frac{-q(\phi_B - \sqrt{qE/4\pi\varepsilon_i})}{kT}\right]$$

where, A^* is the effective Richardson constant,

ϕ_B is the Schottky barrier height,

E is the applied electric field, and

ε_i is the dynamic permittivity of insulator.

The leakage current density as a function of post-annealing temperature is shown in Figure B.4. The leakage current density diminishes slightly except at 750 °C, as the post-annealing temperature increases. The lowering trend of leakage current with different annealing temperature at the electric field of 150 KV/cm (3 V) is presented in Figure 6.5. It is noted, from the XRD patterns analysis as shown in Figure A.12, that the leakage

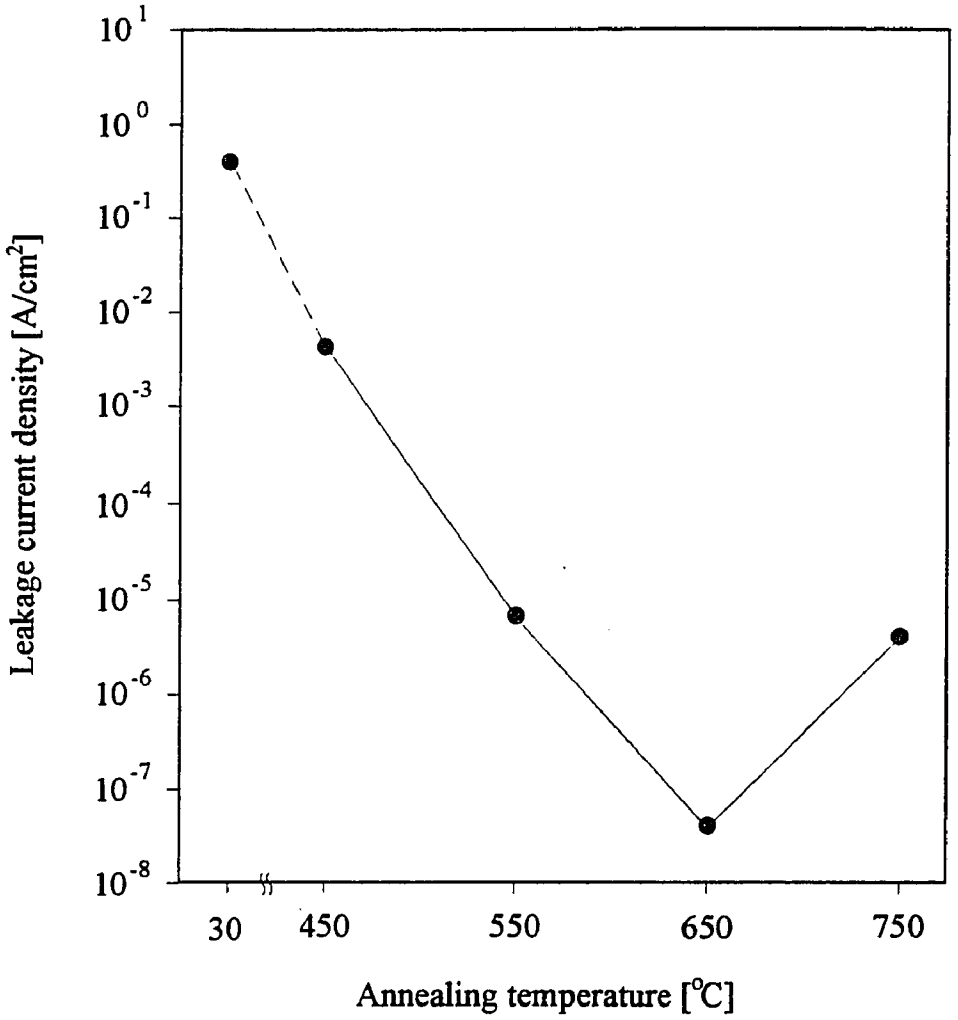

Figure 6.5 Leakage current density as a function of annealing temperature for PLT films at 150 KV/cm (3V).

current density with the increasing annealing temperature is closely related to the degree of crystallinity. Since the intensity of each diffraction peak is proportional to the effect of a rise in post-annealing temperature, the paraelectric PLT (28) thin films are further crystallized into the cubic perovskite phase. The PLT thin film annealed at 750 °C exhibits larger leakage current density than that at 650 °C. This elevation in leakage current observed at high heat treatment shows a similar tendency with the results from Chikarmane et al [91], suggesting that the vaporization of Pb at high annealing temperature leads to the augmentation of oxygen vacancies. It is almost certain, from the results mentioned above, that the optimization between minimum leakage current density and maximum charge storage density is essentially adjusted by the conditions of the post-deposition annealing process.

Figure B.5 shows the dc voltage-induced resistance degradation and the dielectric breakdown in the paraelectric PLT thin film (200 nm) annealed at 650 °C. The leakage current is 85 nA (2.5 $\mu A/cm^2$) at a reference voltage of 5 V. The resistance degradation starts slowly at 5 V (250 KV/cm) prior to the dielectric breakdown at 13.5 V (675 KV/cm). Waser et al [92] and Baiatu et al [93] have shown that the resistance degradation in the perovskite-type titanates under dc voltage stress is closely related to the field-induced segregation of oxygen vacancies and the specific defect structure in the films. The oxygen vacancies, since they are positively charged, tend to segregate toward the cathode under dc voltage stress. According to the theory proposed by Waser et al., such a field-induced segregation results in the growth of the n-conducting cathodic region toward the anode, and then leads to resistance degradation. A positive polarity in the top electrode leads to a rapid reduction of the oxygen vacancies, and this results in the fast growth of the cathodic n-type region toward the top electrode. It is supposed that the dc voltage-induced resistance degradation, in this study, is observed at a somewhat low electric field because the top electrode is biased positively.

Figure B.6 shows the static current-voltage curves for different delay times with a 5 second interval. The I-V characteristics are carried out by a non-switching static current measurement using a HP4145B Semiconductor Parameter Analyzer. The static current is measured by applying a dc bias from 0 to 20 V, and increasing in 0.09 V steps. These measurements are typical of a virgin PLT thin film with a paraelectric perovskite structure. The films are heat-treated at 650 °C for 5 min and its thickness is 200 nm. The static current with repeating delay time decreases at a region of the electric field lower than 2 V (100 KV/cm). However, the static current increases at a moderately high electric field above 2 V. The decreasing static current with a prolonged delay time is due to the fast response at the low voltage under 2 V. The leakage current at the higher voltage is slightly increased, because the PLT thin film is degraded by fatigue effects of the unipolar stress. Duiker et al [94] has observed that this fatigue effect is caused by the increase of the space-charge regions near the electrodes or the oxygen-deficient dendrite growth.

6.4 Voltage-Time Measurements

Voltage-time (V-t) characteristics are another method used to estimate the charge storage density which is calculated from the transient response of a MDM capacitor using the unipolar pulse measurement technique. The switching voltage is monitored with an oscilloscope by measuring the voltage drop across a grounded resistor in series with the film capacitor. Figure 6.6 (a) shows the schematic test circuit with a peak voltage of the unipolar pulse and a 1 KΩ load resistor as a series resistance to simulate the transistor of the DRAM unit cell. The charge storage density is gained by the estimation of the triangular area as shown in Figure 6.6 (b). The switching time (t_S) is defined as the time that decays to a point 90 % down from the maximum current transient value. The simple approximation for the charge storage density is estimated as the following [20]:

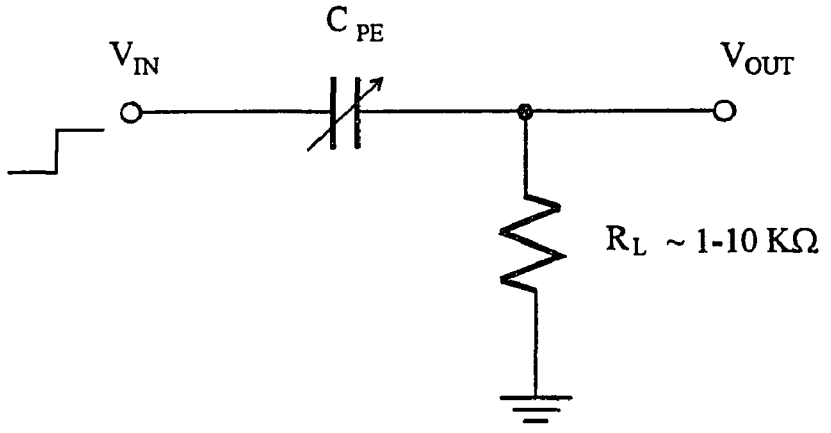

(a)

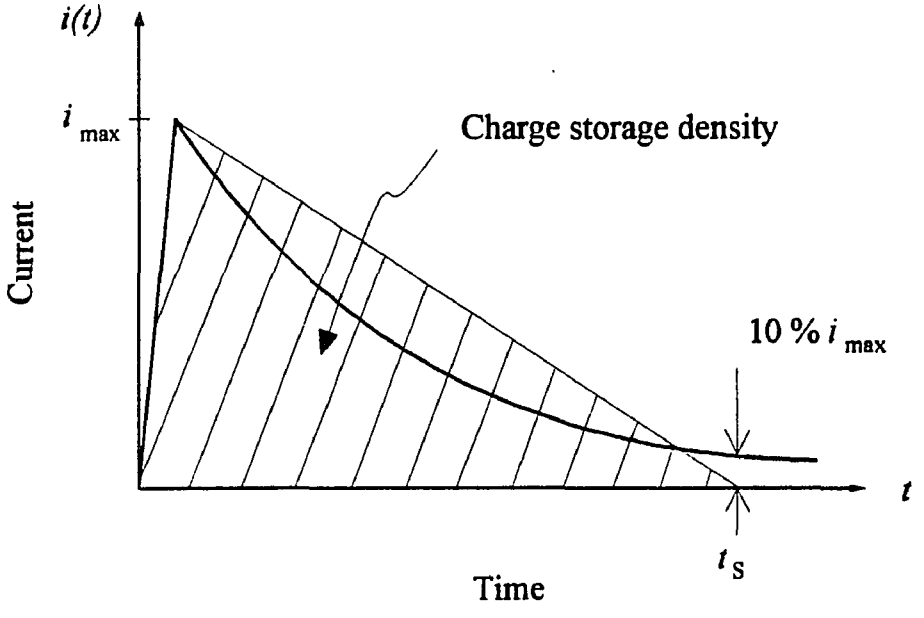

(b)

Figure 6.6 (a) Schematic test circuit with a peak voltage of unipolar pulse and a load resistor, (b) the estimation of triangular area from transient response of I-t curve shows charge storage density.

$$Q_C' = \frac{1}{A}\int i\,dt = \frac{1}{A}\int_0^{\infty} \frac{V_{max}}{R_L} e^{-\frac{t}{\tau}}\,dt$$

$$\cong \frac{V_{max} t_s}{2R_L A}$$

where, V_{max} is the maximum response voltage,

R_L is the load resistance, and

A is the area of the paraelectric MDM capacitor.

The transient response is nearly exponential as shown in Figure 6.6 (b).

Figure B.7 presents the voltage-time curves with the different peak voltage of the unipolar pulse experiments for the estimation of charge storage density and charging time. The triangular area (i.e., charge storage density) is also increased, as the peak voltage of unipolar pulse increases. The detailed results, compared with the data of P-E measurements, are summarized in Table 6.1. It is noted that the charge storage density is 11.3 μC/cm^2 at 4 V (200KV/cm) peak voltages. The charge storage density estimated by the above equation produces an inaccuracy of about 9.7 % by comparison with the P-E characteristics. The charging and discharging times are an important parameter in determining the speed of a MDM capacitor in a DRAM unit cell. The total charging time (t_T) of the capacitors using paraelectric PLT thin films is expressed by:

$$t_T = t_C + t_P = 2.303(R_L C_{eff}) + t_P$$

where, $C_{eff} = \frac{\varepsilon_r \varepsilon_o AE}{d}$,

and t_P is the time of parasitic capacitance due to test setup. Lee et al [40] reported that t_P was estimated to be 0.7 μsec for a capacitor area of 10000 μm^2. The charging and discharging times are dependent significantly on the electrode area, so that the switching

Table 6.1 Charge storage density calculated by V-t measurement in comparison with the results of P-E measurement.

Peak voltage (V)	Electric field (KV/cm)	V-t plot		P-E plot	
		Charge density ($\mu C/cm^2$)	Dielectric constant	Charge density ($\mu C/cm^2$)	Dielectric constant
1	50	5.22	1179	3.2	723
2	100	6.80	768	6.0	678
3	150	8.59	647	—	—
4	200	11.3	638	10.3	580
5	250	13.26	599	—	—

time decreases with a decrease of the electrode area. Larsen et al [95] reported that it was difficult to take measurements for the small capacitor area of a MDM capacitor due to the above-mentioned parasitic capacitance as well as the limitation of the measuring system's respond time.

Figure B.8 shows the switching time response characteristics as a function of load resistance under the same peak voltage of 4 V (200 KV/cm). The smaller the load resistance, the faster the switching time response as shown in this Figure. The transient response is governed by the following:

$$i(t) = I_P \exp\left[-\frac{t}{t_T}\right]$$

where, $t_T = 2.303 R_L C_{eff} + t_P$ and I_p is the maximum current. The switching time response in Figure B.8 appears to correspond to the above equation.

CHAPTER 7

SUMMARY AND CONCLUSIONS

7.1 Summary

Since thin film material with extremely high dielectric constant was required in high density capacitor of ULSI DRAM cell, lanthanum modified lead titanate (PLT; $Pb_{1-X}La_XTi_{1-X/4}O_3$) thin films prepared by various deposition techniques have been concentrated as an attractive candidate. In this research, paraelectric PLT thin films were fabricated in a unique way by reactive magnetron sputtering system using a multi-component metal target which was designed in our laboratory. The content of Pb in the sputtering target appeared to play an important role in the film growth. As-deposited PLT thin films were annealed to cause crystallization into paraelectric perovskite structure at temperatures ranging from 550 to 750 °C.

The chemical composition, crystalline structure and surface morphology of the films were extensively investigated. The semiquantitative analysis of stoichiometric composition, based on RBS data for a standard PLT film, were measured by AES. The best stoichiometric composition observed by AES analysis was Pb, 0.73; La, 0.28; Ti, 0.88; and O, 2.9. The relations of composition, crystalline structure and microstructure in paraelectric PLT thin films annealed by a heat treatment appeared simultaneously important from the results of XRD and SEM. The as-deposited films were altered during post-deposition annealing by the inter-dependent relationship between composition and crystalline structure through Pb evaporation.

The dielectric and electrical characteristics of paraelectric perovskite PLT thin films were conducted under different post-annealing conditions. The dielectric constant increased significantly and the dissipation factor decreased slightly, as the post-annealing temperature increased. The dielectric properties of PLT films were also exhibited as a

function of La content in the general formula of Pb-La-Ti-O system. The dielectric constant increased with a rise in La concentration. The best results of dielectric constant and dissipation factor in the paraelectric capacitor, at low field measurement of 500 V/cm (10 mV), were 1216 and 0.018, respectively. The measured dielectric constant was tremendously different from the value of PLT bulk films reported by Hennings et al [22]. This is due to porosity and segregation phenomena caused by Pb evaporation in post-deposition annealing treatment.

The charge storage density (Q_c') of the film annealed at 650 °C was 10.3 μC/cm^2 at the peak voltage of 4 V. The charge storage density at 750 °C was 12.5 μC/cm^2, and then the effective dielectric constant was about 706. The leakage current density was ordinarily observed to decrease as the annealing temperature increased. But the leakage current for PLT film annealed 750 °C was higher than that of the film heat-treated at 650 °C. The optimal relationship between minimum leakage current density and maximum charge storage density was chosen by the adjustable conditions of the post-annealing technique. Voltage-time (V-t) measurement was also an important tool to determine the charge storage density and the transient response of the paraelectric PLT capacitor. The charge storage density was approximately 11.3 μC/cm^2 at 4 V peak voltage. This estimated value produced an inaccuracy of about 9.7 % in comparison with the value of P-E measurement. The electrical characteristics of paraelectric PLT thin films for the capacitor dielectric of a DRAM cell were compared in Table 7.1 with the results published by other researchers. The results of dielectric constant and leakage current density in PLT films were generally better than those of PZT films for ULSI DRAM applications. But it seemed that the charge storage density of PLT and PZT thin films was somewhat less than the value required in the planar capacitor of 1-T DRAM cell.

In summary, fabrication of the ternary compound PLT thin film could be easily controlled by each metal element on the target. Post-annealing treatment should be optimized as significant factors to improve the dielectric properties and electrical

Table 7.1 Electrical Characteristics in recent researches of PT family for DRAM applications.

Ref./Year	Deposition	Material (La/Zr)	Thickness (μm)	ε_r / $tan\delta$	I_{leak} (μA/Cm^2)	Q_c^* (μC/cm^2)
Watanabe (44) 1993	MOCVD	PLT (15/0)	0.25	330 0.04	N.A.	13 @0.5MV/cm
Dey (30) 1992	Sol-Gel	PLT (28/0)	0.5	1500 0.015	0.1 @5MV/cm	15 @0.2MV/cm
Khan (22) 1992	MOD	PLT (28/0)	0.35	1300 0.02	N.A.	N.A.
Adachi (1) 1991	rf-Mag. Sputter	PLT (0-42/0)	0.4	8000 N.A.	N.A.	N.A.
Schwartz (41) 1991	MOD	PLT (25/0)	0.4	690 0.03	N.A.	11.1 @0.25MV/cm
Moazzami (38) 1992	Sol-Gel	PZT (0/50)	0.2-0.6	1300 N.A.	0.1 @2MV/cm	15 @0.1MV/cm
Chikamane (3) 1992	dc-Mag. Sputter	PZT (0/65)	0.4	N.A.	0.1 @0.2MV/cm	19.6 @0.1MV/cm
Roy (15) 1992	KrF Excimer	PZT (0/52)	0.3-1	860 0.01	N.A.	18 @0.2MV/cm
Krupanidhi (8) 1992	MIBERS	PZT (0/50-56)	0.2-0.8	1150 0.019	N.A.	42 @0.6MV/cm
Carrano (20) 1991	Sol-Gel	PZT (0/50)	0.2-0.6	577 N.A.	25 @2MV/cm	15 @0.125MV/cm
Maderic (96) 1991	Sol-Gel	PZT (0/50)	0.04-0.15	N.A.	0.5 @1MV/cm	29.3 @1.2MV/cm
Sreenivas (62) 1988	dc-Mag. Sputter	PZT (0/52)	1-3.5	820 0.2	N.A.	~30 @0.1MV/cm
NJIT 1994	dc-Mag. Sputter	PLT (28/0)	0.2	1216 0.018	0.1 @0.25MV/cm	12.5 @0.2MV/cm

characteristics of the paraelectric capacitor. Thus, paraelectric perovskite PLT (28) thin films offer critical advantages over the conventional dielectrics (e.g. silicon oxide, silicon nitride and ZrO_2), and the ferroelectric thin films for ULSI DRAM applications.

7.2 Conclusions

The research showed that multi-component metal target sputtering was a promising deposition technique to grow PLT thin films with the paraelectric perovskite structure. The results of this investigation are described as follows.

(1) The paraelectric PLT thin films for the capacitor dielectric of DRAM memory cells were successfully prepared by reactive magnetron sputtering using a multi-component metal target. The individual control of each metal area on the sputtering target had considerable influence on the stoichiometry and electrical properties of the thin films. The relative ratio of each component area on the multi-component metal target was estimated by the base on the chemical composition of the deposited thin films, the sputtering yields for Pb, La and Ti metals and sticking coefficient in substrate.

(2) A post-deposition annealing treatment for the as-deposited PLT thin films affected composition, crystalline structure and surface morphology due to Pb evaporation. Single crystal film at 650 °C were smooth and the PLT thin films annealed at high temperature (750 °C) frequently exhibited segregation phenomenon along the grain boundary on the film surface. Finally, the annealing treatment for a prolonged period of high temperature led to the formation of serious microcrack and craters.

(3) The dielectric characteristics were essentially dependent on the changes in the chemical composition and crystalline phase with variation of annealing heat treatment. The dielectric constant increased significantly and the dissipation factor decreased slightly, as the post-annealing temperature increased. The dielectric constant also increased with a rise in La concentration. The best results of dielectric constant and dissipation factor in the paraelectric PLT film annealed at 750 °C were 1216 and 0.018, respectively.

(4) The best value of the charge storage density in the 200 nm PLT (28) thin film annealed at 750 °C was approximately 12.5 $\mu C/cm^2$, and the effective dielectric constant was about 706. The P-E plot at low electric field was similar with the linear behavior of a normal dielectric material, while P-E characteristics were developed to the paraelectric state of nonlinear behavior at high electric field.

(5) The leakage current density in the paraelectric PLT thin film annealed at 650°C was around 0.1 $\mu A/cm^2$ at the electric field of 0.25 MV/cm. The charge storage density by V-t measurement was about 11.3 $\mu C/cm^2$ at 4 V peak voltage. This estimated value produced an inaccuracy of around 9.7 % in comparison with the value of P-E measurement.

From the above results, the dielectric constant and charge storage density of paraelectric PLT thin films annealed at 750 °C were higher than those of the PLT films annealed at 650 °C. The leakage current density of the films annealed at 750 °C was worse value than that of the films annealed at 650 °C. Therefore, the optimization among maximum dielectric constant, maximum charge storage density and minimum leakage current density for the capacitor dielectric of a DRAM cell was essentially adjusted by the conditions of the post-deposition annealing treatment.

In conclusion, a large charge storage density, high dielectric constant and relatively low leakage current density have been illustrated in the paraelectric perovskite PLT thin films annealed under optimal conditions of post-deposition annealing treatment. Therefore, it is expected that the paraelectric PLT capacitor is an attractive candidate for potential application as capacitor dielectrics in ULSI DRAM cells.

APPENDIX A

TEST RESULTS OF PLT THIN FILM ANALYSIS

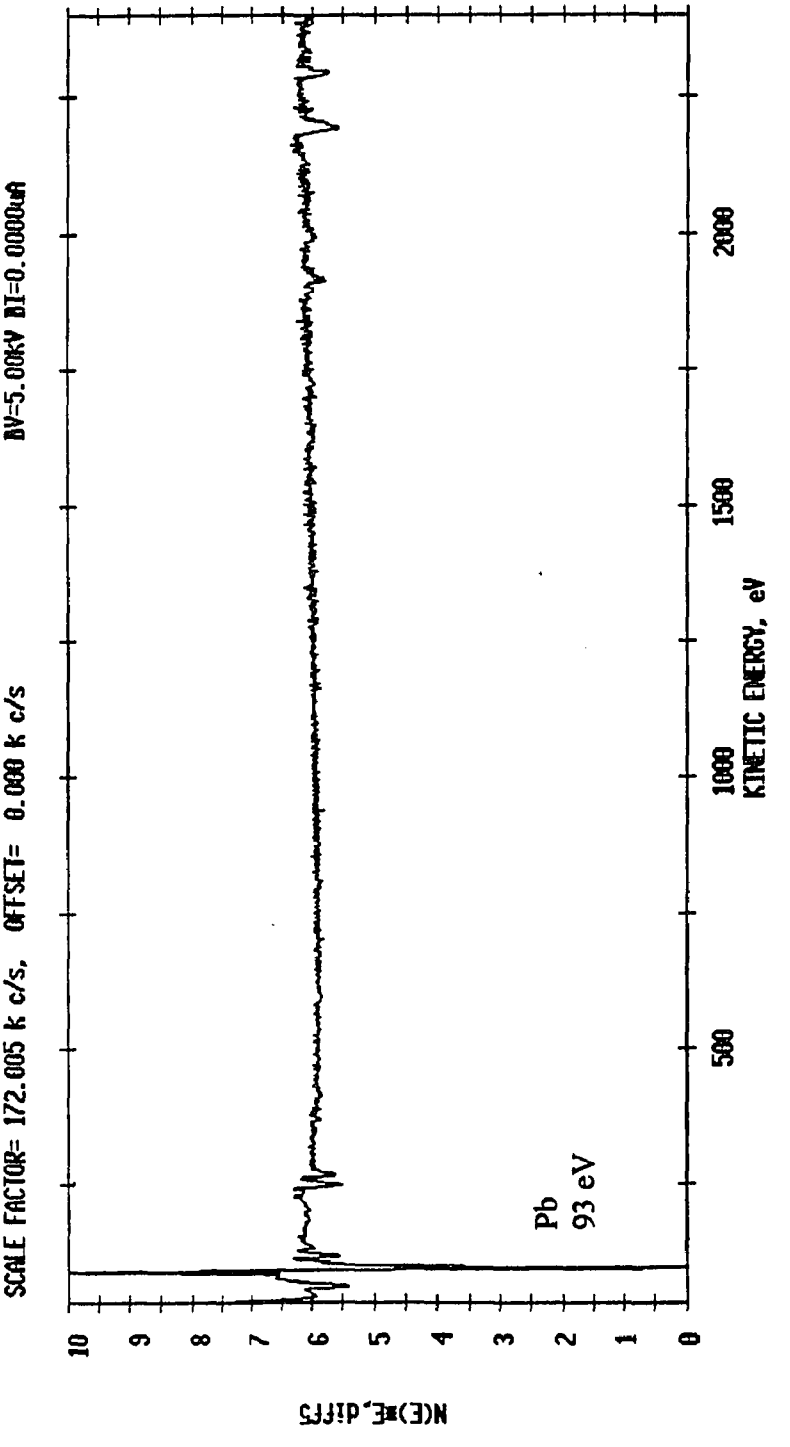

Figure A.1 Auger electron spectroscopy spectrum of pure Pb

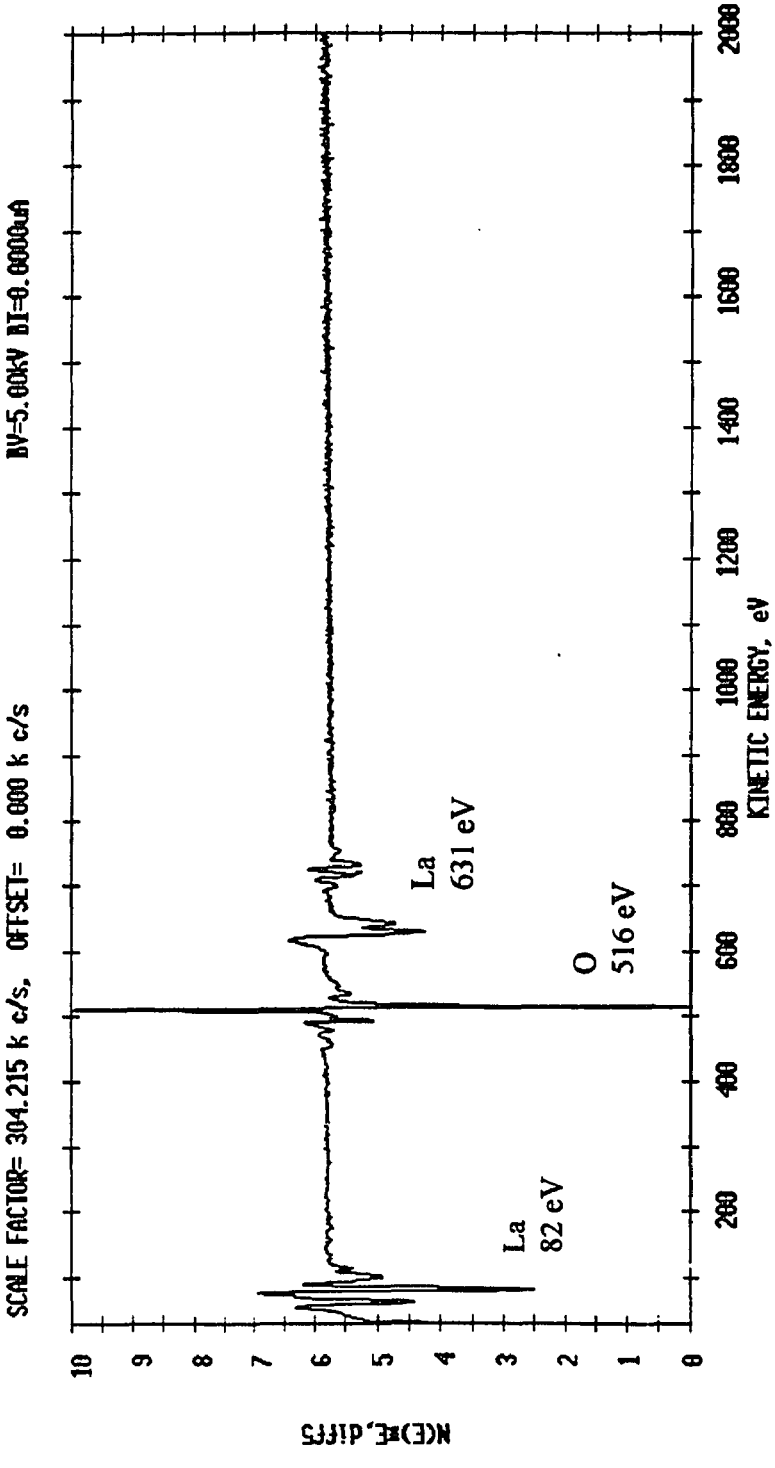

Figure A.2 Auger electron spectroscopy spectrum of pure La

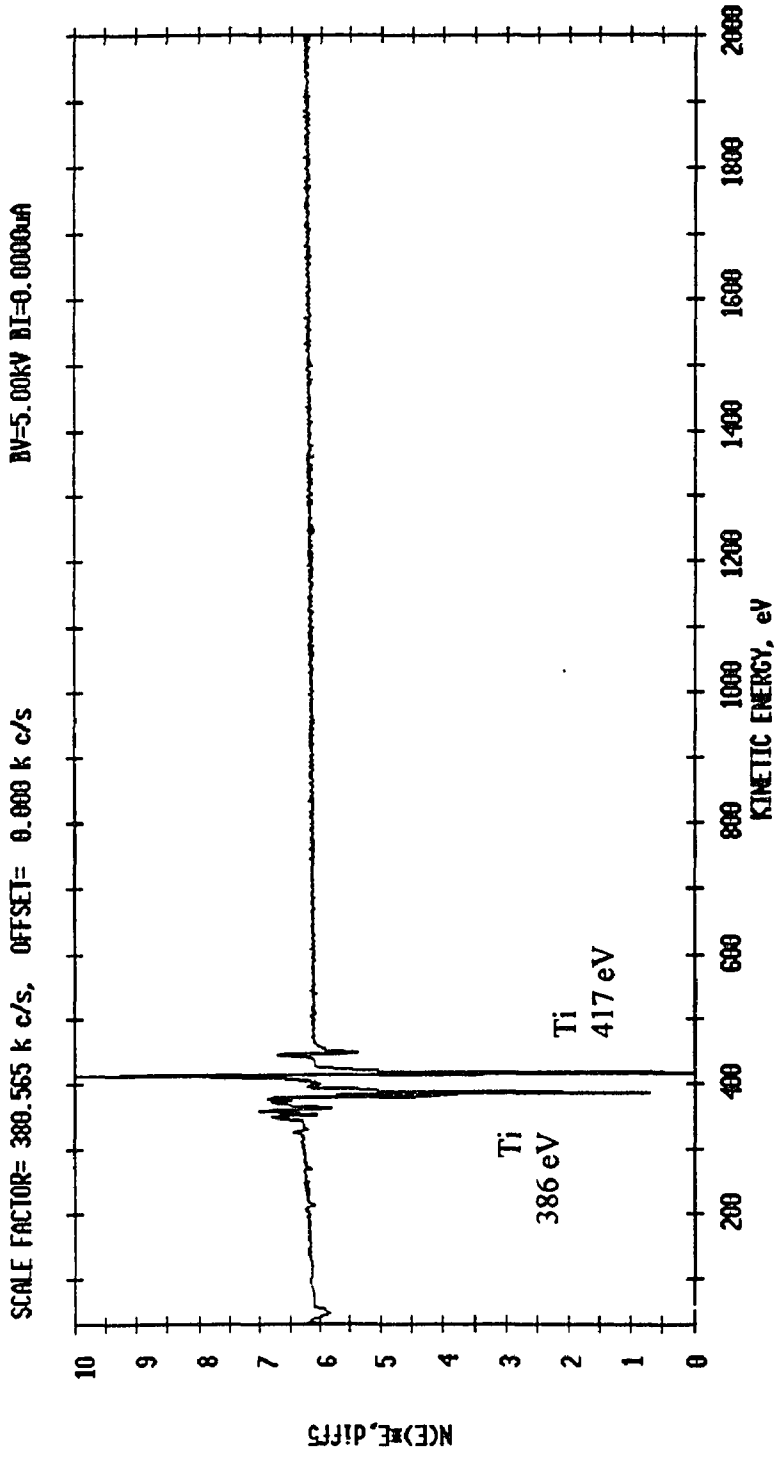

Figure A.3 Auger electron spectroscopy spectrum of pure Ti

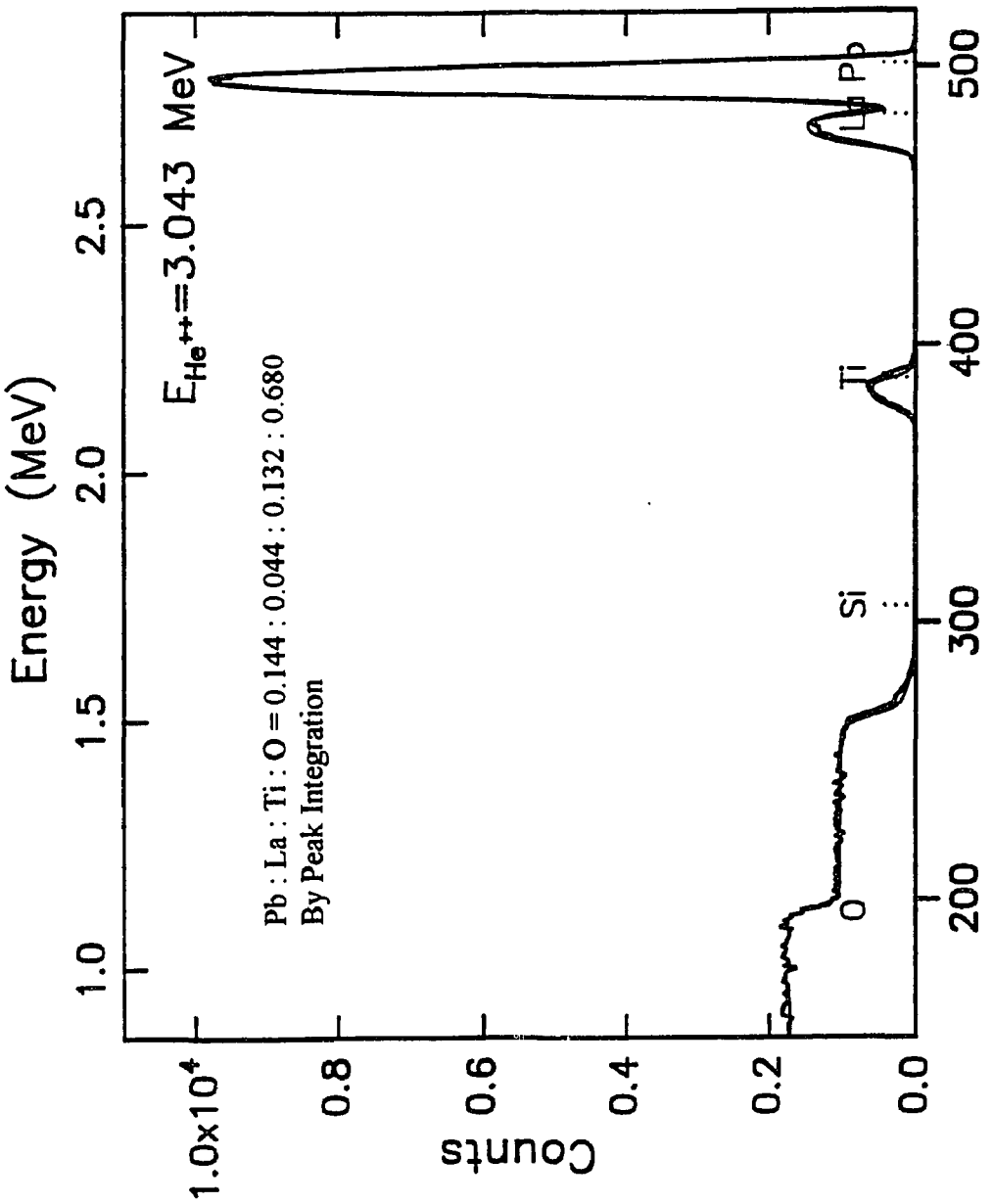

Figure A.4 Typical RBS spectrum of standard PLT film for semiquantitative AES analysis

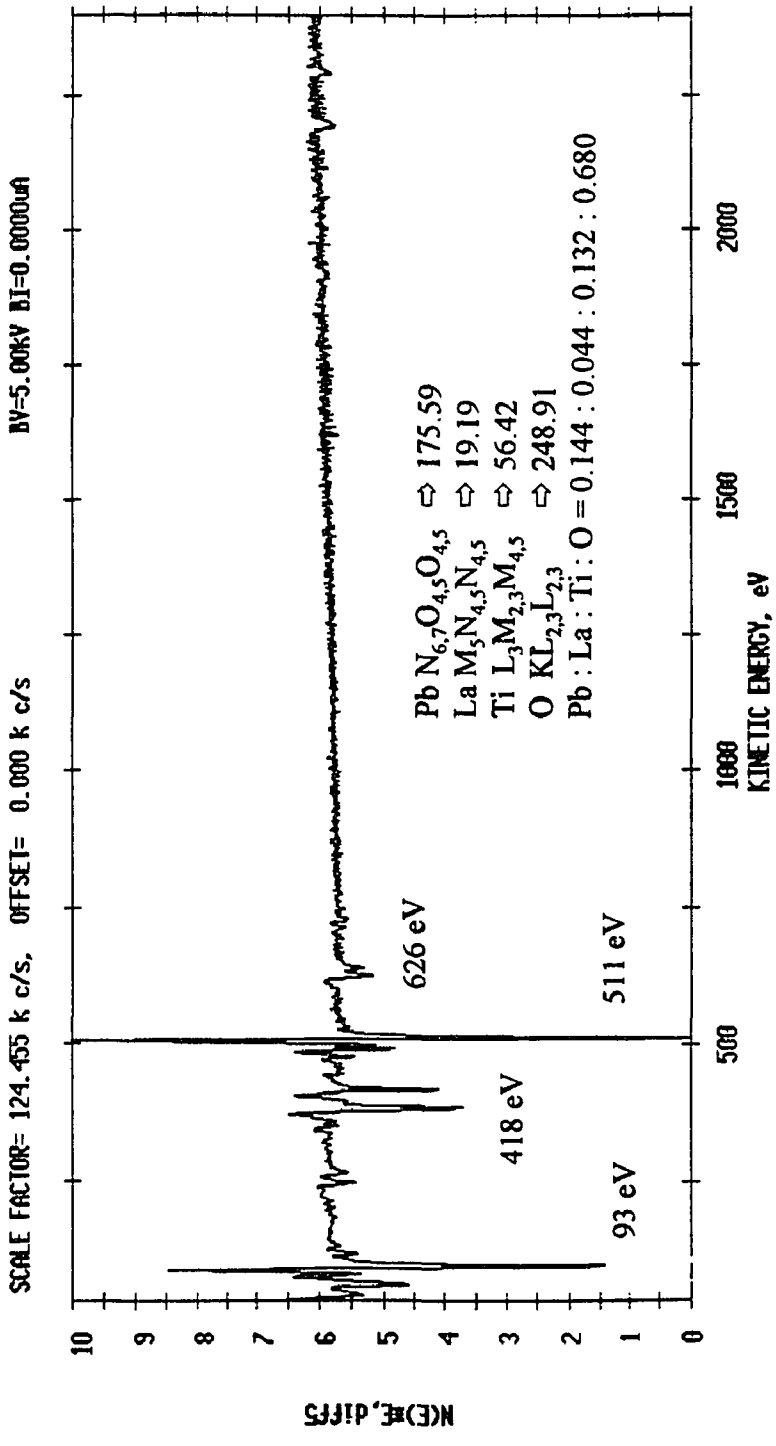

Figure A.5 Typical AES spectrum of standard PLT film

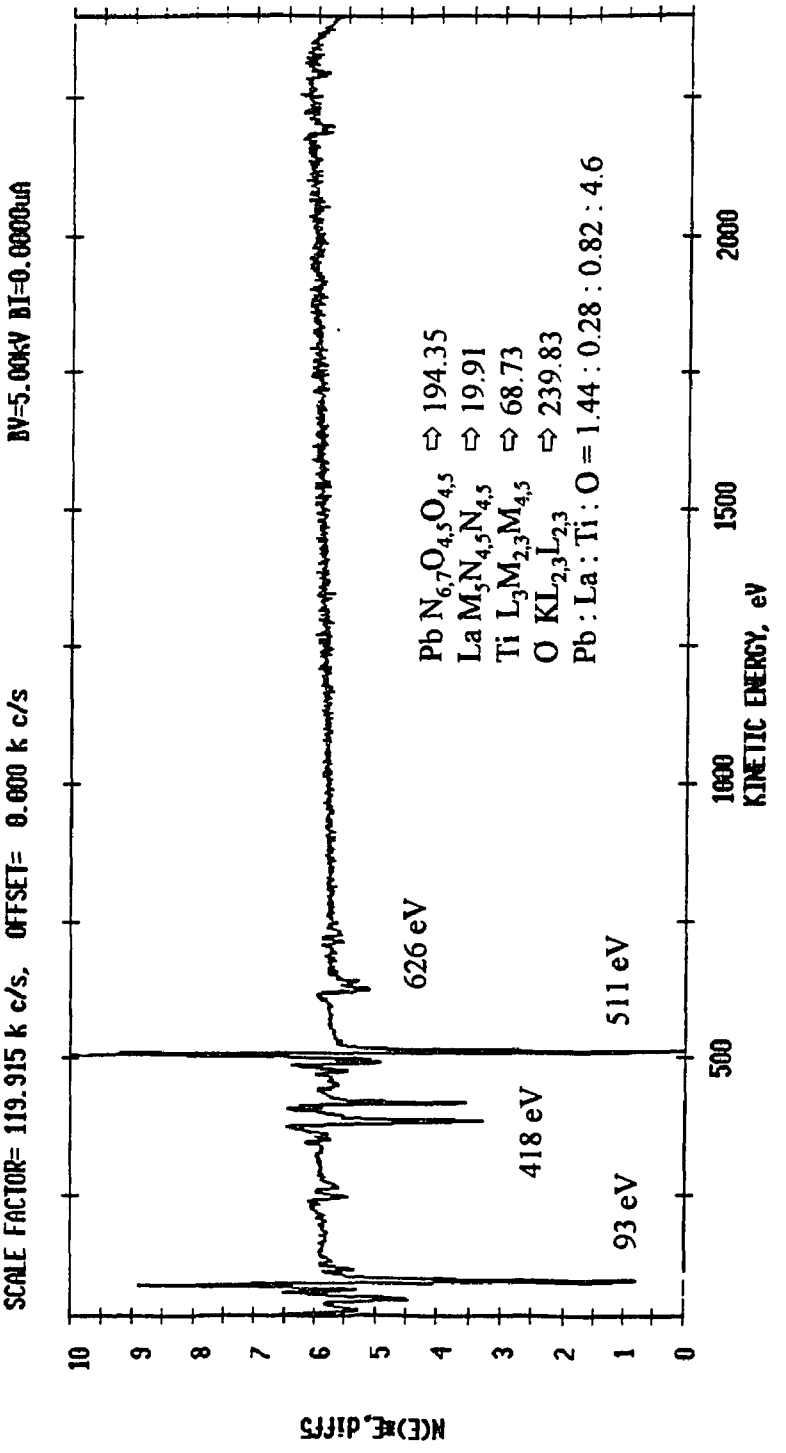

Figure A.6 Typical results of AES analysis on an as-deposited PLT film

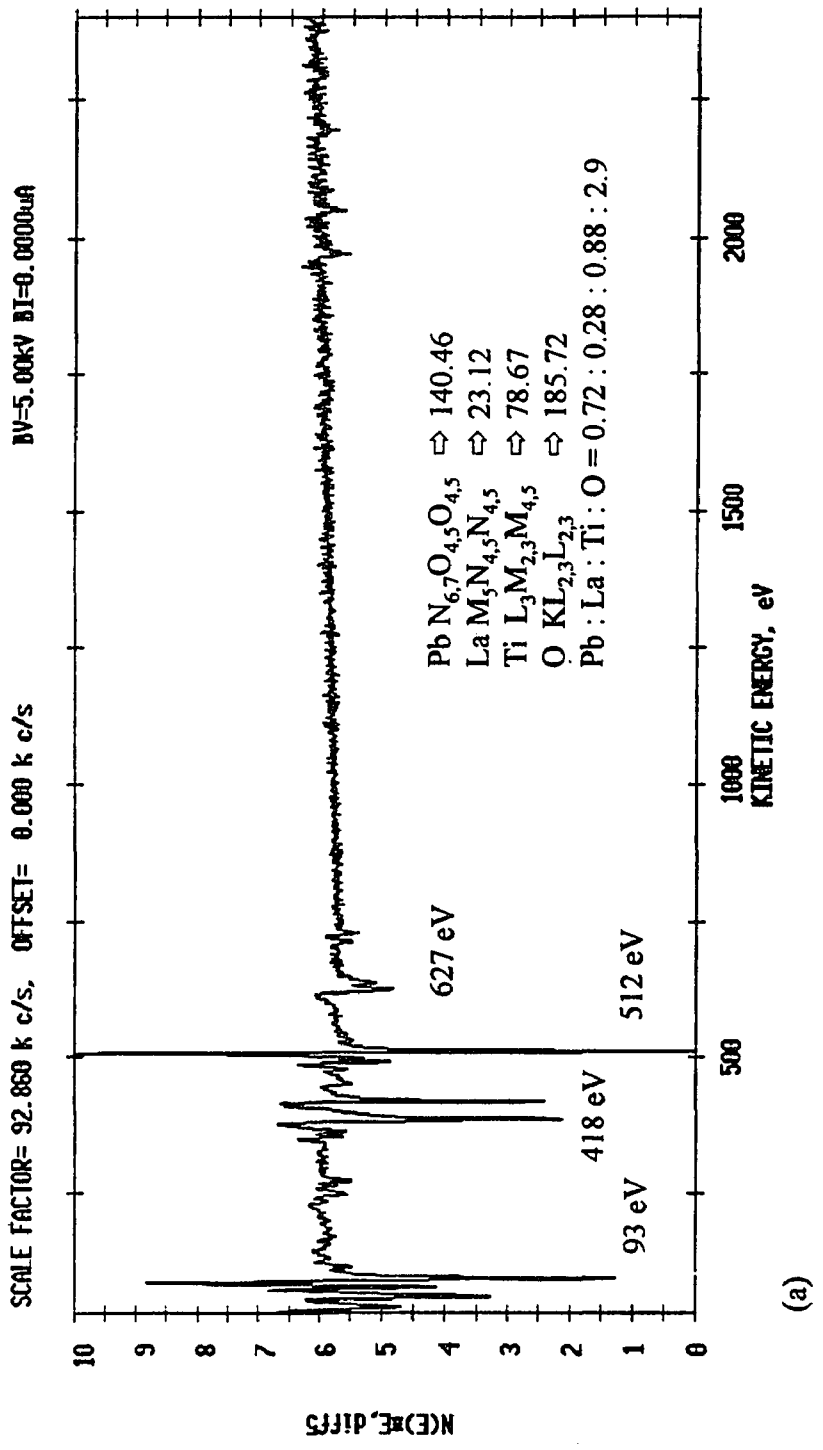

Figure A.7 AES spectrum of PLT (28) thin films with different target area:
(a) Pb : La : Ti = 8.38 : 5.85 : 85.76
(b) Pb : La : Ti = 7.60 : 7.80 : 84.60

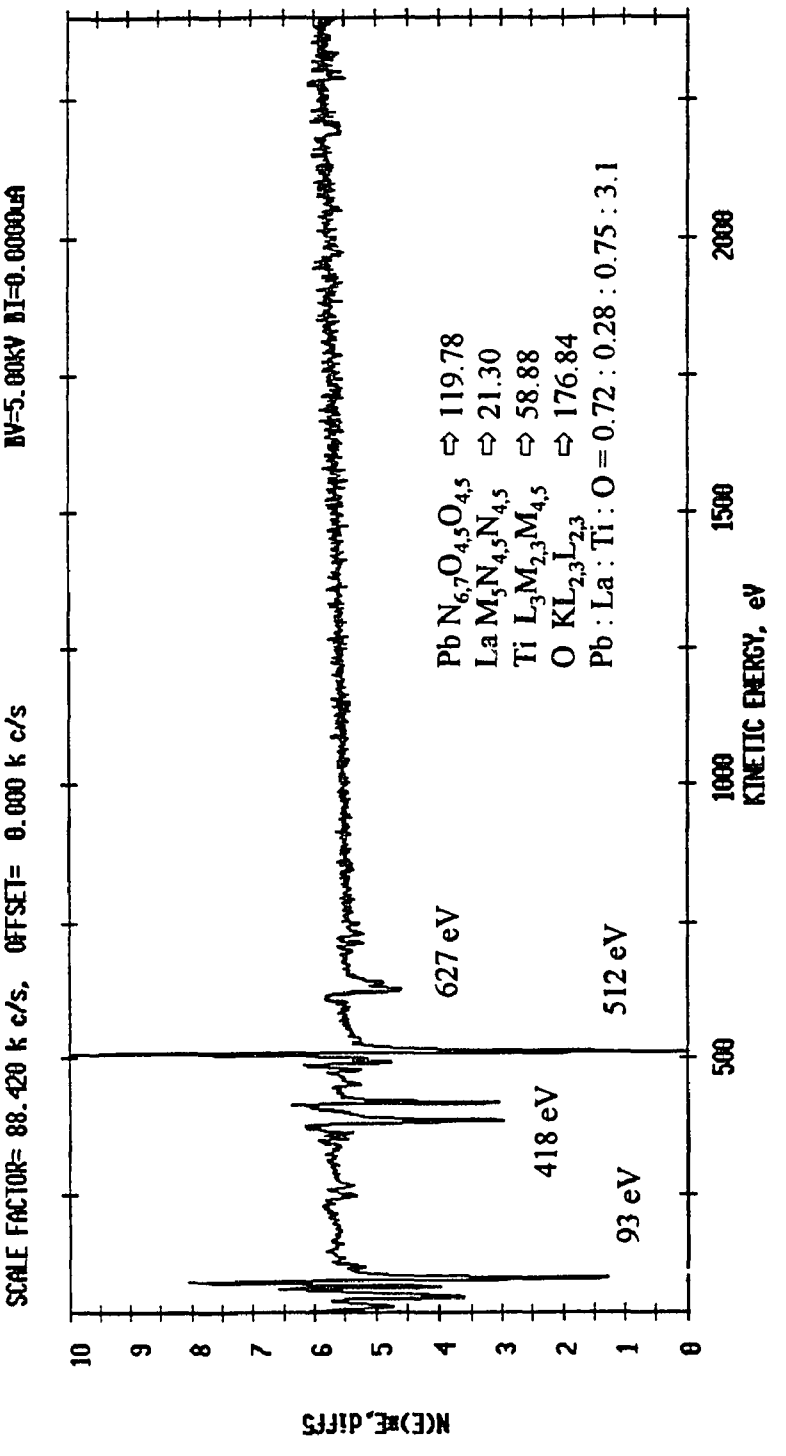
SCALE FACTOR= 88.420 k c/s, OFFSET= 0.000 k c/s
BV=5.00kV BI=0.0000uA
N(E)*E, diffs
KINETIC ENERGY, eV
627 eV
512 eV
418 eV
93 eV
Pb N6,7O4,5O4,5 ⇨ 119.78
La M5N4,5N4,5 ⇨ 21.30
Ti L3M2,3M4,5 ⇨ 58.88
O KL2,3L2,3 ⇨ 176.84
Pb : La : Ti : O = 0.72 : 0.28 : 0.75 : 3.1

(b)

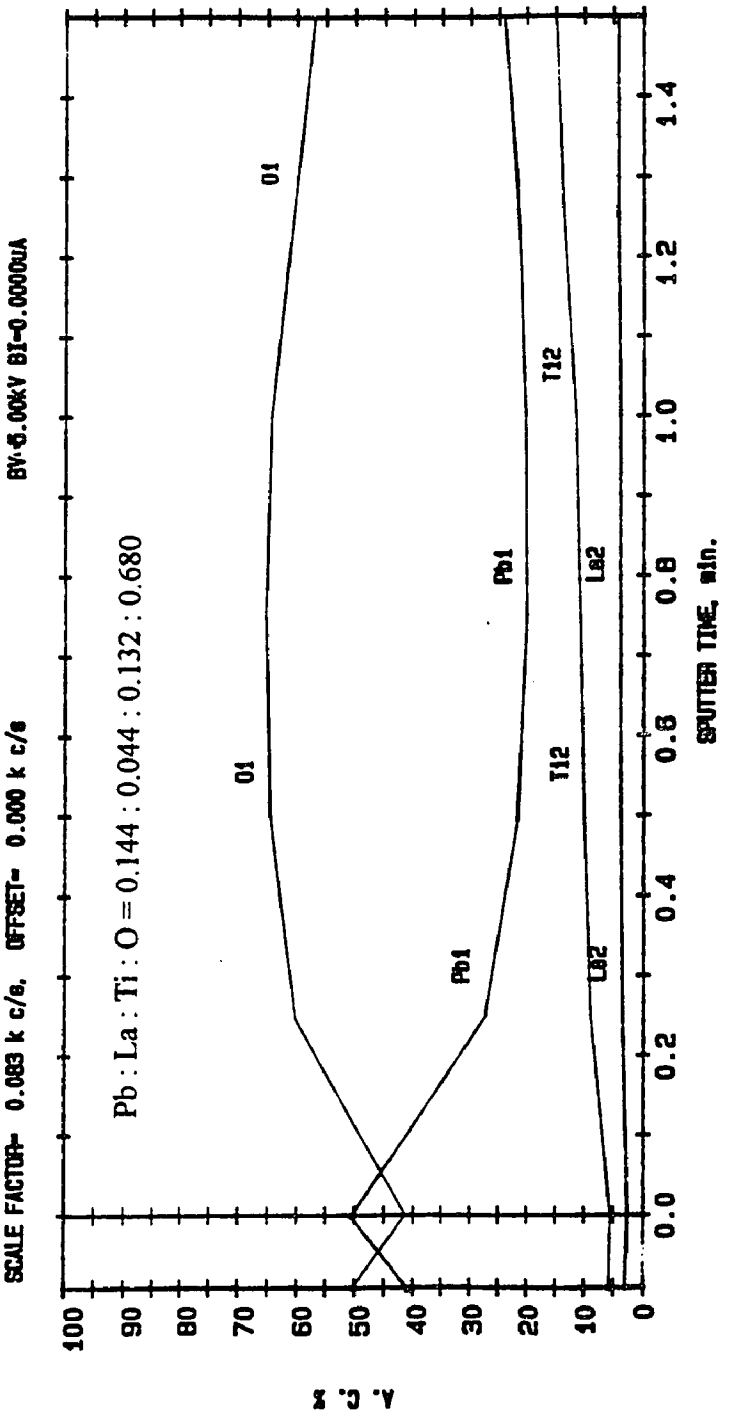

Figure A.8 Auger depth profile of an as-deposited PLT film as a function of etching time

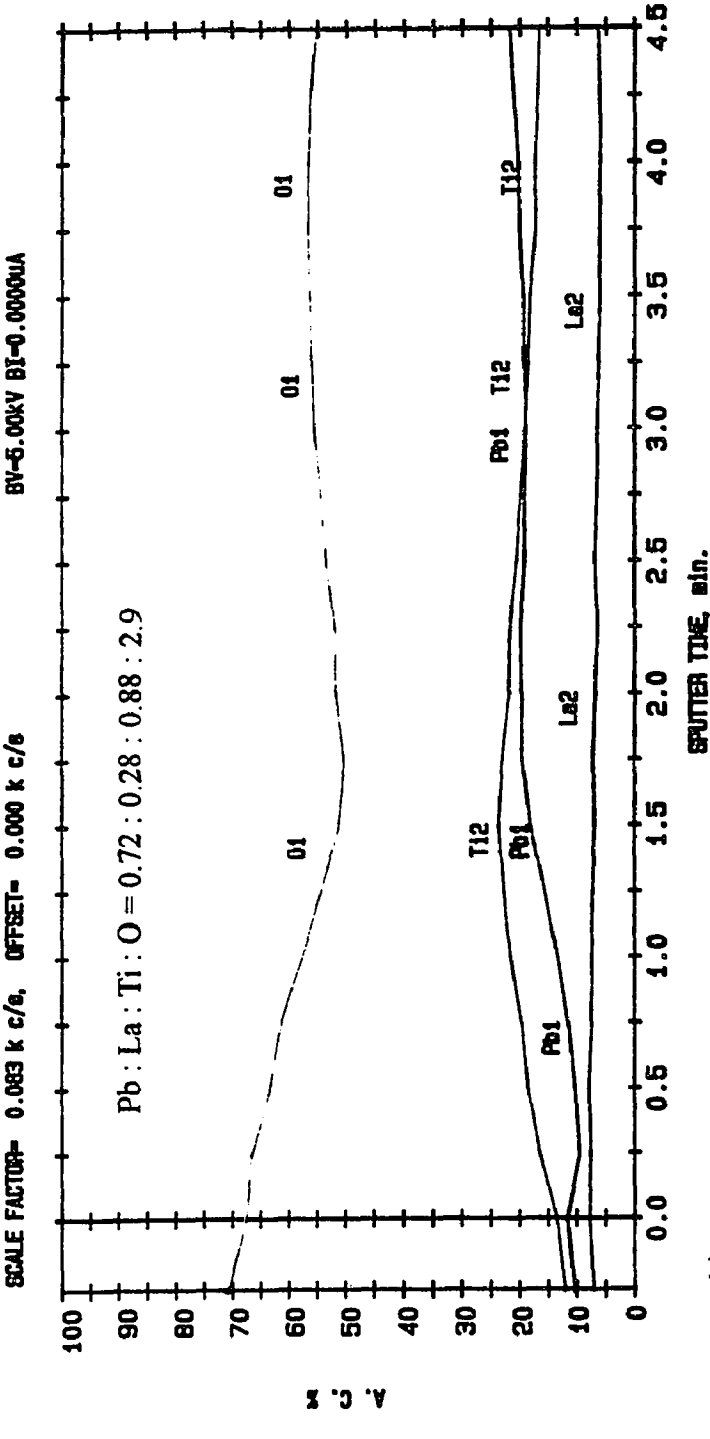

Figure A.9 Auger depth profile of PLT (28) films with different target area:
(a) Pb : La : Ti = 8.38 : 5.85 : 85.76
(b) Pb : La : Ti = 7.60 : 7.80 : 84.60

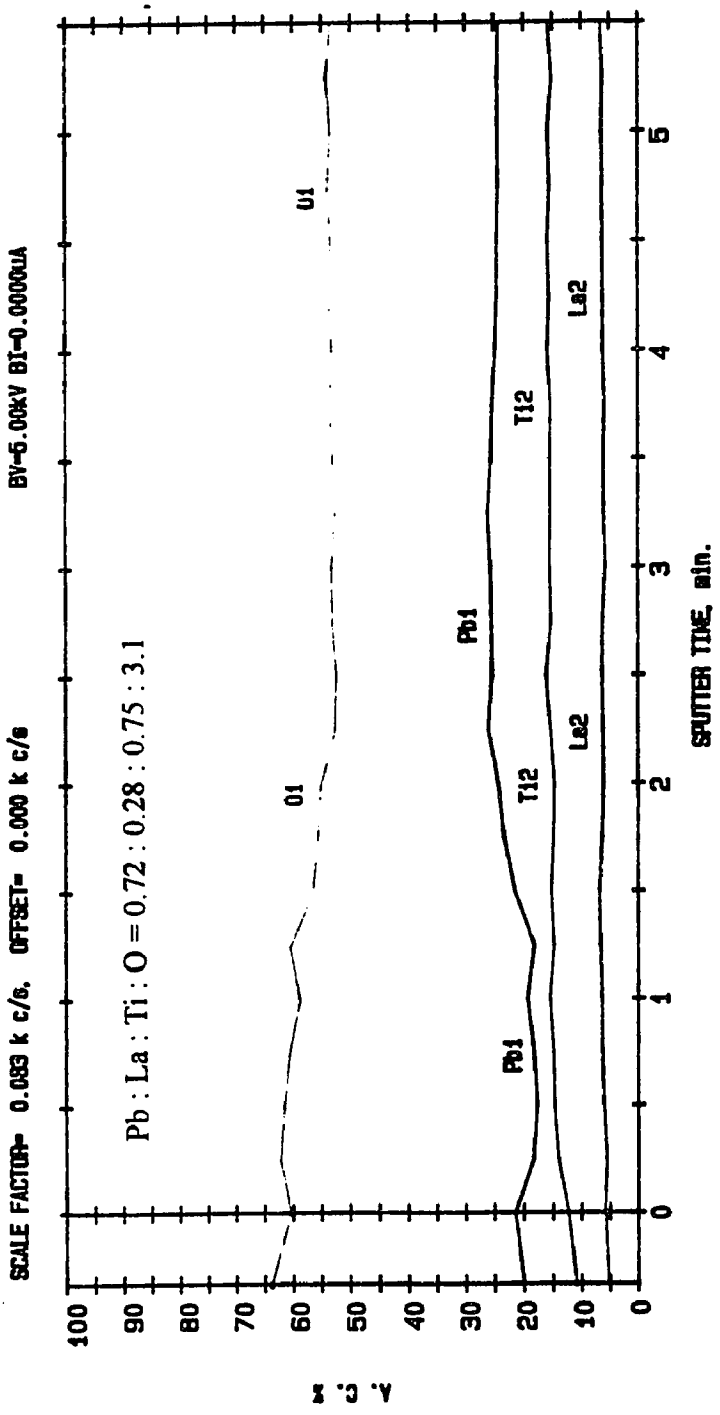
SCALE FACTOR= 0.083 k c/s, OFFSET= 0.000 k c/s
BV=5.00kV BI=0.0000uA
Pb : La : Ti : O = 0.72 : 0.28 : 0.75 : 3.1
O1
U1
Pb1
Ti2
La2
Pb1
Ti2
La2
SPUTTER TIME, min.
100
90
80
70
60
50
40
30
20
10
0
0
1
2
3
4
5

(b)

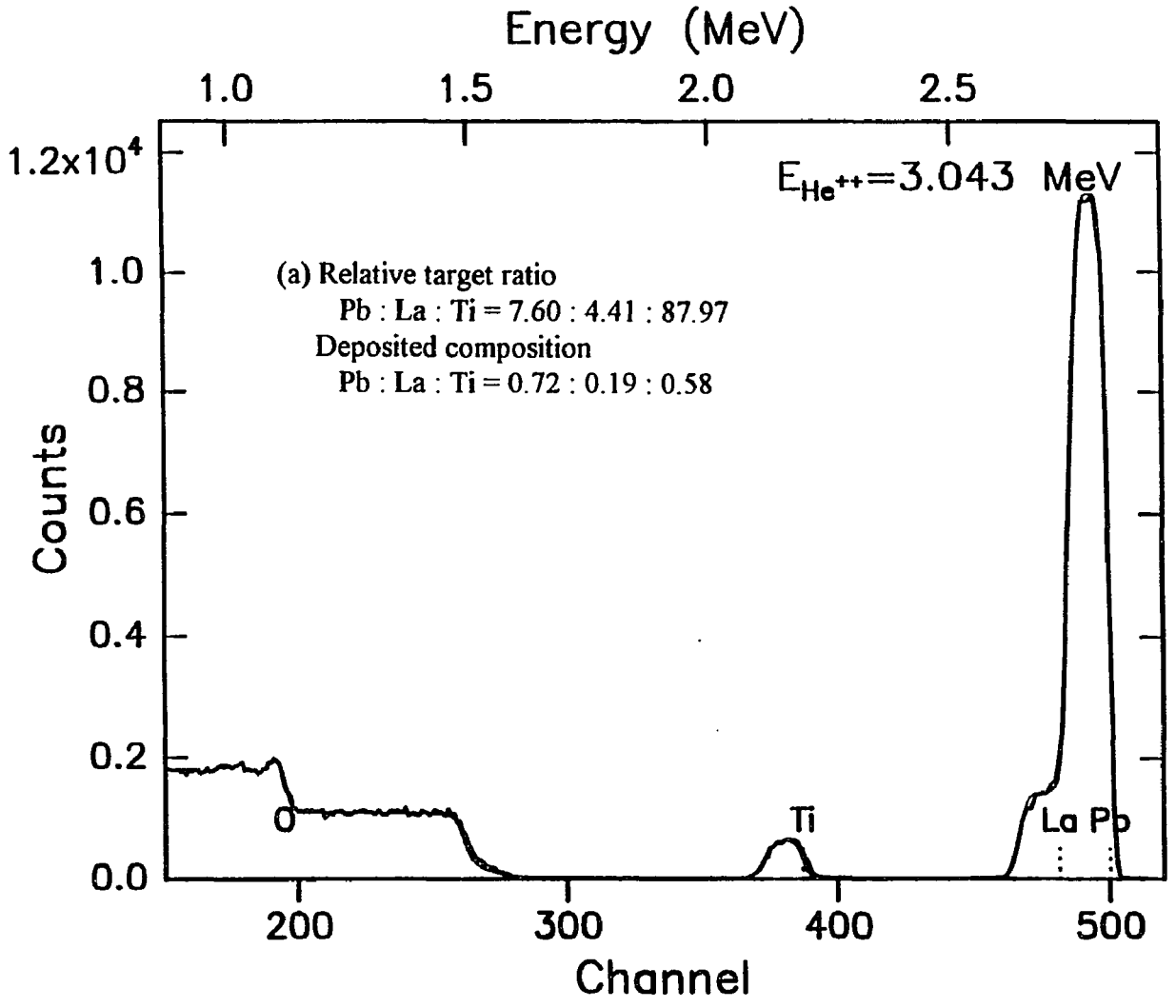

Figure A.10 Rutherford backscattering spectra of PLT thin films with different area ratio of multi-component metal target

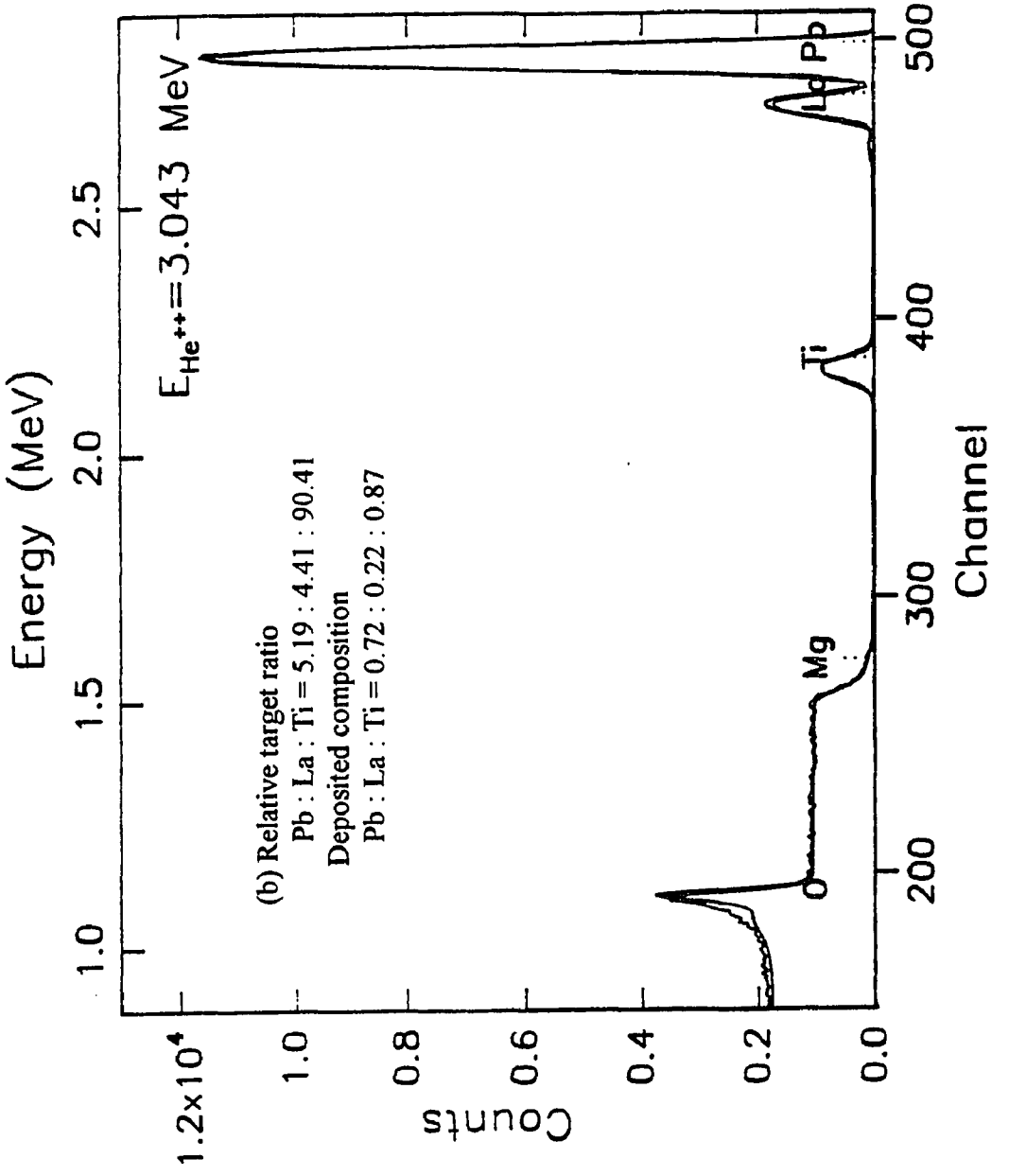
Energy (MeV)
1.0
1.5
2.0
2.5
$E_{He^{++}}$=3.043 MeV
(b) Relative target ratio
Pb : La : Ti = 5.19 : 4.41 : 90.41
Deposited composition
Pb : La : Ti = 0.72 : 0.22 : 0.87
Counts
1.2x10⁴
1.0
0.8
0.6
0.4
0.2
0.0
O
Mg
Ti
La
Pb
200
300
400
500
Channel

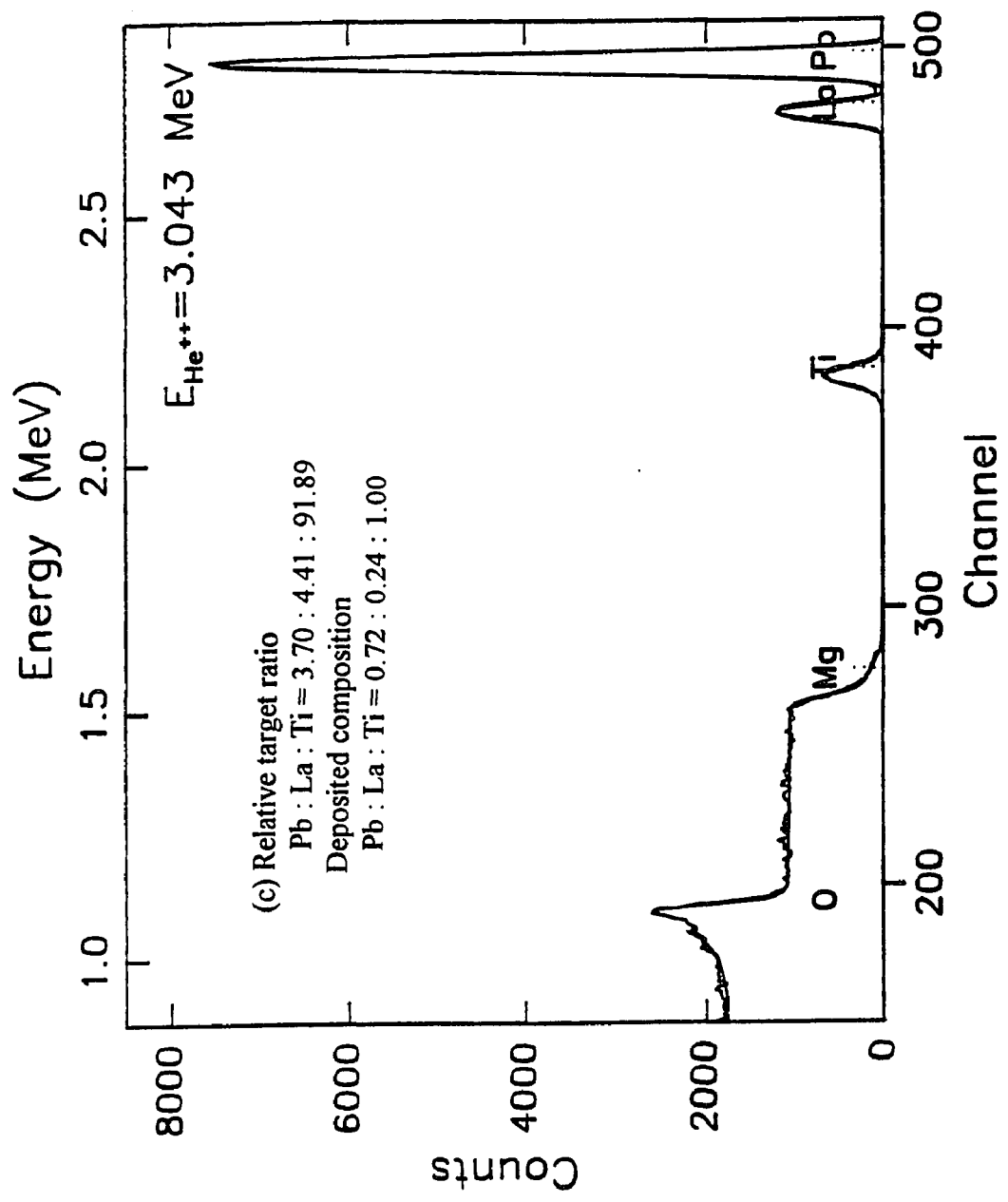
Energy (MeV)
1.0
1.5
2.0
2.5
$E_{He^{++}}$=3.043 MeV
(c) Relative target ratio
Pb : La : Ti = 3.70 : 4.41 : 91.89
Deposited composition
Pb : La : Ti = 0.72 : 0.24 : 1.00
Mg
Ti
Pb
Counts
8000
6000
4000
2000
0
0
200
300
400
500
Channel

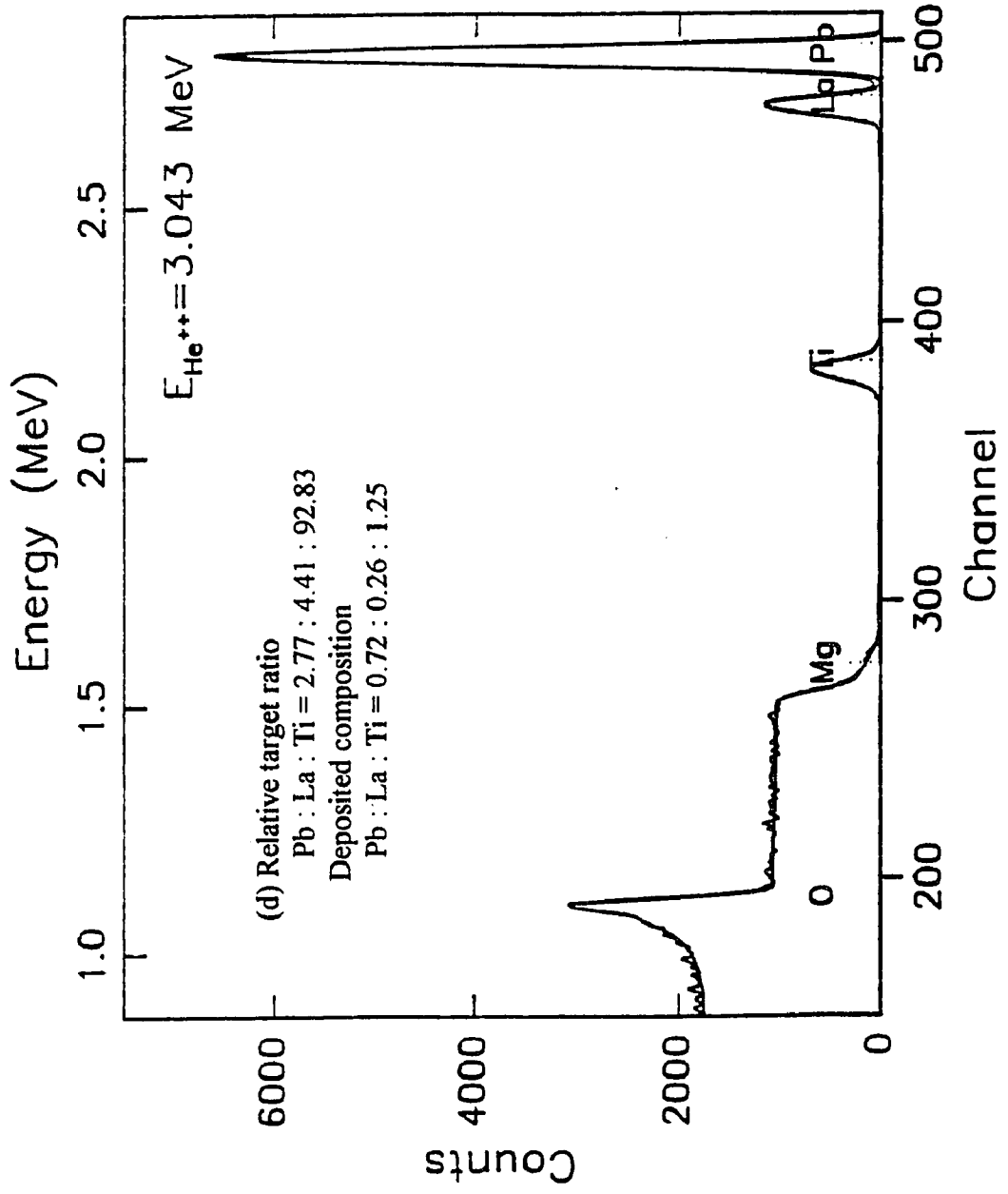
Energy (MeV)
1.0
1.5
2.0
2.5
$E_{He^{++}}$=3.043 MeV
(d) Relative target ratio
Pb : La : Ti = 2.77 : 4.41 : 92.83
Deposited composition
Pb : La : Ti = 0.72 : 0.26 : 1.25
Counts
6000
4000
2000
0
Mg
Ti
La
Pb
0
200
300
400
500
Channel

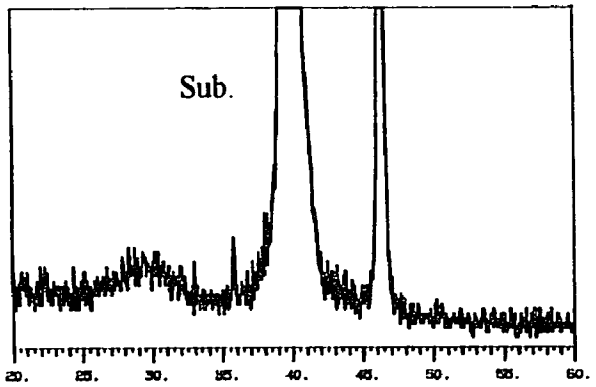

(a) As-deposited PLT film

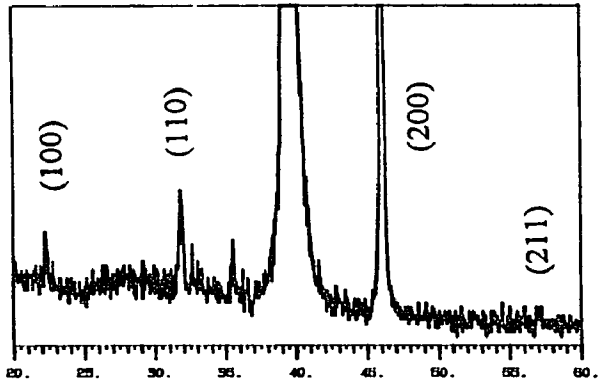

(b) 550 °C

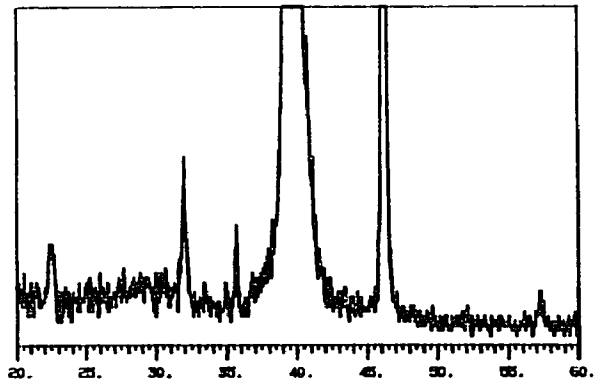

(c) 650 °C

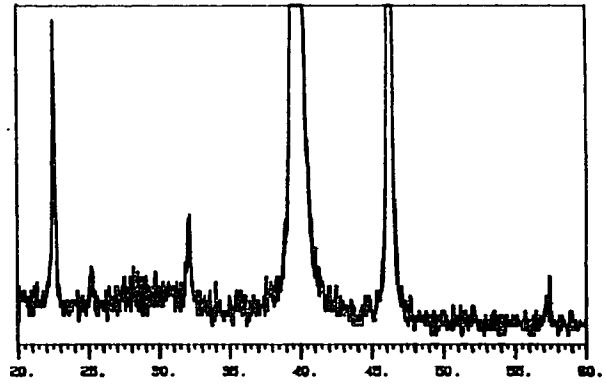

(d) 750 °C

Figure A.11 XRD patterns of PLT thin films with different post-annealing treatment. These PLT films belong to the type D in Table 5.3

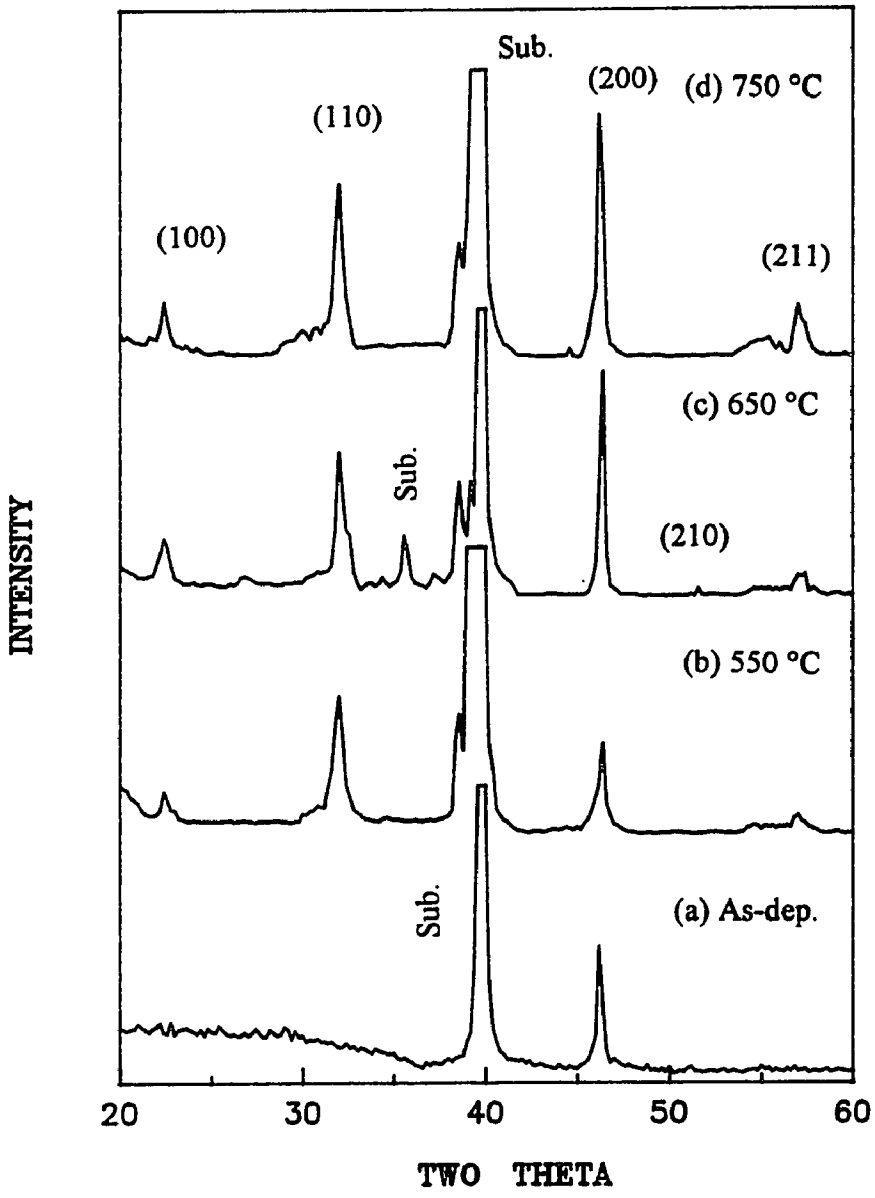

Figure A.12 XRD spectra of the paraelectric PLT (28) thin films as a function of post-annealing temperature. These PLT films belong to the type A in Table 5.3

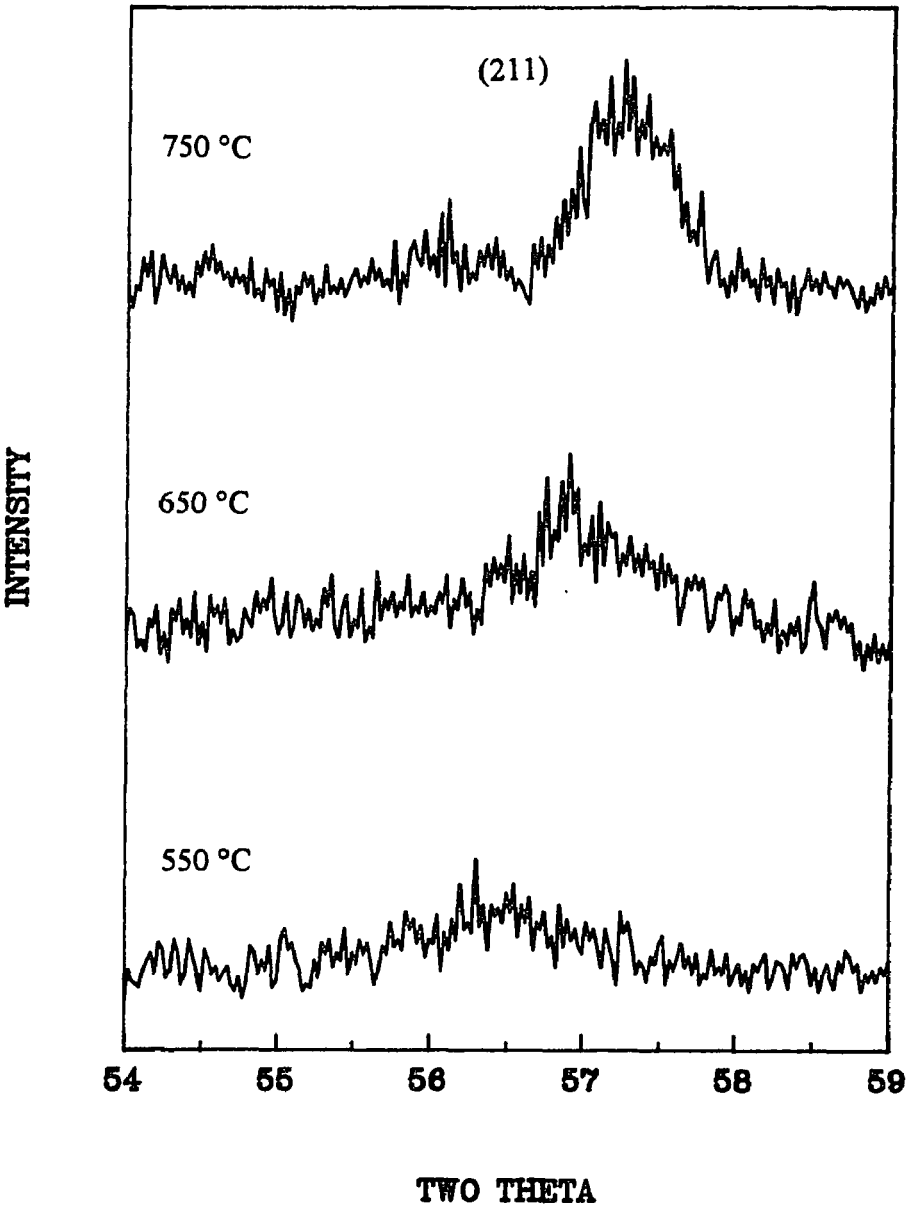

Figure A.13 XRD step scans to observe the (211) peak shift of PLT (28) films at 550, 650, and 750 °C for 5 min

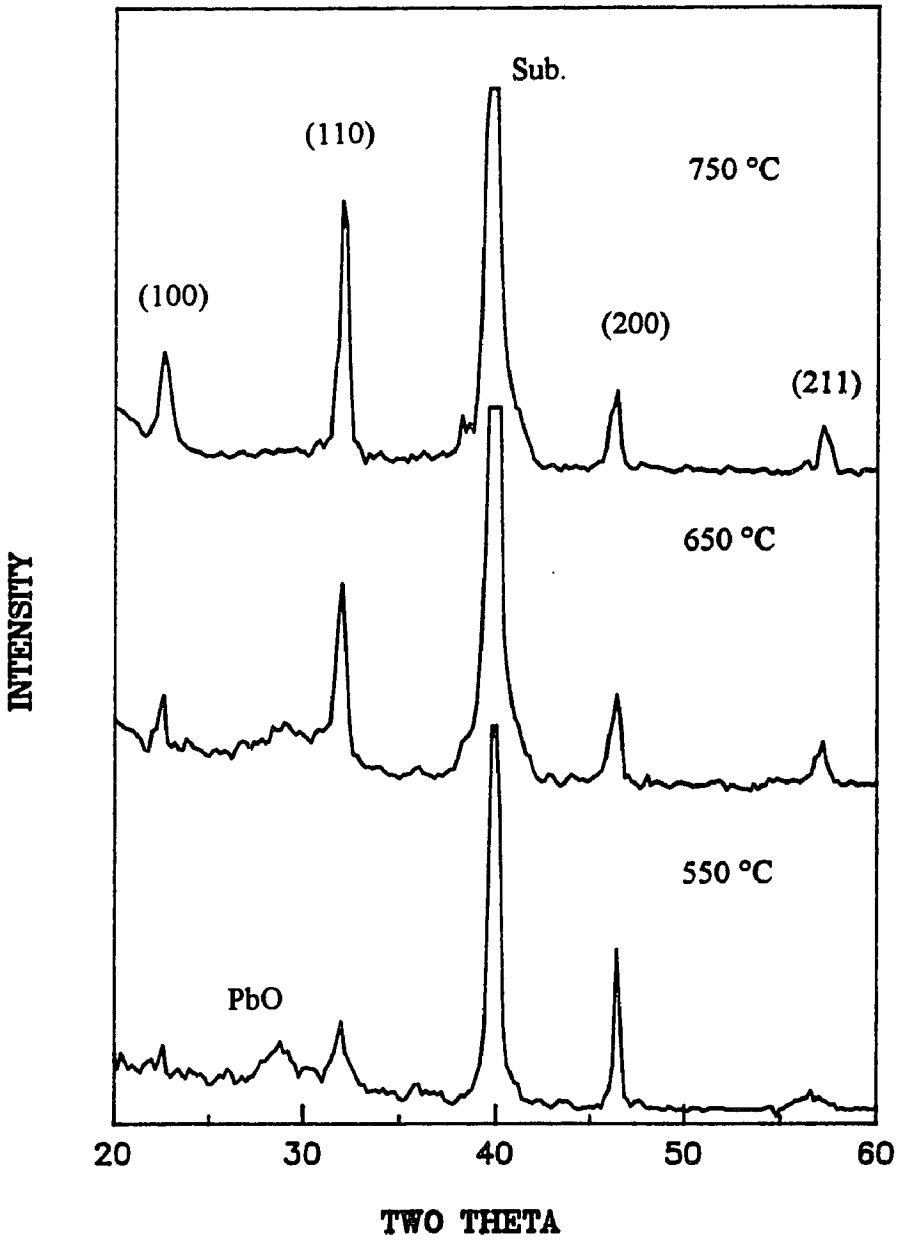

Figure A.14 XRD patterns as a function of annealing temperature for PLT thin films of chemical composition type B in Table 5.3

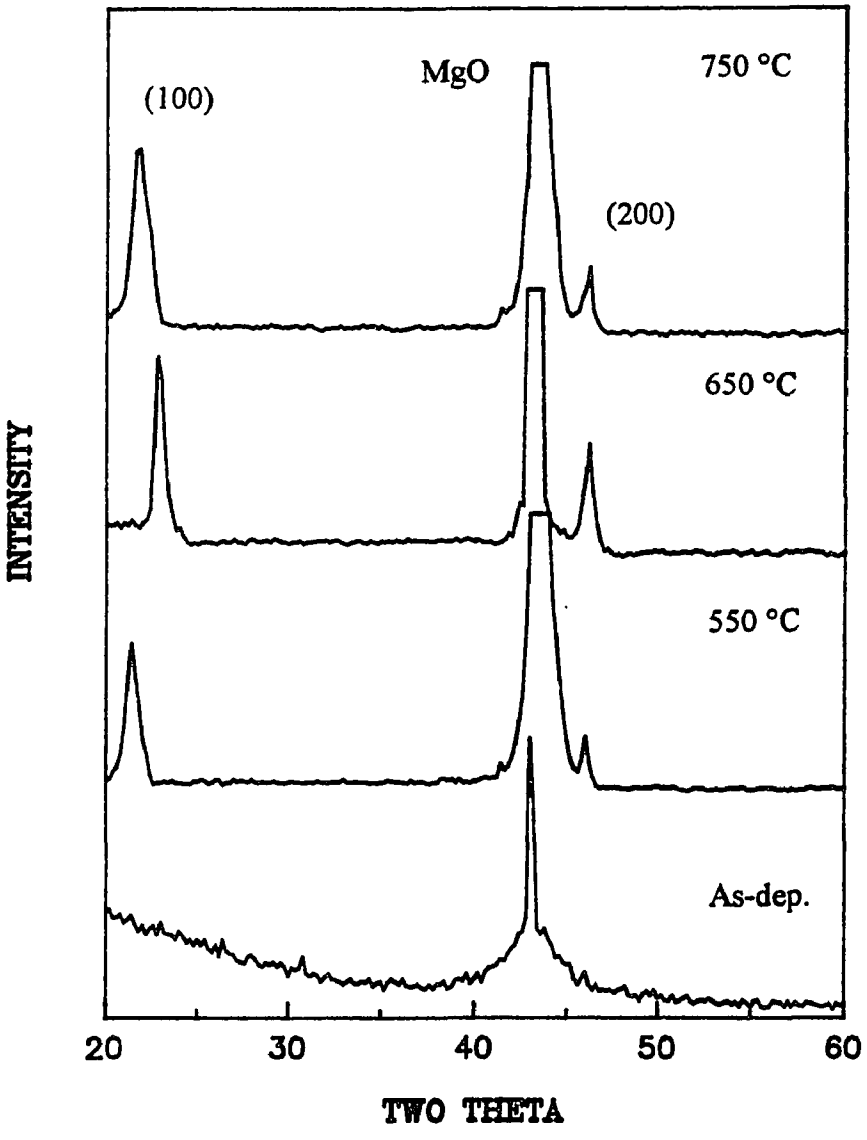

Figure A.15 XRD spectra of PLT thin films on single-crystal MgO (100) substrate

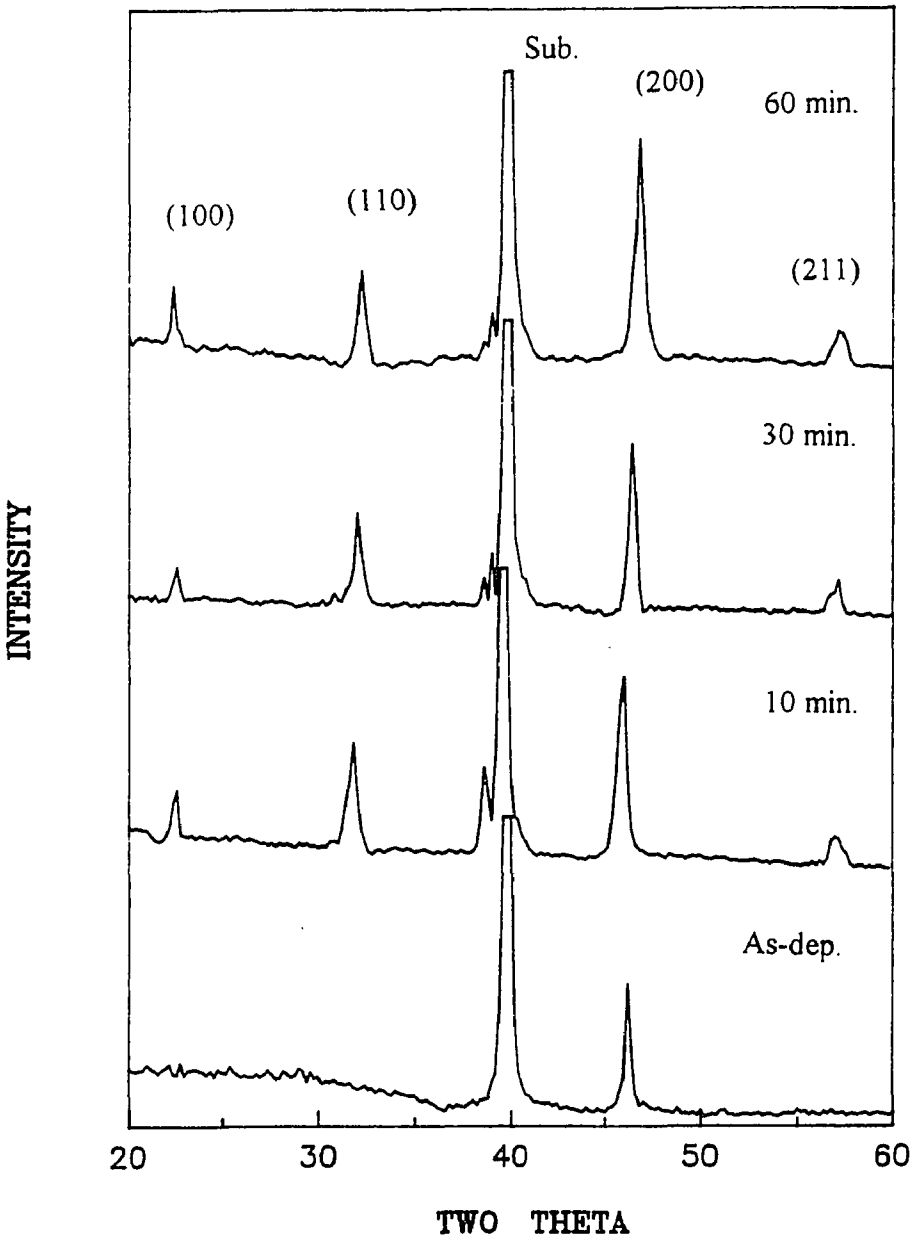

Figure A.16 XRD patterns of the paraelectric PLT (28) thin films as a function of annealing time at 650 °C

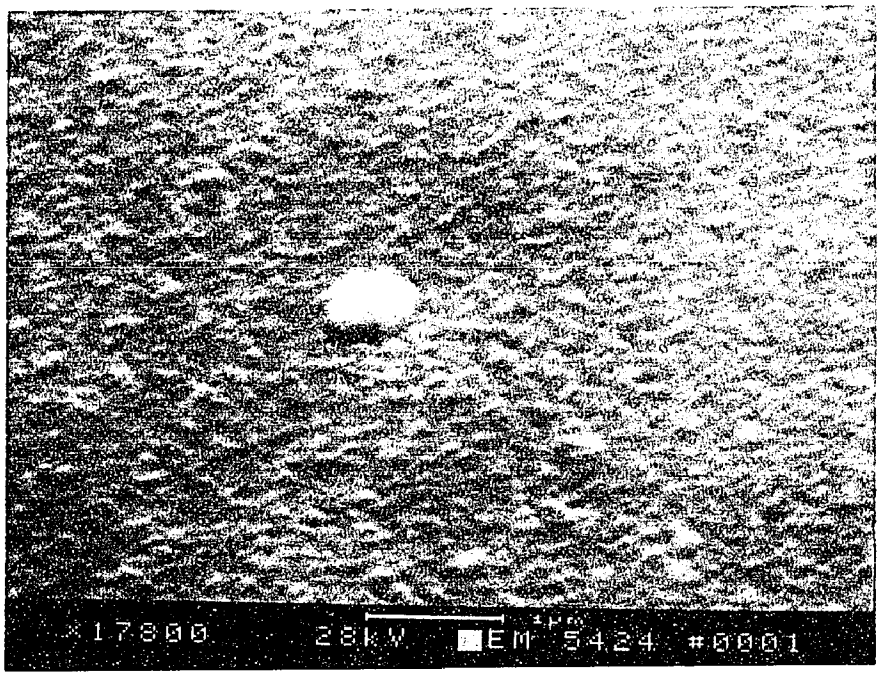

Figure A.17 Typical SEM of as-deposited PLT film with smooth surface

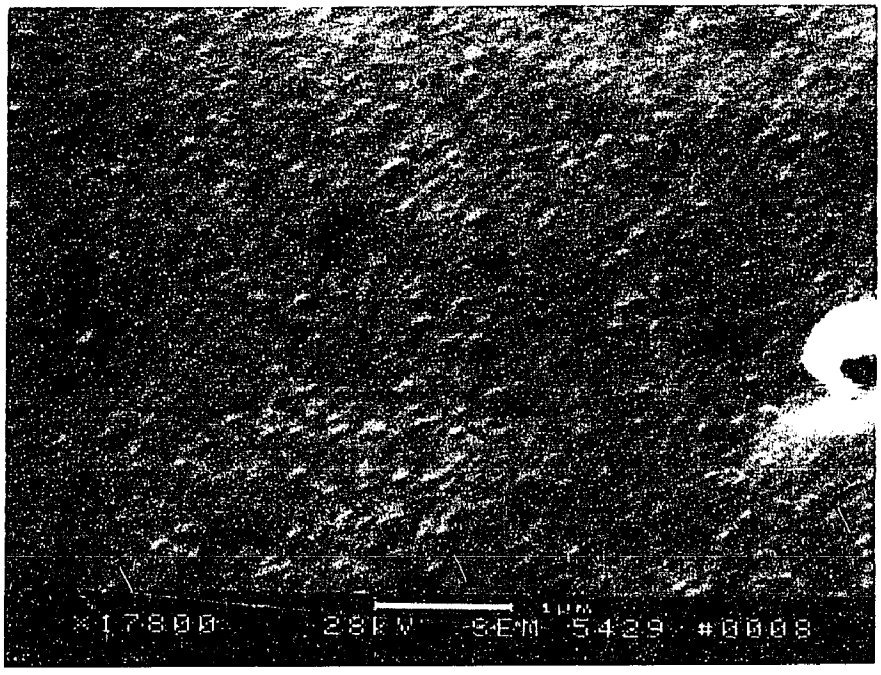

Figure A.18 Typical SEM of PLT thin film annealed at 650 °C for 5 min

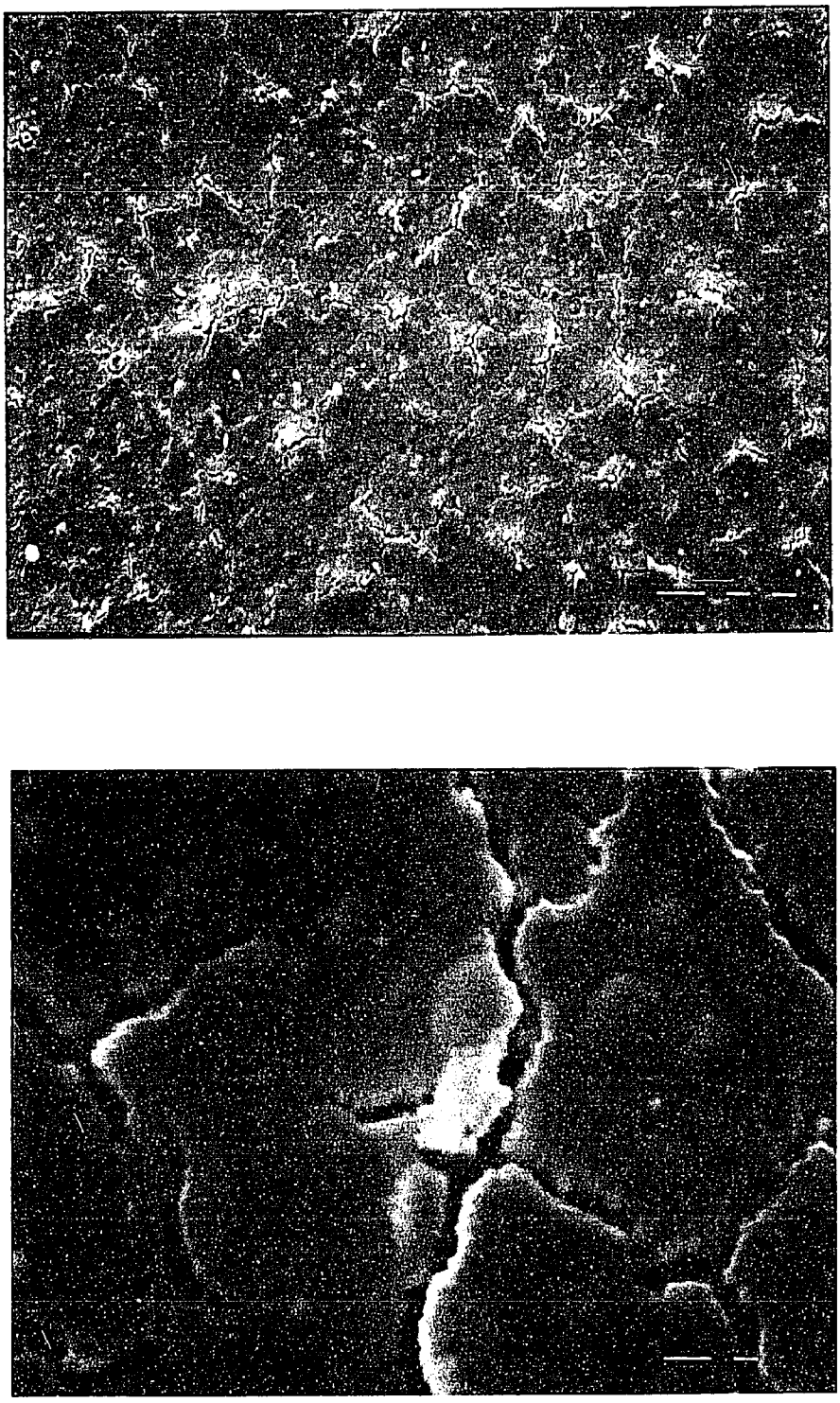

Figure A.19 Segregation of grain boundary in PLT films due to Pb evaporation

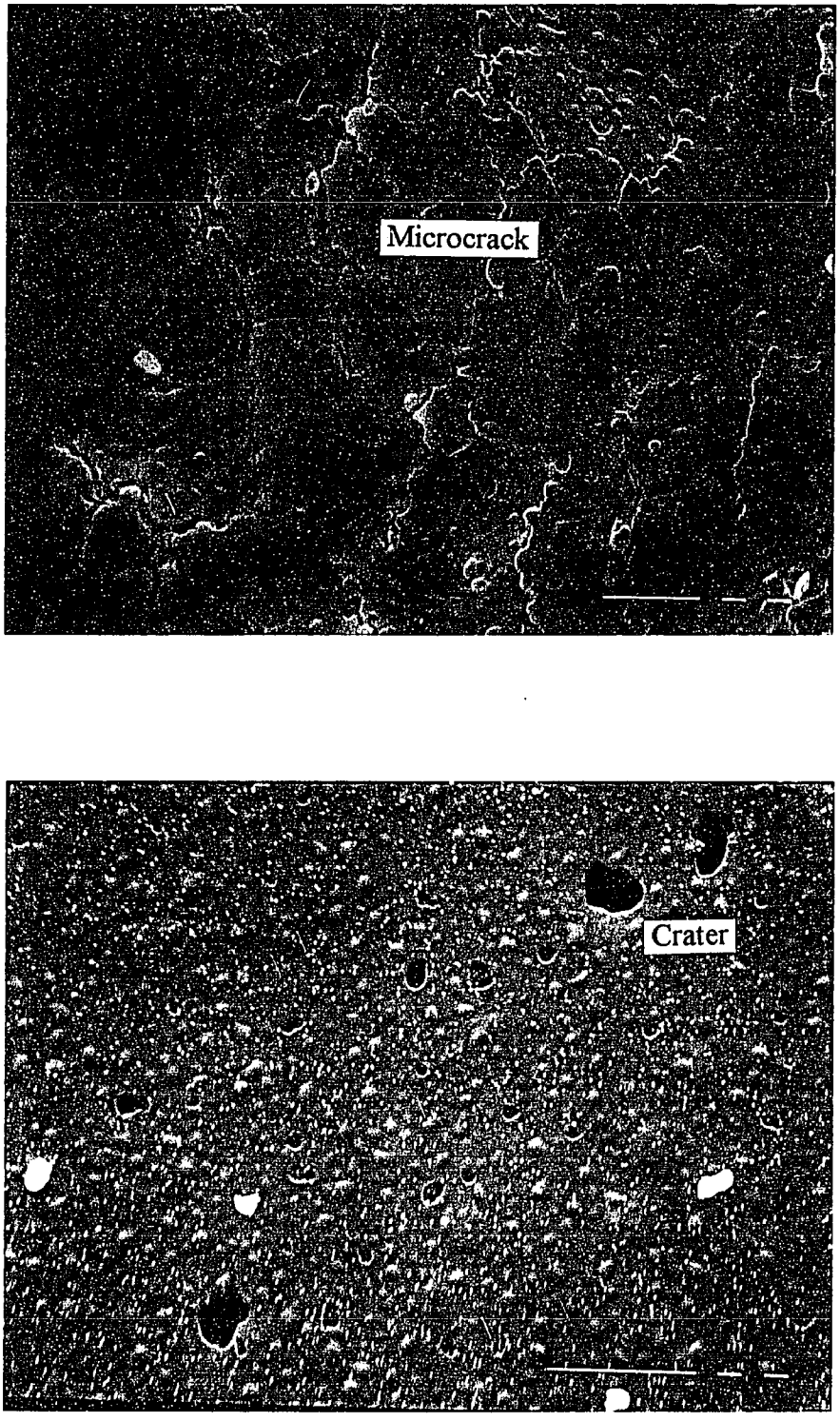

Figure A.20 SEM of typical defects on PLT films annealed at 750 °C for 60 min: (a) crack and (b) craters and holes

APPENDIX B

TEST RESULTS OF ELECTRICAL ANALYSIS

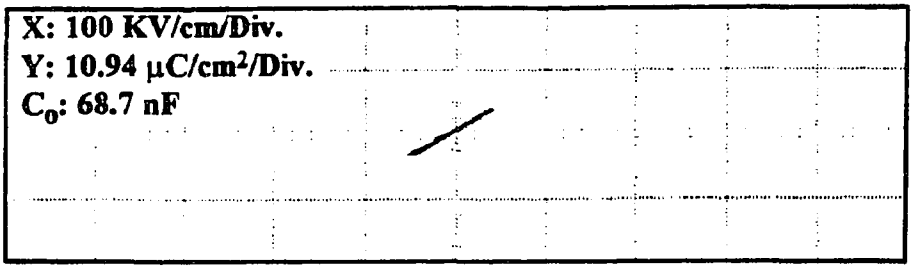

(a) $V_p = 1$ V

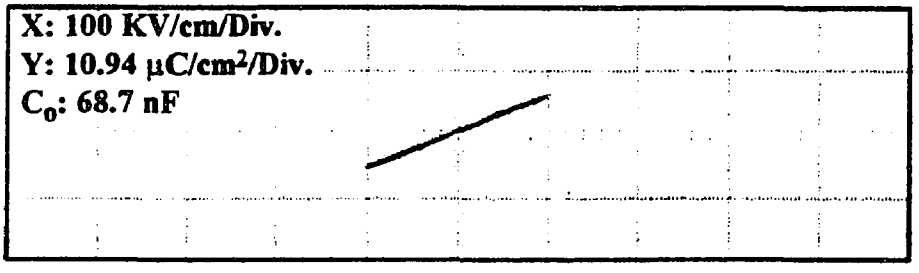

(b) $V_p = 2$ V

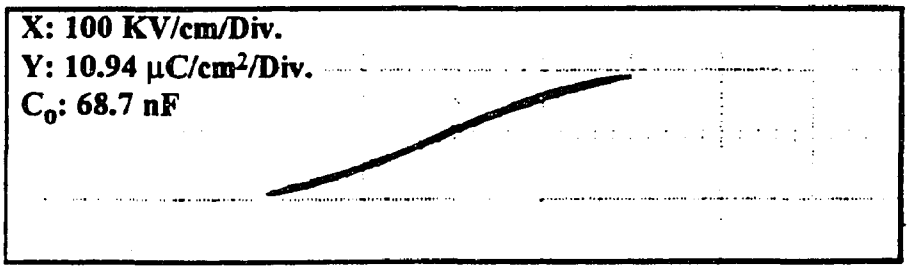

(c) $V_p = 4$ V

Figure B.1 P-E characteristics as a function of peak voltage for 200 nm PLT (28) thin film at 650 °C for 5 min

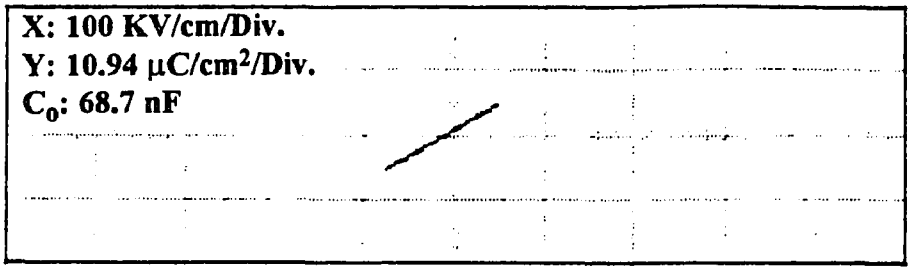

(a) $V_p = 1$ V

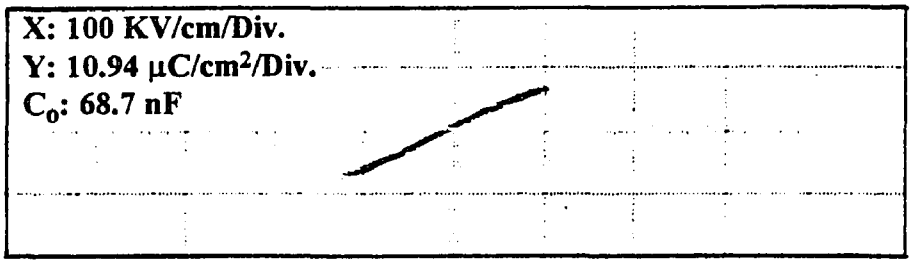

(b) $V_p = 2$ V

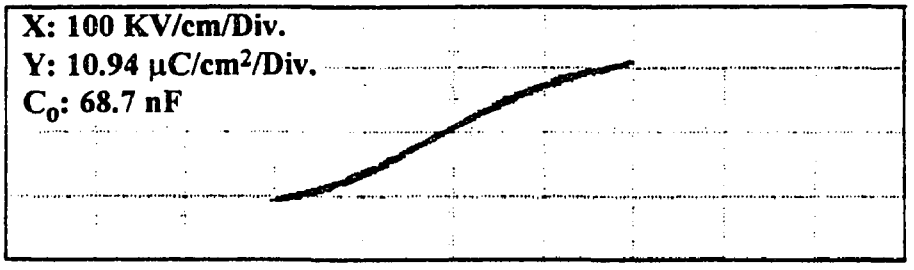

(c) $V_p = 4$ V

Figure B.2 P-E characteristics with different peak voltages for 200 nm PLT (28) thin film at 750 °C for 5 min

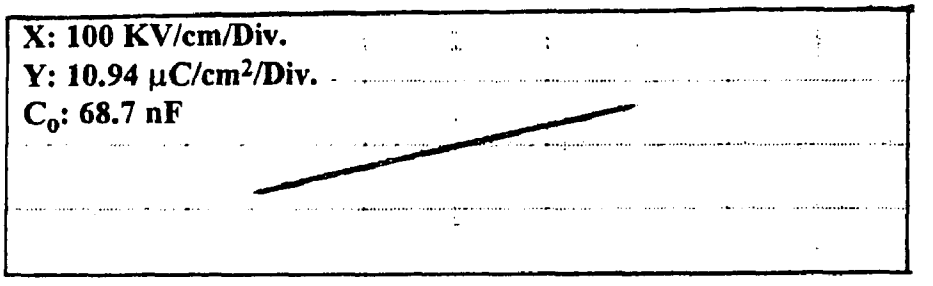

(a) 550 °C

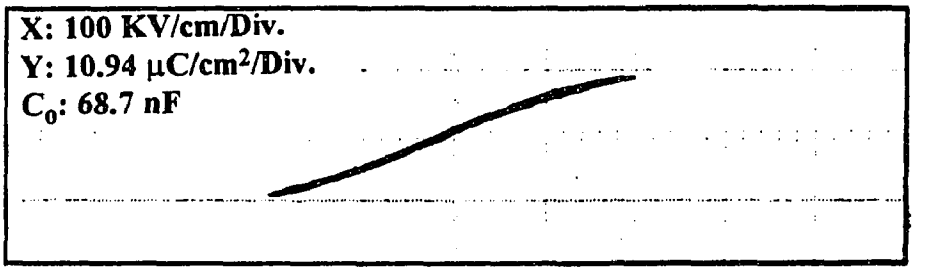

(b) 650 °C

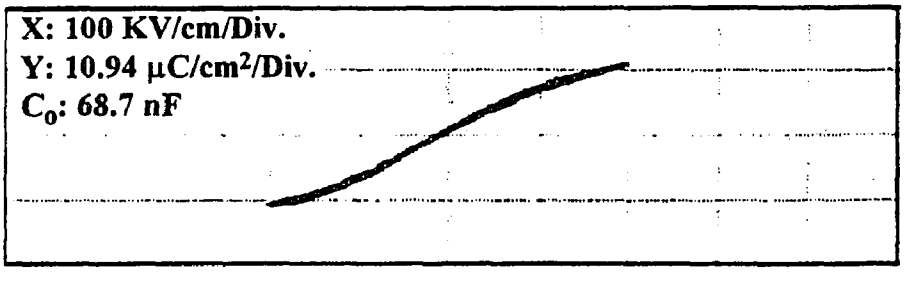

(c) 750 °C

Figure B.3 P-E characteristics as a function of annealing temperature for PLT films at the same peak voltage of 4 V (200 KV/cm)

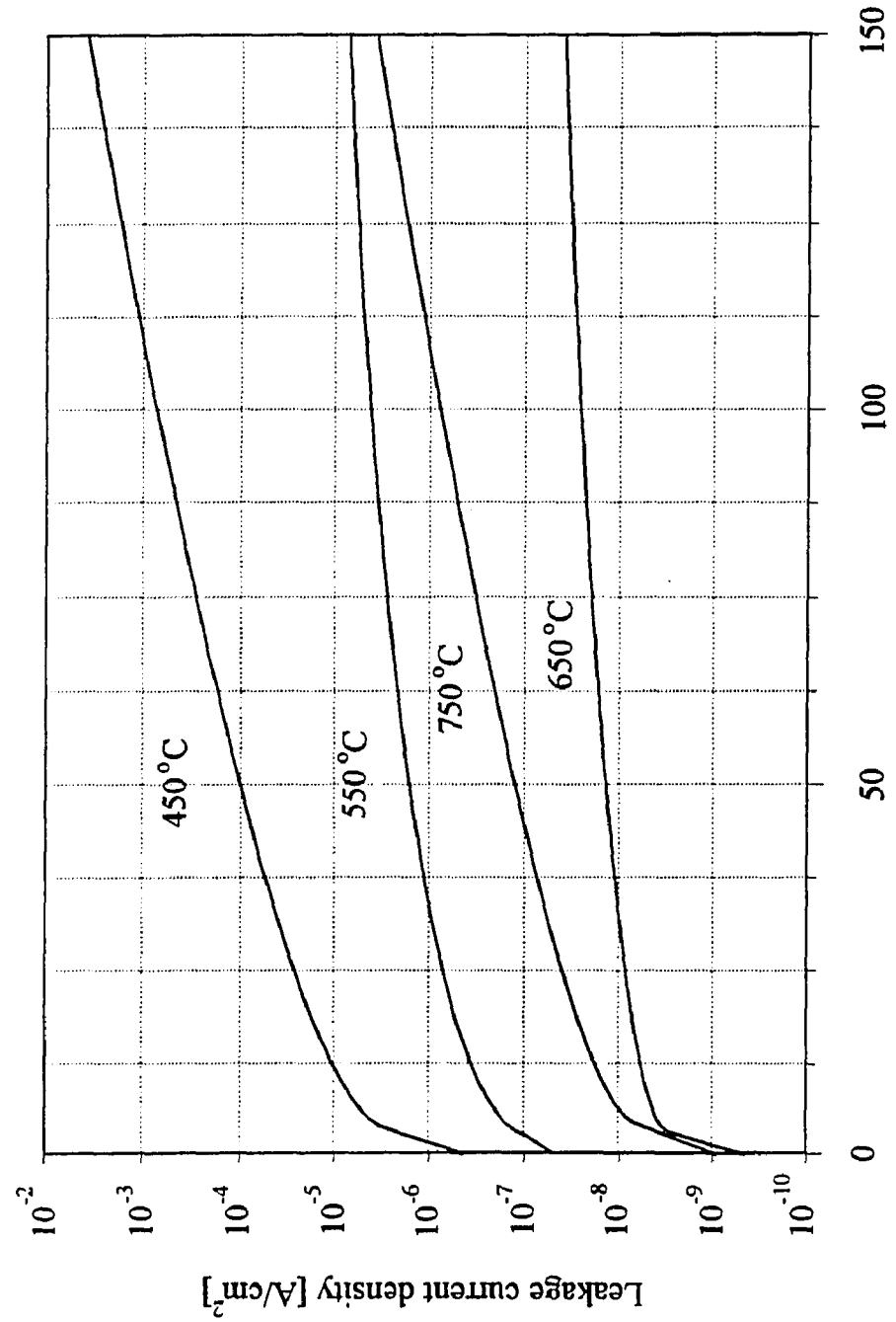

Figure B.4 I-V plot of PLT thin films with different post-annealing temperature for 5 min.

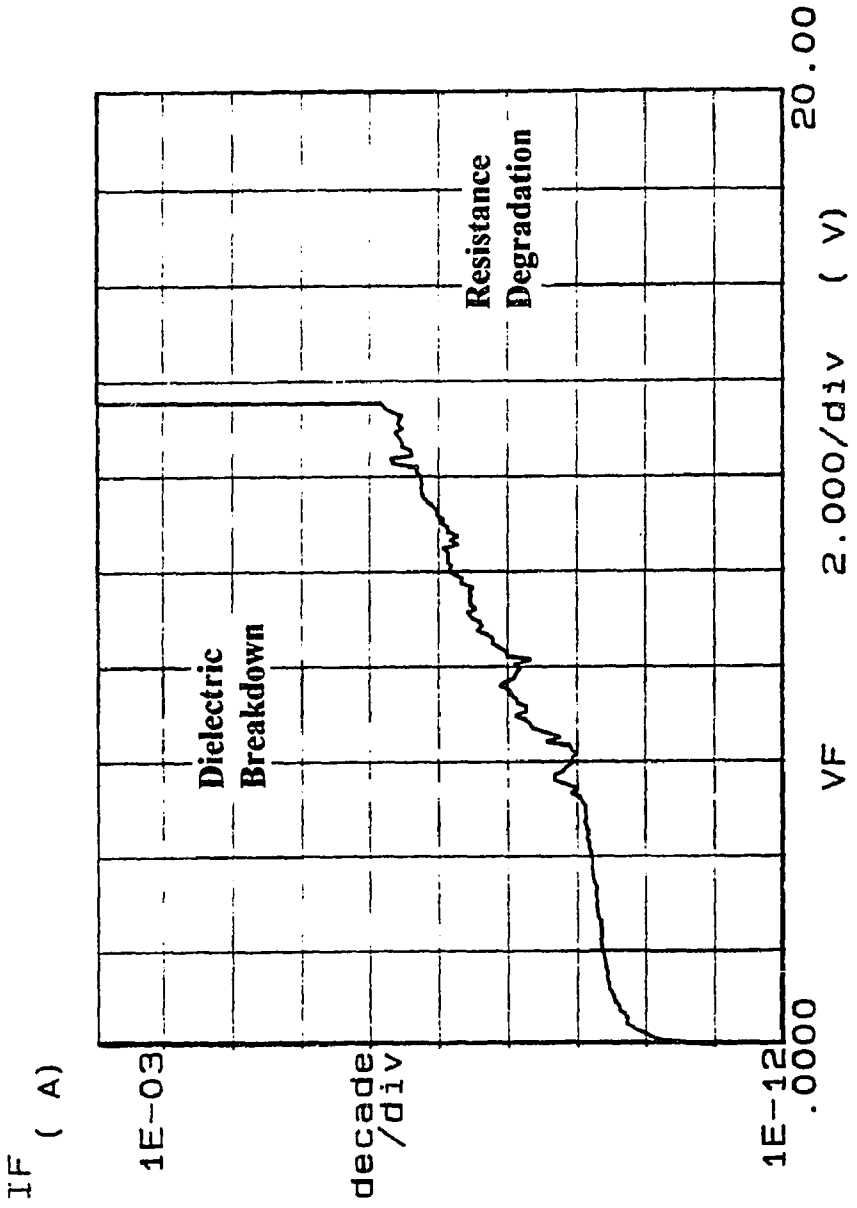

Figure B.5 The phenomena of dc voltage-induced resistance degradation suddenly rising in the leakage current level prior to dielectric breakdown

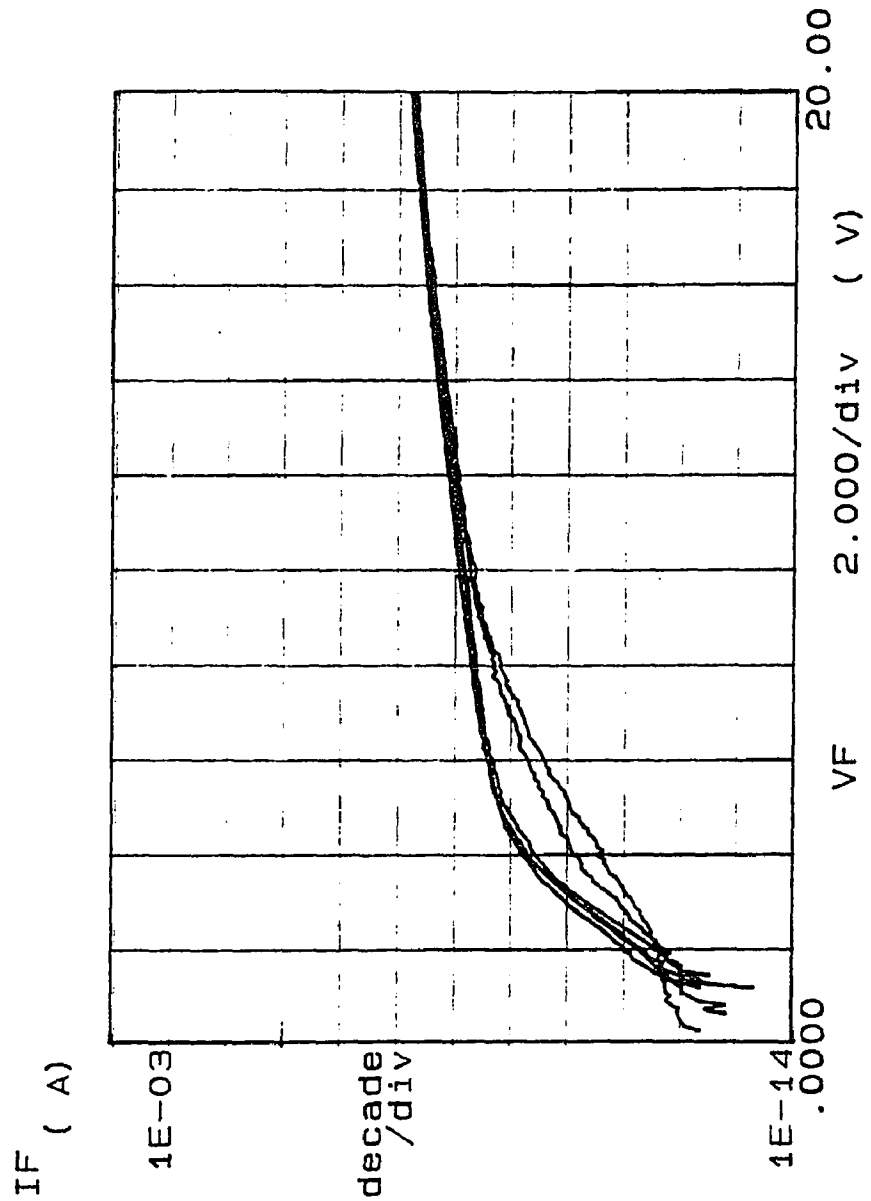

Figure B.6 I-V characteristics for different delay time of a 5 sec using non-switching static current

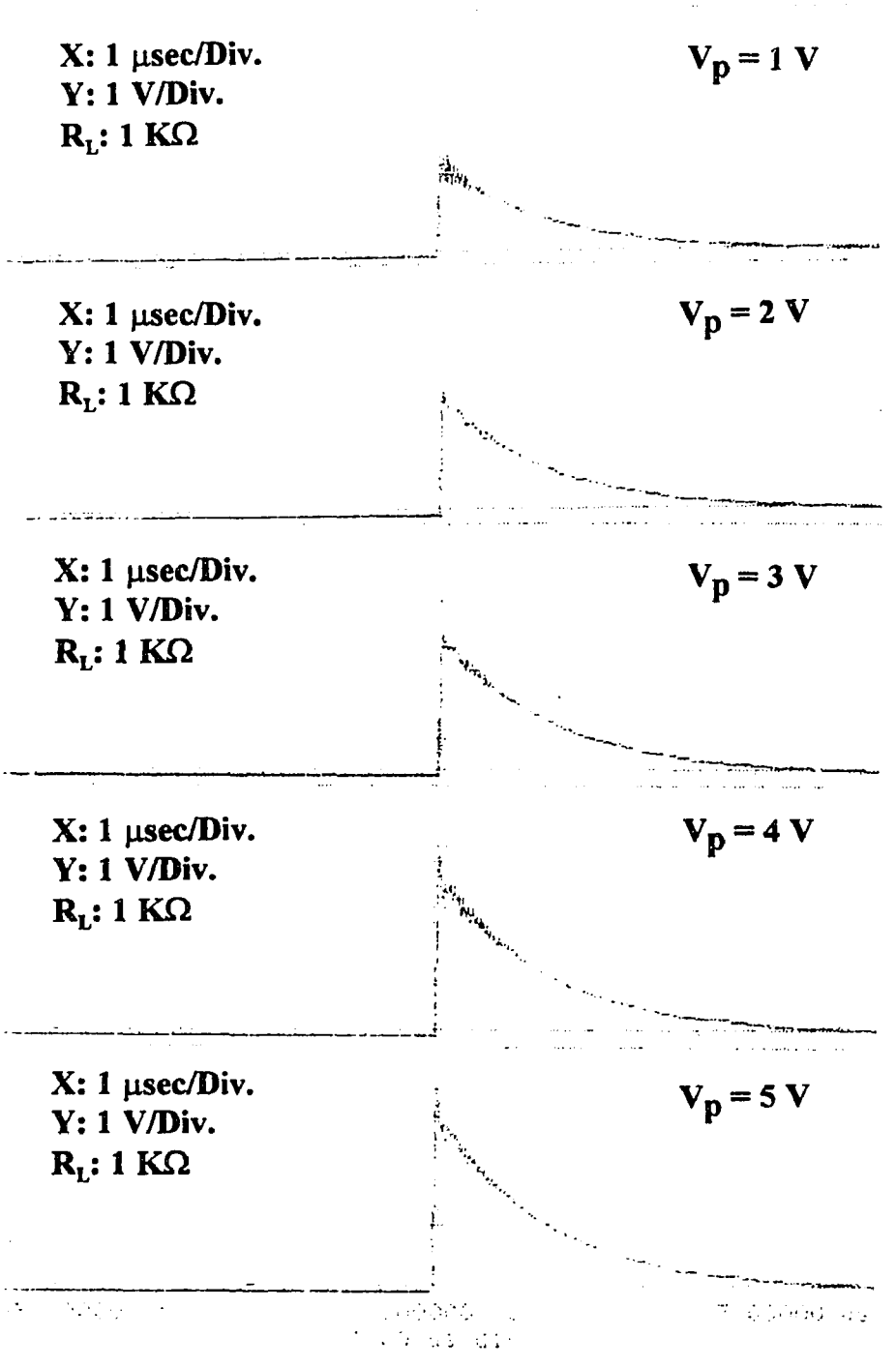

Figure B.7 Voltage-time characteristics of PLT (28) MDM capacitors with different peak voltage of unipolar pulse

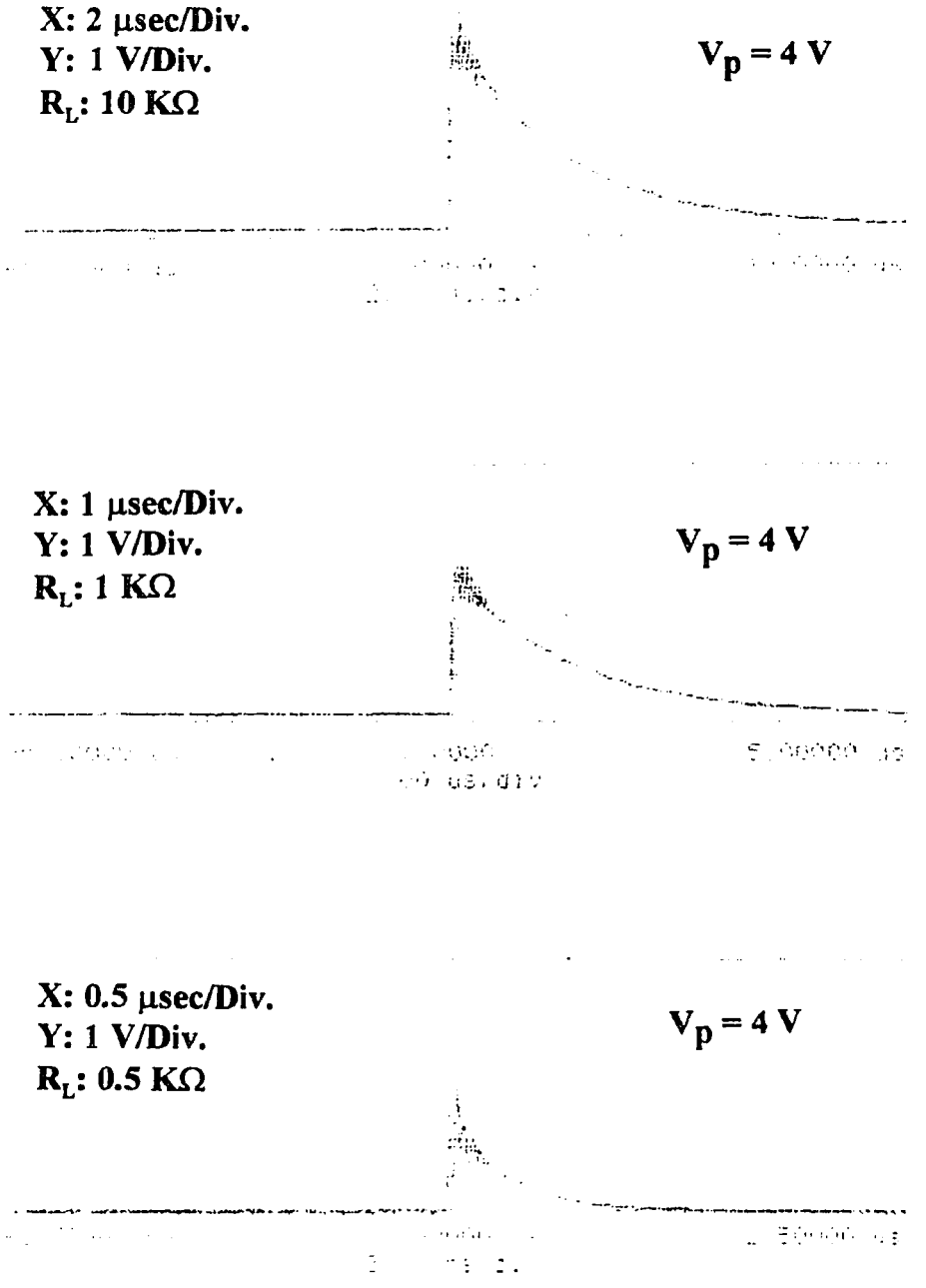

Figure B.8 Switching time response characteristics as a function of load resistance under the same peak voltage of 4 V (200 KV/cm)

REFERENCES

[1] H. Adachi and K. Wasa. "Sputtering Preparation of Ferroelectric PLZT Thin Films and Their Optical Application." IEEE Trans. Ultra. Ferro. Freq. Control, 38(6), 645, 1991.

[2] R. Takayama, Y. Tomita, K. Iijima, and I. Ueda. "Preparation and Characteristics of Pyroelectric Infrared Sensors Made of c-axis Oriented La-Modified $PbTiO_3$ Thin Films." J. Appl. Phys. 61(1), 411, 1987.

[3] V. Chikarmane, J. Kim, C. Sudhama, J. Lee, A. Tasch, and S. Novak. "Annealing of PZT (65/35) Thin Films for ULSI Storage Dielectric Applications: Phase Transformation and Electrical Characteristics." J. Elect. Mater. 21(5), 503, 1992.

[4] L. Wang, A. Pignolet, and F. Levy. "Properties of PZT Thin Films Prepared by rf Magnetron Sputtering and Heat Treatment." Mater. Res. Bull. 25, 1495, 1990.

[5] M. Okuyama, and Y. Hamakawa. "PT Ferroelectric Thin Films and Their Pyroelectric Application." Ferro. 118, 261, 1991.

[6] R. Watton, and M. Todd. "Induced Pyroelectricity in Sputtered PST Films and Their Merit for IR Detector Arrays." Ferro. 118, 279, 1991.

[7] R. Castelland, and L.Feinstein. "Ion-Beam Deposition of Thin Films of Ferroelectric PZT." J. Appl. Phys. 50, 4406, 1979.

[8] B. Krupanidhi, H. Hu, and V. Kumar. "Multi-Ion-Beam Reactive Sputter Deposition of Ferroelectric PZT Thin Films." J. Appl. Phys. 71, 376, 1992.

[9] M. Okada, S. Takai, M. Amemiya, and K. Tominaga. "Preparation of c-axis Oriented $PbTiO_3$ Thin Films by MOCVD under Reduced Pressure." Jpn. J. Appl. Phys. 28, 1030, 1989.

[10] R. Vest. "Metallo-Organic Decomposition Processing of Ferroelectric and Electro-Optic Films: A Review." Ferro. 102, 53, 1990.

[11] G. Haertling. "Ferroelectric Thin Films for Electronic Applications." J. Vac. Sci. Technol. 9(3A), 414, 1991.

[12] S. Dey, and R.Zuleeg. "Integrated Sol-Gel PZT Thin Films on Pt, Si and GaAs for Non-volatile Memory Applications." Ferro. 108, 37, 1990.

REFERENCES
(Continued)

[13] G. Spierings, M. Ulenaers, G. kampschoer, H. Hal, and P. Larsen. "Preparation and Ferroelectric Properties of PZT (53/47) Thin Films by Spin Coating and Metalorganic Decomposition." J. Appl. Phys. 70, 2290, 1991.

[14] H. Buhay, S. Sinharoy, W. Kasner, M. Francombe, D. Lampe, and E. Stepke. "Pulsed Laser Deposition and Ferroelectric Characterization of Bismuth Titanate Films." Appl. Phys. Lett. 58, 1470, 1991.

[15] D. Roy, S. Krupanidhi, and J. Dougherty. "Excimer Laser Ablation of Ferroelectric PZT Thin Films with Low Pressure Direct-Current Glow Discharge." J. Vac. Sci. Technol. 10(4A), 1827, 1992.

[16] M. Lines, and A. Glass. *Principles and Applications of Ferroelectrics and Related Materials.* Clarendon Press, Oxford, 1977.

[17] C. Land, P. Thacher, and G. Haertling. *Electrooptic Ceramics*, in Applied Solid State Science: Vol 4 edited by R.Wolfe, Academic Press, New York, P137, 1974.

[18] H. Adachi, T. Kawaguchi, K. Setsune, K. Ohji, and K. Wasa. "Electro-Optic Effects of PLZT Thin Films Prepared by rf Planar Magnetron Sputtering." Appl. Phys. Lett. 42(10), 867, 1983.

[19] G. Haertling. *Piezoelectric and Electrooptic Ceramics*, in Ceramic Materials for Electronics edited by R.Buchanan, 2nd Edition, Marcel Dekker, Inc., New York, P129, 1991.

[20] J. Carrano, C. Sudhama, V. Chikarmane, J. Lee, A. Tasch, W. Shepherd, and N. Abt. "Electrical and Reliability Properties of PZT Thin Films for ULSI DRAM Applications." IEEE Ultra. Ferro. Freq. Control 38(6), 690, 1991.

[21] D. Hennings, and K. Härdtl. "The Distribution of Vacancies in Lanthana-Doped Lead Titanate." Phys. Stat. Sol. (a) 3, 465, 1970.

[22] A. Khan, I. Yoo, and S. Desu. "Preparation and Characterization of PLT Thin Films by Metalorganic Decomposition." IEEE-92, ISAF, 412, 1992.

[23] D. Hennings. "The Range of Existence of Perovskite Phase in the System PbO-TiO_2-La_2O_3." Mater. Res. Bull. 6, 329, 1971.

REFERENCES
(Continued)

[24] K. Keizer, and A. Burggraaf. "Grain Size Effects on the Ferroelectric-Paraelectric Transition, the Dielectric Constant, and the Lattice Parameters in Lanthana-Substituted Lead Titanate." Phys. Stat. Sol. (a) 26, 561, 1974.

[25] R. Roth, T. Negas, and L. Cook. *Phase Diagrams for Ceramists: Vol 4.* The American Ceramic Society, Inc., Ohio, P223, 1981.

[26] G. Fox, S. Krupanidhi, K. More, and L. Allard. "Composition/Structure/Property Relations of Multi-Ion-Beam Reactive Sputtered Lead Lanthanum Titanate Thin Films: Part I. Composition and Structure Analysis." J. Mater. Res. 7(11), 3039, 1992.

[27] J. Thornton. "Influence of Substrate Temperature and Deposition Rate on Structure of Thick Sputtered Cu Coatings." J. Vac. Sci. Technol. 12(4), 830, 1975.

[28] T. Yamamoto, H. Igarashi, and K. Okazaki. "Dielectric, Electro-mechanical, Optical, and Mechanical Properties of Lanthana-Modified Lead Titanate Ceramics." J. Amer. Ceram. Soc. 66(5), 363, 1983.

[29] K. Keizer, G. Lansink, and A. Burggraaf. "Anomalous Dielectric Behaviour of La (III) Substituted Lead Titanate Ceramics." J. Phys. Chem. Sol. 39, 59, 1978.

[30] S. Dey, and J.Lee. "Cubic Paraelectric (Nonferroelectric) Perovskite PLT Thin Films with High Permittivity for ULSI DRAMs and Decoupling Capacitors." IEEE Elect. Dev. 39(7), 1607, 1992.

[31] L. Parker, and A. Tasch. "Ferroelectric Materials for 64 and 256 Mb DRAMs." IEEE Circuit Dev. Mag. 17, Jan. 1990.

[32] A. Tasch. "Storage Capacitor Dielectric Issues and Requirements in Gigabit One-Transistor Cell MOS RAMs." 184th Electrochem. Soc. Meeting, New Orleans, P238, 1993.

[33] R. Dennard. "Field-Effect Transistor Memory." US Patent 3 387 286, June 4, 1968.

[34] D. Bondurant. "Ferroelectric RAM memory Family for Critical Data Storage." Ferro. 112, 273, 1990.

[35] S. Dey, and R. Zuleeg. "Processing and Parameters of Sol-Gel PZT Thin Films for GaAs Memory Applications." Ferro. 112, 309, 1990.

REFERENCES
(Continued)

[36] C. Hashimoto, H. Oikawa, and N. Honma. " Leakage-Current Reduction in Thin Ta_2O_5 Films for High Density VLSI Memories." IEEE Elect. Dev. 36(1), 14, 1989.

[37] L. Manchanda, and M. Gurvitch. "Yttrium Oxide/Silicon Dioxide: A New Dielectric Structure for VLSI/ULSI Circuits." IEEE Elect. Dev. Lett. 9(4), 180.1988.

[38] R. Moazzami, C. Hu, and W. Shepherd. "Electrical Characteristics of Ferroelectric PZT Thin Films for DRAM Applications." IEEE Elect. Dev. 39(9), 2044, 1992.

[39] R. Moazzami, C. Hu, and W. Shepherd. "A Ferroelectric DRAM Cell for High Density NVRAM." IEEE Elect. Dev. Lett. 11(10), 454, 1990.

[40] J. Lee, and S. Dey. "Sol-Gel Derived PLT Thin Films with High Linear Permittivity for ULSI DRAMs." Ceram. Trans. 25, 235, 1992.

[41] A. Tasch, and L. Parker. "Memory Cell and technology Issues for 64- and 256-Mbit One-Transistor Cell MOS DRAMs." Proc. IEEE 77(3), 374, 1989.

[42] H. Adachi, T. Mitsuya, O. Yamazaki, and K. Wasa. "Ferroelectric PLZT Epitaxial Thin Films on Sapphire Grown by rf planar Magnetron Sputtering." J. Appl. Phys. 60(2), 736, 1986.

[43] R. Schwartz, B. Tuttle, D. Doughty, C. Land, D. Goodnow, C. Hernandez, T. Zender, and S. Martinez. "Preparation and Characterization of Chemically Derived PLT Thin Films." IEEE Ultra. Ferro. Freq. Control, 38(6), 677, 1991.

[44] S. Watanabe, T. Fujiu, and A. Tanaka. "Lanthanum-Modified Lead Titanate Thin Film Formed by Low Temperature Chemical Vapor Deposition and Subsequent Annealing." Appl. Phys. Lett. 62(25), 3377, 1993.

[45] Z. Qian, D. Xiao, J. Zhu, and Z. Li. "X-ray Photoelectron Spectroscopy and Auger Electron Spectroscopy Studies of Ferroelectric PLT Thin Films Prepared by A Multi-Ion-Beam Reactive Cosputtering Technique." J. Appl. Phys. 74(1), 224, 1993.

[46] G. Fox, S. Krupanidhi, and K. More. "Composition/Structure/Property Relations of Multi-Ion-Beam Reactive Sputtered Lead Lanthanum Titanate Thin Films: Part II. Textured Microstructure Development." J. Mater. Res. 8(9), 2191, 1993.

[47] S. Krupanidhi. "Recent Advances in Physical Vapor Growth Processes for Ferroelectric Thin Films." J. Vac. Sci. Technol. 10(4A), 1569, 1992.

REFERENCES
(Continued)

[48] S. Swan. "Magnetron Sputtering." Phys. Technol. 19, 67, 1988.

[49] R. Waits. *Planar Magnetron Sputtering.* in Thin Film Processes edited by J.Vossen and W.Kern, Academic Press, New York, P131, 1978.

[50] Hexetch 640, Asymmetrical Reactive Ion Etch System. Instruction Manual, Plasma-Therm, Inc., Kresson, NJ, 1982.

[51] *Tri-Mag Sputtering Source. 383-BPM-FS-AS-VCOS.* Instruction Manual, L.M.Simard Inc., Oregon, 1989.

[52] The Simion PC/PS2, User's Manual, Version 4.0, Idaho National Engineering Laboratory, EG&G Idaho Inc., Idaho Falls, Idaho, 1988.

[53] B. Chapman. *Glow Discharge Processes: Sputtering and Plasma Etching.* John Wiley and Sons, New York, P263, 1980.

[54] F. Green, and B. Chapman. "Electron Effects in Magnetron Sputtering." J. Vac. Sci. Technol. 13(1), 165, 1976.

[55] A. Kingon, H. Al-Shareef, and S. Summerfelt. "Electrodes Systems for Ferroelectric Capacitor Structures in DRAMs." 184th Electrochem. Soc. Meeting, New Orleans, P263, 1993.

[56] K. Sreenivas, I. Reaney, T. Maeder, N. Setter, C. Jagadish, and R. Elliman. "Investigation of Pt/Ti Bilayer Metallization on Silicon for Ferroelectric Thin Film Integration." J. Appl. Phys. 75(1), 232, 1994.

[57] I. Kondo, T. Yoneyama, O. Takenaka, and A. Kinbara. "Formation of High Adhesive and Pure Pt Layers on TiO_2." J. Vac. Sci. Technol. 10(6A), 3456, 1992.

[58] J. Olowolafe, R. Jones, A. Campbell, R. Hegde, C. Mogab, and R. Gregogy. "Effects of Anneal Ambients and Pt Thickness on Pt/Ti and Pt/Ti/TiN Interfacial Reactions." J. Appl. Phys. 73(4), 1764, 1993.

[59] A. Croteau, and M. Sayer. "Growth and Characterization of PZT Films Deposited by Reactive Sputtering of Metallic Targets." IEEE-86, ISAF, 606, 1986.

REFERENCES
(Continued)

[60] T. Yamamoto, T. Imai, and T. Shiozaki. "Preparation of PZT Thin Films by Reactive rf Magnetron Cosputtering Using Multi-Element Metallic Targets and Their Evaluations." IEEE-92, ISAF, 317, 1992.

[61] M. Sayer. "Fabrication and Application of Multi-Component Piezoelectric Thin Films." IEEE-86, ISAF, 560, 1986.

[62] K. Sreenivas, and M. Sayer. "Characterization of PZT Thin Films Deposited from Multi-Element Metal Targets." J. Appl. Phys. 64(3), 1484, 1988.

[63] Y. Ochiai, K. Aso, M. Hayakawa, H. Matsuda, K. Hayash, W. Ishikawa, and Y. Iwasaki. "On Specimen Preparation by rf Planar Magnetron Sputtering." J. Vac. Sci. Technol. 4(1A), 19, 1986.

[64] T. Fukami, and T. Sakuma. "Composition of Reactively Sputtered PLZT Films." Jpn. J. Appl. Phys. 20(8), 1599, 1981.

[65] T. Hase, and T. Shiosaki. "Preparation and Switching Kinetics of PZT Thin Films Deposited by Reactive Sputtering." Jpn. J. Appl. Phys. 30(9B), 2159, 1991.

[66] P. Sigmund. "Theory of Sputtering. I. Sputtering Yield of Amorphous and Polycrystalline Targets." Phys. Rev. 184(2), 3883, 1969.

[67] P. Sigmund. "Sputtering of Single and Multiple Component Materials." J. Vac. Sci. Technol. 17(1), 396, 1980.

[68] H. Adachi, T. Mitsuyu, O. Yamazaki, and K. Wasa. "Preparation and Properties of PLT Epitaxial Thin Films by Multi-Target Sputtering." Jpn. J. Appl. Phys. Suppl. 24(3), 13, 1985.

[69] R. Cornely. *Film Growth by Ion Beam and Plasma Discharge Sputtering Method.* in Ion Beam Assisted Film Growth edited by T.Itoh. Japan. P9, 1989.

[70] O. Auciello, and A. Kingon. "A Critical Review of Physical Vapor Deposition Techniques for the Synthesis of Ferroelectric Thin Films." IEEE-92, ISAF, 320, 1992.

[71] H. Adachi, K. Hirochi, K. Setsune, M. Kitabatake, and K. Wasa. "Low Temperature Process for the Preparation of High T_c Superconducting Thin Films." Appl. Phys. Lett. 51(26), 2263, 1987.

REFERENCES
(Continued)

[72] R. Sandstrom, W. Gallagher, T. Dinger, R. Koch, R. Laibowitz, A. Kleinsasser, R. Gambino, B. Bumble, and M. Chisholm. "Reliable Single-Target Sputtering Process for High Temperature Superconducting Films and Devices." Appl. Phys. Lett. 53(5), 444, 1988.

[73] N. Terada, H. Ihara, M. Jo, M. Hirabayashi, Y. Kimura, K. Matsutani, K. Hirata, E. Ohno, R. Sugise, and F. Gawashima. "Sputter Synthesis of YBCO As-Deposited Superconducting Thin Films from Stoichiometric Target: A Mechanism of Compositional Deviation and Its Control." Jpn. J. Appl. Phys. 27(4), L639, 1988.

[74] M. Okuyama, T. Ueda, and Y. Hamakawa. "Bias Effect in rf Sputtering of $PbTiO_3$ Thin Films." Proc. 1985 5th Meeting on Ferro. and Their Appl., Kyoto, 1985.

[75] R. Hill. *Physical Vapor Deposition.* Temescal, Berkeley, P57, 1976.

[76] J. Vossen, and J. Cuomo. *Glow Discharge Sputter Deposition.* in Thin Film Processes edited by J.Vossen and W.Kern, Academic Press, New York, P48, 1978.

[77] V. Fridkin. *Ferroelectric Semiconductors.* Consultants Bureau, New York, P70, 1980.

[78] Z. Surowiak, J. Dudek, Y. Goltzov, S. Gach, A. Dranishnikov, L. Shpak, and V. Yurkevich. "The Semiconductor Properties on the System Metal-Semiconductive Ferroelectric-Metal." Ferro. 123, 19, 1991.

[79] L. Davis, N. MacDonald, P. Palmberg, G. Riach, and R. Weber. *Handbook of Auger Electron Spectroscopy.* Physical Electronics Industries, Eden Prairie, Minn. 1976.

[80] C. Chang. "Auger Electron Spectroscopy." Surf. Sci. 25, 53, 1991.

[81] Y. Shimizu, K. Udayakumar, and L. Cross. "Preparation and Electron Properties of Lanthanum-Doped Lead Titanate Thin Films by Sol-Gel Processing." J. Amer. Ceram. Soc. 74(12), 3023, 1991.

[82] G. Samara. "Pressure and Temperature Dependence of the Dielectric Properties and Phase Transitions of the Ferroelectric Perovskites: $PbTiO_3$ and $BaTiO_3$." Ferro. 2, 277, 1971.

[83] S. Dana, K. Etzold, and J. Clabes. "Crystallization of Sol-Gel Derived Lead Zirconate Titanate Thin Films." J. Appl. Phys. 69(8), 4398, 1991.

REFERENCES
(Continued)

[84] T. Ogawa, A. Senda, and T. Kasanami. "Controlling the Crystal Orientations of Lead Titanate Thin Films." Jpn. J. Appl. Phys. 30(9B), 2145, 1991.

[85] M. Murakami. "Thermal Strain in Lead Thin Films VI: Effects of Oxygen Doping." Thin Sol. films, 69, 253, 1980.

[86] R. Opila. "The Role of Grain Boundaries in the Surface Segregation of TiN in TiN-Lead Alloys." J. Vac. Sci. Technol. 4(2A), 173, 1986.

[87] C. Sawyer, and C. Tower. "Rochelle Salt as a Piezoelectric." Phys. Rev. 35, 269, 1930 or Diamant, H., K. Drenck, and R. Pepinsky. "Bridge for Accurate Measurement of Ferroelectric Hystersis." Rev. Sci. Instru. 28(1), 30, 1957.

[88] G. Fox, and S. Krupanidhi. "Composition/Structure/Property Relations of Multi-Ion-Beam Reactive Sputtered Lead Lanthanum Titanate Thin Films: Part III. Electrical Properties." J. Mater. Res. 8(9), 2203, 1993.

[89] S. Sze. *Physics of Semiconductor Devices*. 2th Edition, Wiley, NJ, P403, 1981.

[90] I. Yoo, and S. Desu. "Leakage Current Mechanism and Accelerated Unified Test of Lead Zirconate Titanate Thin Film Capacitor." IEEE-92, ISAF, 225, 1992.

[91] V. Chikarmane, C. Sudhama, J. Kim, J. Lee, A. Tasch, and S. Novak. "Effects of Post-Deposition Annealing Ambient on the Electrical Characteristics and Phase Transformation Kinetics of Sputtering Lead Zirconate Titanate (65/35) Thin Film Capacitors." J. Vac. Sci. Technol. 10(4A), 1562, 1992.

[92] R. Waser, T. Baiatu, and K. Härdtl. "dc Electrical Degradation of Perovskite-Type Titanate: I. Ceramics." J. Amer. Ceram. Soc. 73(6), 1645, 1990.

[93] T. Baiatu, R. Waser, and K. Härdtl. "dc Electrical Degradation of Perovskite-Type Titanate: III. A Model of the Mechanism." J. Amer. Ceram. Soc. 73(6), 1663, 1990.

[94] H. Duiker, P. Beale, J. Scott, C. Araujo, B. Melnick, J. Cuchiaro, and L. McMillan. "Fatigue and Switching in Ferroelectric Memories: Theory and Experiment." J. Appl. Phys. 68(11), 5783, 1990.

REFERENCES
(Continued)

[95] P. Larsen, G. Kampschöer, M. Ulenaers, G. Spierings, and R. Cuppens. "Nanosecond Switching of Thin Ferroelectric Films." Appl. Phys. Lett. 59(5), 611, 1991.

[96] B. Maderic, L. Sanchez, and S. Wu. "Ferroelectric Switching, Memory Retention and Endurance Properties of Very Thin PZT Films." Ferro. 116, 65, 1991.